General Disclaimer

One or more of the Following Statements may affect this Document

- This document has been reproduced from the best copy furnished by the organizational source. It is being released in the interest of making available as much information as possible.

- This document may contain data, which exceeds the sheet parameters. It was furnished in this condition by the organizational source and is the best copy available.

- This document may contain tone-on-tone or color graphs, charts and/or pictures, which have been reproduced in black and white.

- This document is paginated as submitted by the original source.

- Portions of this document are not fully legible due to the historical nature of some of the material. However, it is the best reproduction available from the original submission.

SSL

SPACE SYSTEMS LABORATORY
DEPT. OF AERONAUTICS AND ASTRONAUTICS
MASSACHUSETTS INSTITUTE OF TECHNOLOGY
CAMBRIDGE, MA 02139

ROBUST FAILURE DETECTION FILTERS

Alejandro Miguel San Martin

July 1, 1985 SSL # 17-85

(under NASA Grant # NAG1-126)

ROBUST FAILURE DETECTION FILTERS

by

Alejandro Miguel San Martin

B.S., Syracuse University
(1982)

SUBMITTED TO THE DEPARTMENT OF AERONAUTICS AND ASTRONAUTICS IN PARTIAL FULFILLMENT OF THE REQUIREMENTS FOR THE DEGREE OF

MASTER OF SCIENCE

at the

MASSACHUSETTS INSTITUTE OF TECHNOLOGY

September 1985

Signature of Author _____
Department of Aeronautics and Astronautics
September 1, 1985

Certified by _____
Professor Wallace E. Vander Velde
Thesis Supervisor

Accepted by _____
Professor Harold Y. Wachman, Chairman
Departmental Graduate Committee

Robust Failure Detection Filters

by

Alejandro Miguel San Martin

Submitted to the Department of Aeronautics and Astronautics on September 1, 1985 in partial fulfillment of the requirements for the degree of Master of Science.

Abstract

The robustness of detection filters applied to the detection of actuator failures on a free-free beam is analyzed. This analysis is based on computer simulation tests of the detection filters in the presence of different types of model mismatch, and on frequency response functions of the transfers corresponding to the model mismatch.

The robustness of detection filters based on a model of the beam containing a large number of structural modes varied dramatically with the placement of some of the filter poles. The dynamics of these filters were very hard to analyze.

The design of detection filters with a number of modes equal to the number of sensors was trivial. They can be configured to detect any number of actuator failure events. The dynamics of these filters were very easy to analyze and their robustness properties were much improved. A change of the output transformation allowed the filter to perform satisfactorily with realistic levels of model mismatch.

Thesis Supervisor: Professor Wallace E. Vander Velde
Title: Thesis Supervisor

Acknowledgments

I would like to thank Professor Vander Velde for his technical advice and patience over the past years, as well as for the opportunity to work on this project. My appreciation goes out to Ping Lee for helping secure the computer resources. I express gratitude to my friends and colleagues for their enlightening conversation, suggestions and patient support in the preparation of this thesis. I thank all of my friends and family for their patience displayed while I sang my thesis blues. To my parents, Baby and Salvador, I send my thanks and love for their emotional and financial support, but most of all for their unending encouragement and selflessness in allowing me to pursue my dreams. I would especially like to thank my wife Susan for the encouragement and love demonstrated by volunteering for the arduous and difficult task of typing this thesis.

I would also like to thank the National Aeronautics and Space Administration for sponsoring this work under NASA Grant #NAG1-126.

Table of Contents

List of Figures

List of Tables

Chapter 1
Introduction

It is expected, with the advent of the space shuttle, that large space structures serving a variety of mission requirements will be assembled in space in the near future. Some of the structures being contemplated include antennas, reflectors and solar power satellites. They are characterized by their light weight and very large sizes, which in turn result in low frequency bending properties with very little structural damping.

The active control of large space structures will include station keeping control, attitude control, shape control and vibrational damping. The component unreliability issue is most important in the last of these applications where hundreds of sensors and actuators will be needed in order to actively damp the many vibrational modes to assure mission success. The large number of components in the system result in a high probability of a component failure in a short period of time, even assuming components having very optimistic mean time between failures. For example, a system with 200 components, each having a time between failures of 100,000 hours, is expected to have 17 component failures a year [7]. Even if these control systems are serviced in orbit, it is desired that its service interval be as long as possible, at least one year. Therefore, it will be necessary to design control systems that can tolerate the number of component failures occurring during the service interval. This, in turn, will require systems that can detect and identify a component failure, and will require control systems that can be reconfigured to perform without the failed component in some optimal

fashion.

The failure detection and identification systems (FDI) depend on hardware redundancy or analytic redundancy in order to detect and identify a failed component. An example of hardware redundancy to detect and identify sensor failures is the one that involves triplication of sensors, where the failure of a component is detected when there is a discrepancy between the signals of two sensors and comparison with the third determines which of the two has failed. Because of the large weight and cost resulting from hardware redundancy, these systems are not attractive for applications in large space structures. The FDI systems based on analytic redundancy use knowledge of the plant dynamics to make the detection and identification of the failure. Some of these systems require specification of the failure modes ahead of time.

The Failure Detection Filter is a closed loop method, based on analytic redundancy, to detect and identify actuator and sensor failures, and changes in plant dynamics. A very attractive property of the detection filter is that it does not require specificaton of the mode of failure.

The Failure Detection Filter is a linear filter having the same configuration as an observer but with an additional constraint in the design of the gain matrix D. The output error, the difference between the system measurements and the filter estimate of those measurements, is zero when the system is operating nominally (assuming no model mismatch). When a failure occurs, the output error becomes nonzero, indicating that a component has failed. Moreover, the additional constraint on the gain matrix D keeps the output error in a single direction in the output space. The failed component can then be identified by this direction.

The failure detection filter was first proposed by Beard [1] for deterministic

systems. Jones [5] explained detection filter theory using a more geometric approach and expanded it to stochastic and sampled data systems. Detection Filter Theory was applied by Carignan [2] in the context of flexible space structures, where he considered actuator and sensor failure events, and analyzed the performance of the filter in the presence of unmodeled modes. He developed the computer software used in this thesis to design detection filters and to simulate the dynamics of the plant with the filter.

The goal in this thesis, is to improve the performance of detection filters in detecting and identifying actuator failures in an undamped flexible structure, in the presence of model mismatch. To achieve this goal, the filter performance will be evaluated in the presence of unmodeled modes and different levels of parameter errors. In addition, the transfer properties of the filter will be analyzed and the results compared with the simulations.

In Chapter 2, the main results of detection filter theory are introduced along with analytical procedures for the filter design. Chapter 3 describes the model of the undamped flexible beam, shows some properties of the detection filter design for actuator failures, and simulates the filter with no model mismatch.

In Chapter 4, the detection filter performance in the presence of model mismatch is analyzed using simulations and frequency response functions. Ways of improving the filter performance derived from this analysis are presented in the chapter. Chapter 5 contains the conclusions and recommendations for further research.

Chapter 2
Failure Detection Filter Theory

The **Failure Detection Filter** is a linear filter having the same configuration as a full order observer (Fig. 2-1). It includes a model of the nominal system and is driven by the same actuator commands as the actual system. The output error, the difference between the system measurements and the filter estimate of those measurements, is multiplied by the gain matrix D and fed-back to the filter.

In a full order observer, the only constraint placed upon the gain matrix D is that the eigenvalues of the matrix (A - DC) must have negative real parts. When this is the case, the observer is stable and the state and output errors become zero (except for noise and other unmodeled effects) during nominal operation. When a component failure occurs, the output error will become nonzero. Therefore, any stable observer can detect when the system has failed. What distinguishes a Failure Detection Filter from such an observer is that the gain matrix D has the additional constraint of restricting the output error due to a particular failure to a single line in the output space. The direction of that line is used to identify which component has failed.

Pole placement in Detection Filter design can be used not only to assure the stability of the filter, but to improve the performance of the filter in the presence of unmodeled system dynamics. Therefore, complete control of the Detection Filter poles is required. This requirement together with the output directionality constraint are the bases of Detection Filter Theory and are present in the definition

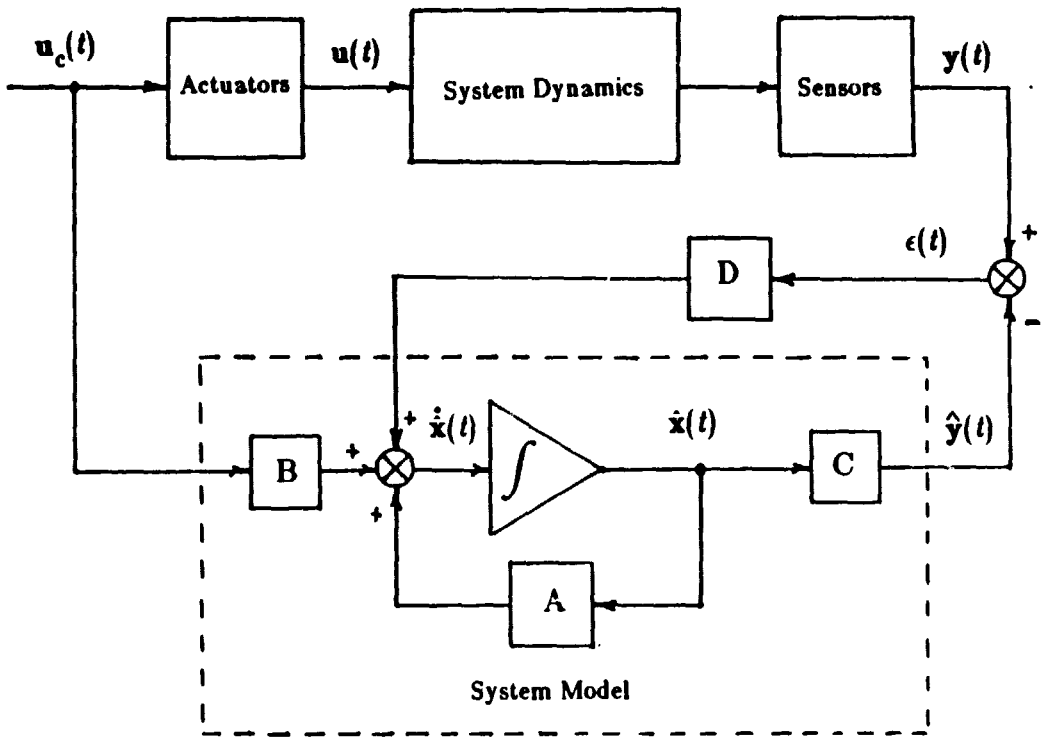

Figure 2-1: The Failure Detection Filter

of **Failure Detectability**.

Detection Filter Theory consists mainly of two parts: 1) a set of necessary and sufficient conditions that must be satisfied for the solution of a particular detection filter problem to exist, and 2) a set of algorithms to achieve the design.

In this chapter, the state and output error equations are presented for both nominal and failed system operation. The concept of **Failure Detectability** will then be introduced, and important results concerning necessary and sufficient conditions will be stated. Finally, an algorithm for filter design based on annhilating minimal polynomials will be presented.

2.1 The Failure Detection Filter Problem

The model that describes the plant dynamics must be linear, time-invariant and observable. It is not necessary that the system be observable but only that the model be observable. An observable model can be obtained by removing the unobservable dynamics from it. This does not reduce the effectiveness of the FDI system because failures that affect only the unobservable part of the plant dynamics cannot be detected.

The unfailed system is represented by the equations:

$$\dot{\mathbf{x}}(t) = \mathrm{A}\,\mathbf{x}(t) + \mathrm{B}\,\mathbf{u}(t) \tag{2.1}$$

$$\mathbf{y}(t) = \mathrm{C}\,\mathbf{x}(t)$$

where

$\mathbf{x}(t)$ is the n dimensional state vector,

$\mathbf{u}(t)$ is the m dimensional control vector,

$\mathbf{y}(t)$ is the p dimensional measurement vector.

The structure of the **Failure Detection Filter** is shown in (2-1). Due to the similarity between detection filters and observers, the filter state vector $\hat{\mathbf{x}}$ is called the state estimate and $\hat{\mathbf{y}}$ is called the measurement estimate.

The filter equations are:

$$\dot{\hat{\mathbf{x}}}(t) = \mathrm{A}\,\hat{\mathbf{x}}(t) + \mathrm{B}\,\mathbf{u}_c(t) + \mathrm{D}\left[\,\mathbf{y}(t) - \hat{\mathbf{y}}(t)\,\right] \tag{2.2}$$

$$\hat{\mathbf{y}}(t) = \mathrm{C}\,\hat{\mathbf{x}}(t)$$

The state error is defined as:

$$\mathbf{e}(t) = \mathbf{x}(t) - \hat{\mathbf{x}}(t)$$

The measurement error is defined as:

$$\epsilon(t) = \mathbf{y}(t) - \hat{\mathbf{y}}(t)$$

The state and measurement equations are obtained by subtracting equations (2.1) from (2.2). In the normal mode, $\mathbf{u}(t) = \mathbf{u}_c(t)$, and

$$\dot{\mathbf{e}}(t) = (\mathrm{A} - \mathrm{DC})\, \mathbf{e}(t) \tag{2.3}$$

$$\epsilon(t) = \mathrm{C}\, \mathbf{e}(t)$$

If the eigenvalues of the matrix (A - DC) have negative real parts, the state and measurement errors will become zero in the steady state. This is true, however, only when the system is operating nominally. When a component failure occurs, the state and output error equations (2.3) are no longer valid since equations (2.1) no longer represent the true system. The new state and output error equations will depend on the type of component that failed.

Consider the failure of actuator j. The true control $\mathbf{u}(t)$ that is being applied to the plant is

$$\mathbf{u}(t) = \mathbf{u}_c(t) + \hat{\mathbf{e}}_{mj}\, \eta(t)$$

where $\mathbf{u}_c(t)$ is the desired control, $\hat{\mathbf{e}}_{mj}$ is a unit vector in the jth direction of dimension m, and $\eta(t)$ is a scalar time function equal to the difference between the commanded input to actuator j and the actual control being applied by this actuator.

The new system equations are

$$\dot{\mathbf{x}}(t) = \mathrm{A}\,\mathbf{x}(t) + \mathrm{B}\,\mathbf{u}_c(t) + \mathbf{b}_j\,\eta(t) \tag{2.4}$$

$$\mathbf{y}(t) = \mathrm{C}\,\mathbf{x}(t)$$

where $\mathbf{b}_j$ is the column of B corresponding to the *jth* actuator.

The new state and output error equations with actuator j failure are obtained by combining (2.2) and (2.4)

$$\dot{\mathbf{e}}(t) = (\mathrm{A} - \mathrm{DC})\,\mathbf{e}(t) + \mathbf{b}_j\,\eta(t) \tag{2.5}$$

$$\epsilon(t) = \mathrm{C}\,\mathbf{e}(t)$$

The goal of **Detection Filter** design, in this example, is to find a gain matrix D such that $\mathbf{e}(t)$ maintains a fixed direction in the output space when actuator j fails (and at the same time assign almost arbitrarily the eigenvalues of matrix [A-DC]). Since only directionality is important in the identification of the failed component, the vector $\mathbf{b}_j$ is the only element in equation (2.5) that characterizes the failure of actuator j. For this reason, the vector $\mathbf{b}_j$ is called the **event vector** associated with actuator j failure. The forcing function $\eta(t)$ depends on the mode of failure of the actuator, and knowledge of this signal (or of the failure mode) is not needed in the use of a detection filter. This characteristic makes **Failure Detection Filters** very attractive for failure detection and identification.

For the rest of the chapter, the detection problem is generalized to the detection and identification of the component failure associated with the event vector **f**, and whose corresponding state and output error equations are

$$\dot{\mathbf{e}}(t) = (\mathrm{A} - \mathrm{DC})\,\mathbf{e}(t) + \mathbf{f}\,\eta(t) \tag{2.6}$$

$$\epsilon(t) = \mathbf{e}(t)$$

The discussion in this section, so far, can be summarized by the following

definition of **detectability** found in Beard [1].

Definition: The failure event associated with event vector **f** in (2.6) is **detectable** if there exists a matrix D such that

(1) C $\mathbf{e}_s(t)$ maintains a fixed direction in the output space (where $\mathbf{e}_s(t)$ is the settled-out solution of (2.6)) and,

(2) at the same time, all eigenvalues of (A - DC) can be specified almost arbitrarily.

Condition (1) is the distinguishing feature of the failure detection filter and serves to identify which component has failed. Condition (2) is needed to assure that the matrix (A - DC) is stable so that during nominal operation, equation (2.3), the initial state and output errors die out to zero, and in the presence of component failure, equation (2.6), the output error is unidirectional. Condition (2) also allows the designer of a failure detection filter to adjust the bandwidth of the filter to suppress the effects of unmodeled system dynamics, as will be shown in Chapter 5.

Given a failure event, the **detection filter problem** consists of: determining whether the event is **detectable** and, if it is detectable, to find the gain matrix that makes the output error unidirectional and assigns the desired poles to the filter.

In the next section, the detection filter problem is solved for both fully measurable systems (rank C = n) and partially measurable systems (rank C < n).

2.2 Fully Measurable Systems

A **fully measurable system** is a system whose state vector $\mathbf{x}(t)$ can be solved uniquely given the measurement vector $\mathbf{y}(t)$, for any time t. Therefore, a system is fully measurable if and only if

$$\text{rank } C = n$$

this implies that the number of sensors $p \geq n$.

The solution of the detection filter problem for this type of system is very simple. Choose a gain matrix D such that

$$(A - DC) = -\sigma I \tag{2.7}$$

where I is the identity matrix and σ is a positive scalar constant. Then all the eigenvalues of (A - DC) are $-\sigma$, and the resulting filter is stable. The matrix D that satisfies (2.7) is given uniquely by

$$D = (A + \sigma I)\, C^{-1} \tag{2.8}$$

if rank $C = n = p$, and non-uniquely by

$$D = (A + \sigma I)\, (C^T C)^{-1}\, C^T \tag{2.9}$$

if rank $C = n < p$.

To prove that this choice of D satisfies condition (1) of detectability, a result from linear systems theory will be used. When the failure associated with event vector $\mathbf{f}$ occurs, the state error in (2.6) will be driven by $\mathbf{f}\,\eta(t)$ within a subspace of R^n called the controllable space of $\mathbf{f}$. This subspace is given by the range space of the matrix W_f defined as

$$W_f = \begin{bmatrix} f & (A - DC)f & \cdots & (A - DC)^{n-1}f \end{bmatrix} \tag{2.10}$$

Since $\epsilon = C\,e$, the output error will lie in a subspace of R^p given by the range space of the matrix CW_f.

For this choice of matrix D, the matrix CW_f becomes

$$CW_f = \begin{bmatrix} Cf & -\sigma Cf & \sigma^2 Cf & \cdots & (-\sigma)^{n-1}Cf \end{bmatrix}$$

and the range space of CW_f is simply the one-dimensional space spanned by the vector Cf. Therefore, when the failure occurs, the output error will remain in a single direction given by the vector Cf. Hence, the gain matrix D given by (2.8) or (2.9) also satisfies condition (1) of detectability. Any matrix D which satisfies this condition is called a **detector gain** for f.

From the preceding proof, note that this choice of D (2.8) or (2.9) is a **detector gain** for any event vector f in R^n. This implies that a single detection filter can be used to detect and identify every failure associated with every event vector f in R^n (except that it wouldn't be able to identify two failures that have the same event vector f).

The solution of the **failure detection filter** problem in the case of fully measurable systems is trivial. Choosing $(A - DC) = -\sigma I$ assured the stability of the filter and also produced unidirectional output errors in the event of component failures.

2.3 Partially Measurable Systems

In a **partially measurable system** rk C $< n$ and therefore, the state vector $\mathbf{x}(t)$ cannot be solved uniquely given the measurements $\mathbf{y}(t)$. In the previous section it was shown that when a system is **fully measurable**, a single detection filter can be designed to detect and identify every event **f** in R^n. This property is lost when the system is partially measurable, and more than one detection filter may be needed to detect a given set of failure events. Moreover, in such detection filters, there are subspaces of R^n containing event vectors that produce the same unidirectional output. These subspaces are called **Detection Spaces** and are very important in the analysis and design of detection filters, for both single and multiple detection.

2.3.1 Single Failure Detection

This section explores the detection problem for a single failure event. The definition of **detection space** is introduced and is later used to prove the **detection theorem**. Algorithms for the design of detection filters, based on the proof of the detection theorem, are then discussed.

2.3.1.1 The Detection Space

Assuming that (A,C) is an observable pair, Jones defines the **detection space** for the event **f** in the following way:

Definition 2.3-1 Assume that Cf is not zero. The **detection space** for **f** is denoted by $\underline{R}_f$ and is the direct sum:

$$\text{i) } \underline{R}_f = \mathbf{f} \oplus R_f$$

where $R_f \subset R^n$ is the largest subspace which satisfies the two

conditions:

ii) $R_f \subset \eta(C)$

iii) $A\,R_f \subset \underline{R}_f$

This definition is motivated by condition (1) of detectability, and serves to derive a formula to generate **detector gains**. By condition ii) and iii) of Definition 2.3-1:

$$(A - DC)\,R_f \subset A\,R_f \subset \underline{R}_f$$

$$(A - DC)\,R_f \subset \underline{R}_f \tag{2.11}$$

Assuming that $Cf \neq 0$, condition i) and ii) imply that:

$$C\,\underline{R}_f = Cf \oplus C\,R_f = Cf \oplus 0 = Cf$$

$$\dim\left(C\,\underline{R}_f\right) = \dim\left(Cf\right) = 1 \tag{2.12}$$

Now, assume that D is chosen such that:

$$(A - DC)\,f = \xi \in \underline{R}_f \tag{2.13}$$

for some arbitrary ξ in $\underline{R}_f$. From (2.11), (2.13) and i), it follows that $\underline{R}_f$ is an **invariant space** with respect to (A - DC) for this choice of D since:

$$(A - DC)\,\underline{R}_f = (A - DC)\,(f \oplus R_f) \subset \underline{R}_f$$

$$(A - DC)\,\underline{R}_f \subset \underline{R}_f \tag{2.14}$$

Since $\underline{R}_f$ contains the event vector f, and since $\underline{R}_f$ is invariant with respect to (A - DC) (for this choice of D), the controllable space of f, spanned by the columns of the matrix W_f defined in (2.10), is a subspace of $\underline{R}_f$:

$$C_f \subset \underline{R}_f \tag{2.15}$$

where C_f is the controllable space of **f**.

Then, from (2.12) and (2.15):

$$CC_f = Cf \tag{2.16}$$

$$\dim (CC_f) = 1$$

and the failure associated with **f** generates unidirectional output errors along **Cf**. Therefore, the gain matrix D chosen in (2.13) is a **detector gain**. Moreover, by the same argument that led to (2.16) and since (A - DC,C) is an observable pair, any event vector in $\underline{R}_f$ produces the same unidirectional output **Cf**. Jones [5] calls this property **detection equivalence** and proved that the detection space $\underline{R}_f$ contains **all** the event vectors that are **detection equivalent** to **f**.

Since, as it was proved, the gain D satisfying (2.13) is a detector gain, this equation can be solved for D to obtain an expression for the **detector gain** of **f**.

Equation (2.13) can be written as:

$$D\,Cf = A\,f - \xi \tag{2.17}$$

where $\xi \in \underline{R}_f$, and its solution is

$$D = D_p + D_H$$

where

$$D_p = (A\,f - \xi)\,[(Cf_j)^T\,Cf]^{-1}\,(Cf)^T \tag{2.18}$$

$$D_H = D' \left[I - Cf\,[\,(Cf)^T\,Cf]^{-1}\,(Cf)^T \right]$$

with $\xi \in \underline{R}_f$ and D' an arbitrary matrix with the same dimension as D.

The **detector gain** of **f** is given by (2.18) with any $\xi \in \underline{R}_f$ and arbitrary D' The eigenvalues of (A - DC) will depend on the choice if $\xi \in \underline{R}_f$ and D', and the question is whether **all** the eigenvalues of (A - DC) can be arbitrarily specified by the proper choice of $\xi \in \underline{R}_f$ and D'. This question is addressed in the next section.

Up to this point, it has been assumed that $\mathbf{Cf} \neq \mathbf{0}$. If $\mathbf{Cf} = \mathbf{0}$, it can be shown that the definition of detection space and all the results derived so far, can be extended by replacing **f** by $\mathbf{A^u f}$, where $u \geq 0$ is the smallest integer, such that $\mathbf{CA^u f} \neq \mathbf{0}$. To simplify the analysis, it will be assumed for the rest of this chapter that $\mathbf{Cf} \neq \mathbf{0}$.

2.3.1.2 Detection Theorem

In this section, it will be shown that the freedom represented by the choice of $\xi \in \underline{R}_f$ and D' in equation (2.18) is enough to assign **all** the eigenvalues of (A - DC) arbitrarily.

First, a theorem proved by Beard and Jones is stated.

Theorem 2.3.1 Let dim $(\underline{R}_f) = \upsilon_f$. There exists a unique vector $\mathbf{g} \in \underline{R}_f$, called the **detection generator** of $\underline{R}_f$, such that:

i) $\mathbf{A^k g} \in \mathbf{R_f} \quad \mathbf{k} = 0, 1, 2, \ldots, (\upsilon_f - 2)$

ii) $\mathbf{C\, A^{\upsilon_f - 1}\, g} = \mathbf{Cf}$

This theorem implies that the vectors $\mathbf{g}, \mathbf{A\,g}, \ldots, \mathbf{A^{\upsilon_f - 1}\, g}$ are a basis for $\underline{R}_f$. Since $\mathbf{f} \in \underline{R}_f$, **f** can be expressed as

$$\mathbf{f} = \alpha_1 \mathbf{g} + \alpha_2 \mathbf{A\,g} + \ldots + \alpha_{\upsilon_f - 1} \mathbf{A^{\upsilon_f - 2}\, g} + \mathbf{A^{\upsilon_f - 1}\, g} \qquad (2.19)$$

where $\alpha_{\nu_f} = 1$ by ii).

Also, since $\xi \in \underline{R}_f$, ξ can be written as

$$\xi = a_1 \mathbf{g} + a_2 A \mathbf{g} + \ldots + a_{\nu_f} A^{\nu_f - 1} \mathbf{g} \tag{2.20}$$

Write (2.13) as

$$D\,Cf = A\,\mathbf{f} - \xi \tag{2.21}$$

and use (2.19) and (2.20) to get

$$A\,\mathbf{f} - \xi = -a_1 \mathbf{g} + (\alpha_1 - a_2)\, A \mathbf{g} + (\alpha_2 - a_3) A^2 \mathbf{g} + \ldots$$
$$\ldots + (\alpha_{\nu_f - 1} - a_{\nu_f}) A^{\nu_f - 1} \mathbf{g} + A^{\nu_f} \mathbf{g} \tag{2.22}$$

Define $p_1 = -a_1$, $p_2 = \alpha_1 - a_2, \ldots, p_{\nu_f} = \alpha_{\nu_f - 1} - a_{\nu_f}$, and write (2.22) as

$$A\,\mathbf{f} - \xi = p_1 \mathbf{g} + p_2 A \mathbf{g} + \ldots + p_{\nu_f} A^{\nu_f - 1} \mathbf{g} + A^{\nu_f} \mathbf{g} \tag{2.23}$$

Equation (2.21) can now be written as

$$D\,Cf = p_1 \mathbf{g} + \ldots + p_{\nu_f} A^{\nu_f - 1} \mathbf{g} + A^{\nu_f} \mathbf{g} \tag{2.24}$$

It is easy to prove, using Theorem 2.3.1, that

$$A^k \mathbf{g} = (A - DC)^k \mathbf{g} \qquad \text{for } 0 \leq k < \nu_f \tag{2.25}$$

Therefore, (2.24) can be expressed as

$$0 = p_1 \mathbf{g} + p_2 (A - DC) \mathbf{g} + \ldots + p_{\nu_f} (A - DC)^{\nu_f - 1} \mathbf{g} + A^{\nu_f} \mathbf{g} - D\,Cf$$

and, since $Cf = C\,A^{\nu_f - 1} \mathbf{g}$, using (2.25) we get

$$0 = p_1 \mathbf{g} + p_2 (A - DC) \mathbf{g} + \ldots + p_{\nu_f} (A - DC)^{\nu_f - 1} \mathbf{g} + (A - DC)^{\nu_f} \mathbf{g} \tag{2.26}$$

Write (2.26) as

$$\psi(A - DC)\, g = 0$$

where the polynomial $\psi(\cdot)$ is defined

$$\psi(\gamma) = p_1 + p_2\,\gamma + \ldots + p_{\upsilon_f}\,\gamma^{\upsilon_f - 1} + \gamma^{\upsilon_f}$$

The polynomial $\psi(\cdot)$ is the minimal **annihilating polynomial** of **g** with respect to (A - DC) (5). Therefore, the eigenvalues of (A - DC) associated with the detection space $\underline{R}_f$ are given by the roots of

$$\psi(\lambda) = 0$$

or

$$p_1 + p_2\,\lambda + \ldots + p_{\upsilon_f}\,\lambda^{\upsilon_f - 1} + \lambda^{\upsilon_f} = 0 \qquad (2.27)$$

For each set of eigenvalues of (A - DC) associated with $\underline{R}_f$, there is a unique set of coefficients $p_1, p_2, \ldots, p_{\upsilon_f}$ a unique set of coefficients $a_1, a_2, \ldots, a_{\upsilon_f}$ and, therefore, there is a unique $\xi \in \underline{R}_f$. Hence, the υ_f detection space eigenvalues of (A - DC) can be assigned **arbitrarily** by the proper choice of $\xi \in \underline{R}_f$ in (2.18). Condition ii) of detectability will be satisfied only if the remaining $n - \upsilon_f$ eigenvalues can be assigned arbitrarily by choice of D' in (2.18).

By replacing D from (2.18) into (A-DC) get

$$A - DC = A' - D'C'$$

where

$$A' = A - D_p C$$

and

$$C' = \left[I - Cf \left[(Cf)^T Cf \right]^{-1} (Cf)^T \right] C \tag{2.28}$$

Matrix D from (2.18) makes $\underline{R}_f$ invariant with respect to (A - DC) and (A'-D'C'). Since D' is an arbitrary matrix, $\underline{R}_f$ is also invariant with respect to A':

$$A' \underline{R}_f \subset \underline{R}_f \tag{2.29}$$

Since:

$$C' \underline{R}_f = C' (f \oplus R_f) = C'f \oplus C'R_f = 0$$

the detection space $\underline{R}_f$ is in the null space of C':

$$\underline{R}_f \subset \eta(C') \tag{2.30}$$

From (2.29) and (2.30), it can be concluded that the detection space $\underline{R}_f$ is a subspace of the unobservable space of the (A', C') pair:

$$\underline{R}_f \subset \eta(M) \tag{2.31}$$

where M is defined as

$$M = \begin{bmatrix} C' \\ C'A' \\ \vdots \\ C'A'^{n-1} \end{bmatrix}$$

Since:

$$C' \eta(M) = 0$$

using equation (2.28) get

$$C\,\eta(M) = Cf \tag{2.32}$$

But since $\eta(M)$ is an invariant space with respect to A' and to (A - DC), equation (2.32) implies that

$$\eta(M) \subset \underline{R}_f \tag{2.33}$$

Hence, by (2.31) and (2.33):

$$\underline{R}_f = \eta(M) \tag{2.34}$$

Given an unobservable pair (A', C'), the theory of linear systems says that all of the eigenvalues of (A' - D'C') can be placed arbitrarily by choice of D' **except** those eigenvalues associated with the unobservable space of (A', C'), which are fixed. But since the unobservable space of (A', C') is the detection space of $\underline{R}_f$, the fixed eigenvalues of (A' - D'C') are the υ_f eigenvalues associated with $\underline{R}_f$, and were assigned by the choice of $\xi \in \underline{R}_f$ in (2.18). Therefore, the matrix D' in (2.18)) assigns arbitrarily the remaining $n - \upsilon_f$ eigenvalues of (A - DC) and condition ii) of detectability is satisfied.

The results of this section are summarized with the statement of the **Detectability Theorem**.

Theorem 2.3.2 Every vector in the state space R^n is detectable if and only if (A,C) is observable.

2.3.1.3 Algorithms

The algorithms presented in this section are based on the proof of the **detectability theorem**, and were suggested by Beard (1).

(1) Detection Space Algorithm

This algorithm is used to obtain the detection space $\underline{R}_f$ and its dimension υ_f of the event **f**. From (2.34), the detection space $\underline{R}_f$ is in the null space of the matrix M defined in (2.31). The matrices C' and A' present in this definition were introduced in (2.28), where C' depends only on **f** and A' is a function of D_p. The detector gain D_p is defined in (2.18) for any $\xi \in \underline{R}_f$. Therefore, the detection space $\underline{R}_f$ is in the null space of any M that results from any choice of $\xi \in \underline{R}_f$ in (2.18). Since, from definition(2.3-1), the only vectors ξ known to be in $\underline{R}_f$ are the ones in the subspace spanned by **f**, the vector $\xi = \mathbf{0} \in \underline{R}_f$ is chosen and the A' resulting from this choice is called K_f:

$$K_f = A - A\,\mathbf{f}\,[(C\mathbf{f})^T\,C\mathbf{f}]^{-1}\,(C\mathbf{f})^T\,C \tag{2.35}$$

Hence the algorithm to obtain $\underline{R}_f$ and υ_f is

$$\underline{R}_f = \eta(M_f)$$

$$\upsilon_f = n - \text{rank } M_f$$

where

$$M_f = \begin{bmatrix} C' \\ C'K_f \\ \vdots \\ C'K_f^{n-1} \end{bmatrix} \tag{2.36}$$

with C' given by (2.28) and K_f by (2.35).

(2) Detection Gain Algorithms

These algorithms perform the actual detection filter design. They calculate the gain matrix D that satisfies condition i) of detectability, and assigns the matrix (A - DC) the desired eigenvalues.

The gain D given by equation (2.18) is a detector gain, and therefore satisfies condition i) of detectability. The choice of $\xi \in \underline{R}_f$ assigns the υ_f eigenvalues of (A - DC) associated with $\underline{R}_f$, and the choice of D' assigns the remaining n - υ_f eigenvalues associated with the completion of the state space R^n.

(a) D_p Algorithm

This algorithm calculates D_p in (2.18) given a specified set of υ_f eigenvalues to be assigned to (A - DC), and that will be associated with $\underline{R}_f$. If the υ_f eigenvalues are specified as the roots of the polynomial

$$s^{\upsilon_f} + p_{\upsilon_f}\, s^{\upsilon_f - 1} + \ldots + p_2\, s + p_1 = 0$$

then, as it was proved, the matrix (A **f** - ξ) must satisfy equation (2.23). Hence, by substituting (2.23) into (2.18) get

$$D_p = \mathbf{q}\,[(C\mathbf{f})^T\, C\mathbf{f}]^{-1}\,(C\mathbf{f})^T \tag{2.37}$$

where

$$\mathbf{q} = p_1\,\mathbf{g} + p_2\,A\,\mathbf{g} + \ldots + p_{\upsilon_f}\,A^{\upsilon_f - 1}\,\mathbf{g} + A^{\upsilon_f}\,\mathbf{g}$$

The detection generator **g** can be found by first using algorithm 1) to obtain the detection space $\underline{R}_f$ and then apply the property of **g** stated in Theorem 2.3.1 to get $\mathbf{g} \in \underline{R}_f$. A convenient way of executing these two steps is using orthogonal reduction, as suggested by Beard [1].

Once **g** is obtained, the matrix D_p is simply calculated using (2.37) and is unique for a given set of υ_f eigenvalues.

(b) D_H Algorithm

This algorithm assigns the remaining n - υ_f eigenvalues of (A - DC) by

choosing the appropriate D' in (2.18) to calculate D_H. These $n - \upsilon_f$ eigenvalues are associated with the **completion** of the state space R^n, and their specifications do not determine a unique D' (and a unique D_H and D). Therefore, given an event **f** and a complete set of eigenvalues to be assigned to (A - DC), the solution of the detection problem will not be unique. For simplicity, the algorithm presented here is based on the same procedure used to assign the eigenvalues to $\underline{R}_f$ and obtain D_p. For this reason, this algorithm adds certain constraints to the detection problem and generates a **unique** D_H that together with D_p give a **unique** gain D as the solution of the detector problem.

The matrix D_H is given by (2.18), where D' can be considered as the gain matrix of the system (A', C'):

$$A - DC = A' - D'C'$$

with A' and C' given by (2.28).

Beard showed that there are a set of vectors $\mathbf{w}_i$ that have the same property with respect to (A', C') as the detection generator **g** with respect to (A, C):

$$C'A'^{\rho}\,\mathbf{w}_j = 0 \qquad \text{for } 0 \leq \rho < q_j - 1$$

$$C'A'^{q_j-1}\,\mathbf{w}_j \neq 0$$

There are (rank C - # of events) of these vectors. They and the corresponding q_j can be obtained as a byproduct, when applying orthogonal reduction to find the null space of M in (2.31) or M_f in (2.36) (Beard showed that M $= M_f$).

The vectors $\mathbf{w}_j$, $A'\mathbf{w}_j$, . . . , $A'^{q_j-1}\,\mathbf{w}_j$ span a subspace called **completion space** $\underline{C}_j$. These spaces are the equivalent of $\underline{R}_f$ to (A', C'). It can be shown that

the spaces $\underline{R}_f$, $\underline{C}_1$, $\underline{C}_2$, . . . , $\underline{C}_l$ are all nonintersecting and

$$R^n = \underline{R}_f \oplus \underline{C}_1 \oplus \underline{C}_2 \oplus \ldots \oplus \underline{C}_l \tag{2.38}$$

where

$$\underline{C}_i \cap \underline{C}_j = 0 \ , \ i \neq j$$

$$\underline{R}_f \cap \underline{C}_j = 0$$

and

$$\sum_{j=1}^{l} q_j = n - \upsilon_f$$

This algorithm assigns q_j eigenvalues to (A' - D'C') by making $\underline{C}_j$ an **invariant** space with respect to (A' - D'C'). Therefore, the same algorithm used to find D_p is used to get D'. Equation (2.37) is modified by substituting A' for A, $\mathbf{w}_i$ for **g** and $C'A'^{q_i-1}\mathbf{w}_i$ for **f**. Hence, the D' that makes all $\underline{C}_j$ invariant and assigns the remaining $n - \upsilon_f$ eigenvalues of (A'-D'C'), is given by

$$D' = \Psi \left[(C' W)^T C' W \right]^{-1} (C' W)^T \tag{2.39}$$

where

$$\Psi = \left[\psi_1 , \psi_2 , \ldots , \psi_l \right]$$

$$\psi_j = p_1^j \mathbf{w}_j + \ldots + p_{q_j}^j A'^{q_j-1} \mathbf{w}_j + A'^{q_j} \mathbf{w}_j$$

$$W = \left[A'^{q_1-1} \mathbf{w}_1 , \ldots , A'^{q_l-1} \mathbf{w}_l \right]$$

Beard showed that W can also be calculated as

$$W = \left[K_f^{q_1-1} \mathbf{w}_1 , \ldots , K_f^{q_l-1} \mathbf{w}_l \right]$$

where K_f is defined in (2.35).

2.3.2 Multiple Failure Detection

This section deals with the problem of designing a **single** detection filter to detect a **set** of failure events $\{\mathbf{f}_1 \ldots \mathbf{f}_r\}$. This set of events is **mutually detectable** by a single detection filter, if there exists a D that satisfies the conditions of detectability for all the $\mathbf{f}_i$. For single failure detection, if (A,C) is an observable pair, any event $\mathbf{f} \in R^n$ is detectable. But for multiple failure detection, complete observability is not a sufficient condition. The **Group Detection Theorem** states a necessary and sufficient condition for a set of **output separable** vectors, as defined below, to be mutually detectable.

Definition: The vectors $\{\mathbf{f}_1 \ldots \mathbf{f}_r\}$ are **output separable** if

$$\text{rk } CF = r$$

where

$$F = \left[A^{u_1} \mathbf{f}_1 , \ldots , A^{u_r} \mathbf{f}_r \right] \tag{2.40}$$

with $u_i \geq 0$ defined as the smallest integer, such that $CA^{u_i} \mathbf{f}_i \neq 0$.

It can be shown that if the set of events are output separable

$$\underline{R}_{f_i} \cap \underline{R}_{f_j} = 0 \ , \ i \neq j \tag{2.41}$$

Before stating the Group Detection Theorem, the following definition is necessary.

Definition: The **group detection order** of the set $\{\mathbf{f}_1 \ldots \mathbf{f}_r\}$ is defined as the dimension of the null space of M_F, (n - rk M_F) where M_F is defined as M_f in

(2.36) with **f** replaced by F in C' and K_f.

Group Detection Theorem The output separable vectors $\{\mathbf{f}_1 \ldots \mathbf{f}_r\}$ are mutually detectable if and only if the sum of the individual detection orders of the set $\mathbf{f}_i$ is equal to the group detection order.

2.3.2.1 Algorithms

Given a set of event vectors $\{\mathbf{f}_1 \ldots \mathbf{f}_r\}$, the algorithm must first determine whether the events are **output separable** by using (2.40). If they are output separable, it must then determine whether they are **mutually detectable** by applying the **group detection theorem**.

If the events are **output separable** and **mutually detectable**, the procedure to calculate D is the same as the one described in the previous section for single failure detection, but with **f** replaced by F.

$$D = D_p + D_H$$

where

$$D_p = Q\,[(CF)^T\,CF]^{-1}\,(CF)^T \tag{2.42}$$

with

$$Q = \left[\, \mathbf{q}_1 , \ldots , \mathbf{q}_r \,\right]$$

$$\mathbf{q}_i = p_1^i\,\mathbf{g}_i + \ldots + p_{\upsilon_i}^i\,A^{\upsilon_i - 1}\,\mathbf{g}_i + A^{\upsilon_i}\,\mathbf{g}_i$$

where $\mathbf{g}_i$ and υ_i are the detection generator and detection order of the event $\mathbf{f}_i$.

$$D_H = D'\left[\, I - CF\,[(CF)^T\,CF]^{-1}\,(CF)^T \,\right]$$

where

$$D' = \Psi \left[(C'_F W)^T C'_F W \right]^{-1} (C'_F W)^T$$

with

$$W = \left[K^{q_1 - 1} \mathbf{w}_1, \ldots, K^{q_l - 1} \mathbf{w}_l \right]$$

and

$$\Psi = \left[\psi_1, \ldots, \psi_l \right]$$

$$\psi_j = p_1^j \mathbf{w}_j + \ldots + p_{q_j}^j A'^{q_j - 1} \mathbf{w}_j + A'^{q_j} \mathbf{w}_j$$

where C'_F and A' are defined in (2.28), with A' calculated using D_p in (2.42) and C'_F calculated using F in place of **f**.

Beard [1] shows a method to obtain the vectors $\mathbf{w}_j$ and the corresponding q_j, that consists of applying orthogonal reduction to find the null space of the matrix M_F.

Chapter 3
Dynamics of Flexible Space Structures

Flexible structures are characterized by very low natural damping and by infinitely dimensioned plant dynamics. The design of detection filters for flexible space structures must, therefore, be based on a reduced order model of the system. Moreover, the parameters of the reduced order model are not exactly known, and the effect of parameter errors and of unmodeled dynamics can be very serious.

In this thesis, the dynamics of a uniform flexible beam are used to analyze the performance of detection filters in the presence of model mismatch. The model of this flexible beam corresponds to an experimental beam that was assembled at NASA Langley Research Center. In this chapter, the model of the experimental beam will be described along with the design of detection filters for actuator failure events. The detection filter will then be evaluated with no model mismatch.

3.1 The Flexible Beam Model

The beam is made of aluminum (M = 0.502 slugs) and is twelve feet long with a 6" x 3/16" cross section [4]. It is equipped with four force actuators and four colocated displacement sensors (Fig. 3-1), that apply forces and measure displacement along the same direction in the vibration plane.

The partial differential equation that describes the dynamics of the undamped beam is

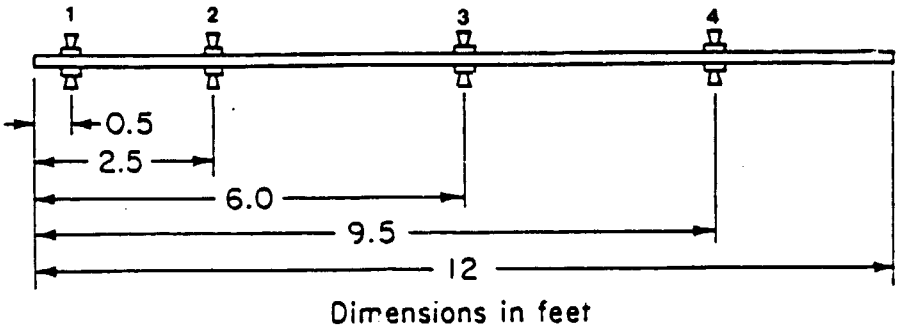

Mass = 0.5031 slugs

Figure 3-1: The Simulated Uniform Beam

$$E\,I\,\frac{\partial^4 y}{\partial \epsilon^4} + m\,\frac{\partial^2 y}{\partial t^2} = f(\epsilon\,,\,t) \tag{3.1}$$

where ϵ = position along the beam

y = displacement

E = modulus

m = mass per unit length

I = cross section inertia

f = distributed force per unit length

The distributed force $f(\epsilon\,,\,t)$ given by the four point actuators is

$$f(\epsilon\,,\,t) = \sum_{j=1}^{4} \delta(\epsilon - \epsilon_j)\,u_j(t) \tag{3.2}$$

where ϵ_j is the position of the *jth* actuator and $u_j(t)$ is the control being applied by it.

The solution of the partial differential equation is

$$y(\epsilon, t) = \sum_{i=1}^{\infty} \phi_i(\epsilon)\, \psi_i(t) \tag{3.3}$$

where $\phi_i(\epsilon)$ are the mode shapes and $\psi_i(t)$ are the modal amplitudes. The mode shapes $\phi_i(\epsilon)$ comprise an orthogonal and normalized set of functions over (0, l), and the modal amplitudes $\psi_i(t)$ satisfy an uncoupled set of differential equations

$$\frac{d^2\psi_i(t)}{dt^2} + \omega_i^2\, \psi_i(t) = \frac{1}{M} \sum_{j=1}^{4} \phi_i(\epsilon_j)\, u_j(t) \qquad i = 1, 2, \ldots \infty \tag{3.4}$$

where $M = m \times l$ is the mass of the beam and ω_i is the natural frequency of the *ith* mode.

The orthogonal mode shapes ϕ_i and the natural frequencies ω_i were obtained for the first ten modes at Langley, by performing a finite element analysis [4]. In Table (3-I) the natural frequencies and mode shape values at positions 0.5 ft., 2.5 ft., 6.0 ft., and 9.5 ft., are given for the first eight modes - two rigid body modes (translation and rotation) and the first six bending modes.

The *kth* sensor y_k is located at ϵ_k, and from equation (3.3)

$$y_k(t) = \sum_{i=1}^{\infty} \phi_i(\epsilon_k)\, \psi_i(t) \tag{3.5}$$

Equations (3.5) and (3.4) can be put into a state space representation by defining

Mode #	Modal frequency rad/sec	Mode shape values at x=0.5 ft	x=2.5 ft	x=6.0 ft	x=9.5 ft
1	0	1.000	1.000	1.000	1.000
2	0	-1.590	-1.010	0.000	1.010
3	11.418	-1.600	-0.123	1.210	-0.123
4	31.360	1.320	-0.876	0.000	0.876
5	61.258	1.040	-1.300	1.410	-1.300
6	100.900	-0.753	1.090	0.000	-1.090
7	150.185	-0.465	0.356	1.400	0.356
8	209.004	-0.181	-0.553	0.000	0.553

Table 3-I: Modal Frequencies and Normalized Mode Shapes (taken from reference [4])

the control vector

$$\mathbf{u}^T = [\, u_1 \;\; u_2 \;\; u_3 \;\; u_4 \,]$$

the measurement vector

$$\mathbf{y}^T = [\, y_1 \;\; y_2 \;\; y_3 \;\; y_4 \,]$$

and the state vector

$$\mathbf{x}^T = [\, \psi_1 \;\; \dot{\psi}_1 \;\; \psi_2 \;\; \dot{\psi}_2 \;\; \ldots \;\; \psi_N \;\; \dot{\psi}_N \,]$$

Then, the state space representation of the beam model is

$$\dot{\mathbf{x}}(t) = \mathrm{A}\,\mathbf{x}(t) + \mathrm{B}\,\mathbf{u}(t) \tag{3.6}$$

$$\mathbf{y}(t) = \mathrm{C}\,\mathbf{x}(t)$$

where

$$A = \begin{bmatrix} 0 & 1 & & & & \\ -\omega_1^2 & 0 & & & & \\ & & 0 & 1 & & \\ & & -\omega_2^2 & 0 & & \\ & & & & \ddots & \\ & & & & & \begin{matrix} 0 & 1 \\ -\omega_N^2 & 0 \end{matrix} \end{bmatrix}$$

$$B = \begin{bmatrix} 0 & 0 & 0 & 0 \\ \frac{1}{M}\phi_1(\epsilon_1) & \frac{1}{M}\phi_1(\epsilon_2) & \frac{1}{M}\phi_1(\epsilon_3) & \frac{1}{M}\phi_1(\epsilon_4) \\ 0 & 0 & 0 & 0 \\ \frac{1}{M}\phi_2(\epsilon_1) & \frac{1}{M}\phi_2(\epsilon_2) & \frac{1}{M}\phi_2(\epsilon_3) & \frac{1}{M}\phi_2(\epsilon_4) \\ \vdots & \vdots & \vdots & \vdots \\ 0 & 0 & 0 & 0 \\ \frac{1}{M}\phi_N(\epsilon_1) & \frac{1}{M}\phi_N(\epsilon_2) & \frac{1}{M}\phi_N(\epsilon_3) & \frac{1}{M}\phi_N(\epsilon_4) \end{bmatrix}$$

$$C = \begin{bmatrix} \phi_1(\epsilon_1) & 0 & \phi_2(\epsilon_1) & 0 & \cdot & \cdot & \cdot & \phi_N(\epsilon_1) & 0 \\ \phi_1(\epsilon_2) & 0 & \phi_2(\epsilon_2) & 0 & \cdot & \cdot & \cdot & \phi_N(\epsilon_2) & 0 \\ \phi_1(\epsilon_3) & 0 & \phi_2(\epsilon_3) & 0 & \cdot & \cdot & \cdot & \phi_N(\epsilon_3) & 0 \\ \phi_1(\epsilon_4) & 0 & \phi_2(\epsilon_4) & 0 & \cdot & \cdot & \cdot & \phi_N(\epsilon_4) & 0 \end{bmatrix}$$

where $\epsilon_1 = 0.5$ ft., $\epsilon_2 = 2.5$ ft., $\epsilon_3 = 6.0$ ft. and $\epsilon_4 = 9.5$ ft., and N is the number of modes included in the model.

The block diagonal structure of matrix A results from the zero coupling between the modes, which in turn, is due to the lack of damping in the beam. The structure of matrices B and C correspond to having force actuators and deflection sensors respectively. It is important to note that any flexible structure with negligible damping having force actuators and displacement sensors, will be described by a state model with matrices A, B and C of the same structure as the ones corresponding to the beam. Therefore, most of the results obtained in this thesis can be applied to most flexible space structures.

3.2 Filter Design for Actuator Failure Events

The actuator failure model was described in section 2.1 and is given by equation (2.5). The event vector $\mathbf{f}_j$ associated with the failure of actuator j is equal to $\mathbf{b}_j$, the *jth* column of matrix B:

$$\mathbf{f}_j = \mathbf{b}_j \qquad j = 1, 2, 3, 4$$

Let's first consider the design of a failure detection filter to detect and

identify the four actuator failure events. Applying the definition of output separability given in section 2.3.2, it was found that $u_j = 1$ and that the events { $\mathbf{f}_1, \mathbf{f}_2, \mathbf{f}_3, \mathbf{f}_4$ } are output separable if and only if the number of modeled modes N is equal to or larger than four: $N \geq 4$. The detection generator $\mathbf{g}_j$ corresponding to these events was found to be equal to $\mathbf{f}_j$, and the detection order equal to two for any $N \geq 1$:

$$\mathbf{g}_j = \mathbf{f}_j = \mathbf{b}_j \qquad j = 1, 2, 3, 4$$

$$\nu_j = 2$$

The number of completion spaces is (rank C - r) . Then, since rank C = 4 and r = 4, there are no completion spaces, and, therefore the group detection order is equal to 2 × N, the number of filter states. Moreover, since the sum of the individual detection orders ν_j is 8, it can be concluded from the group detection theorem that the events { $\mathbf{f}_1, \mathbf{f}_2, \mathbf{f}_3, \mathbf{f}_4$ } are mutually detectable if N = 4. If N > 4, the set of four actuator failure events will not be mutually detectable, but the set of any combination of up to three of these events will be.

A failure detection filter was designed to detect the failures of actuators number 3 and 4. The design was made using the algorithms of Chapter 2 and was based on a model of the beam containing the first 7 modes, resulting in a 14 state filter. This design produced a state space partitioned in this way:

$$R^{14} = \underline{R}_3 \oplus \underline{R}_4 \oplus \underline{C}_1 \oplus \underline{C}_2$$

where $\underline{R}_3$ and $\underline{R}_4$ are the two dimensional detection spaces corresponding to actuators number 3 and 4 respectively, and $\underline{C}_1$ and $\underline{C}_2$ are six and four dimensional completion spaces. In this first design, the 14 filter poles were rather arbitrarily placed at -10 rad/sec. This filter is named Detection Filter #1.

Detection Filter #1:

# of modes = 7

failure events = Actuators 3 and 4

Poles:

4 detection space poles at -10 rad/sec

10 completion space poles at -10 rad/sec

3.3 Computer Simulation

In all the computer simulations, the system and filter start with zero initial conditions at time 0 sec.. The controls applied by the actuators are randomly-chosen command forces uniformly distributed between -1 and 1 pound, and held constant during 1/32 seconds. The actuator failure occurs at t = 1 sec. and the failure mode chosen is **complete failure**, that is $u_j(t) = 0$ or equivalently, $\eta(t) = u_{c_j}(t)$ in equation (2.4).

The dynamics of the system and filter are simulated using a fifth order Runge-Kutta integration routine. The step size is chosen automatically by this routine, and is always smaller than 1/192 seconds. Therefore, since the period of the highest frequency mode being simulated is 1/33.2 seconds, the continuity of the system and filter dynamics is preserved.

The detection filter #1, described in the previous section, is first tested with **no model mismatch** (the evaluation model of the beam consists of the first 7 structural modes.) When the actuators are operating nominally, the output error is zero. When actuator 3 fails, the output error lies in the direction $CA^{u}3\ \mathbf{f}_3 = CA\mathbf{b}_3$, and when actuator 4 fails, it lies in the direction $CA^{u}4\ \mathbf{f}_4 = CA\mathbf{b}_4$ (since u_3

$= u_4 = 1.$) One way of reading this directionality information from the output, in order to identify the failed actuator, is by transforming the output space:

$$\mathbf{E}(t) = \mathrm{R}\ \epsilon(t) \tag{3.7}$$

where $\epsilon(t)$ is the four dimensional output error vector,

$$\mathbf{E}(t) = [\ \mathrm{E}_3\ \ \mathrm{E}_4\ ]^{\mathrm{T}}$$

is the two dimensional transformed output error vector, and

$$\mathrm{R} = [(\mathrm{CF})^{\mathrm{T}}\ \mathrm{CF}]^{-1}\ (\mathrm{CF})^{\mathrm{T}}$$

is the pseudoinverse (F is defined in section 2.3.2).

With no model mismatch and before the failure occurs, the output error $\epsilon(t)$ and transformed output error $\mathbf{E}(t)$ are both zero. When actuator 3 fails $\epsilon(t) = \mathrm{CA}\mathbf{b}_3\ \kappa(t)$, where $\kappa(t)$ is a scalar time function. Therefore,

$$\mathbf{E}(t) = \mathrm{R}\ \epsilon(t) = \mathrm{R}\ \mathrm{CA}\mathbf{b}_3\ \kappa(t)$$

and since $\mathrm{CA}\mathbf{b}_3 = \mathrm{CF} \begin{bmatrix} 1 \\ \\ 0 \end{bmatrix}$,

then

$$\mathbf{E}(t) = [(\mathrm{CF})^{\mathrm{T}}\ \mathrm{CF}\ ]^{-1}\ (\mathrm{CF})^{\mathrm{T}}\ \mathrm{CF} \begin{bmatrix} 1 \\ \\ 0 \end{bmatrix} \kappa(t)$$

and

$$\mathbf{E}(t) = \begin{bmatrix} 1 \\ \\ 0 \end{bmatrix} \kappa(t) \tag{3.8}$$

Hence, when actuator 3 fails, E_3 becomes nonzero and E_4 remains zero. In a similar way, it can be shown, when actuator 4 fails, E_4 becomes nonzero and E_3 remains zero.

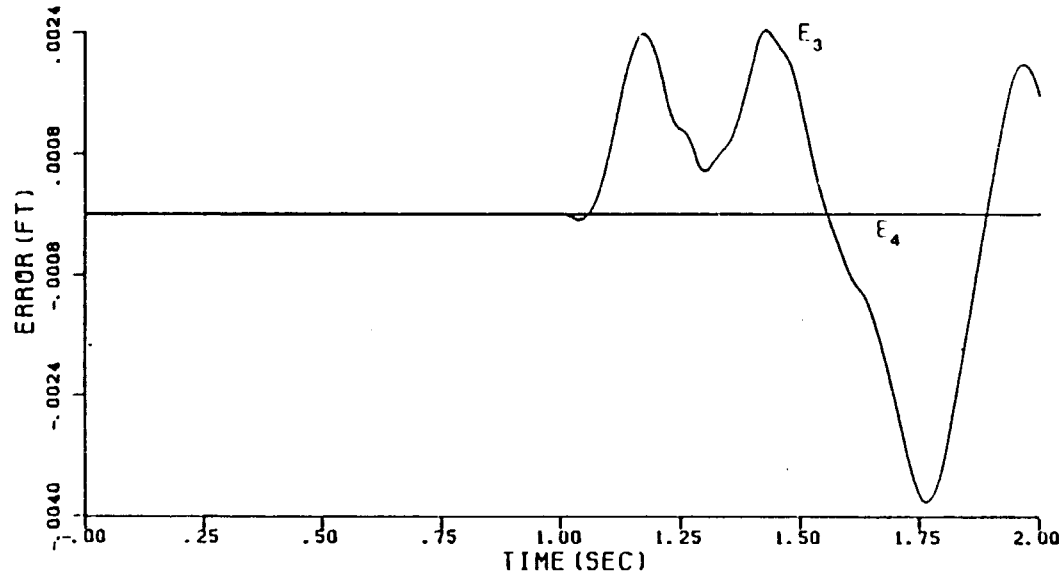

Figure 3-2: Detection Filter #1. No model mismatch.
Actuator 3 failure at T = 1 sec.

These results were verified with simulations. Figure 3-2 shows the transformed output error (E_3 and E_4) resulting from the simulation of the beam and detection filter #1 with **no model mismatch**, and with the failure of actuator number 3 at T = 1 sec.. The transformed output error is zero until T = 1 sec., at which point E_3 starts growing, clearly indicating the failure of actuator number 3. Figure 3-3 shows the results of the simulation with no model mismatch and with

failure of actuator number 4 at T = 1 sec..

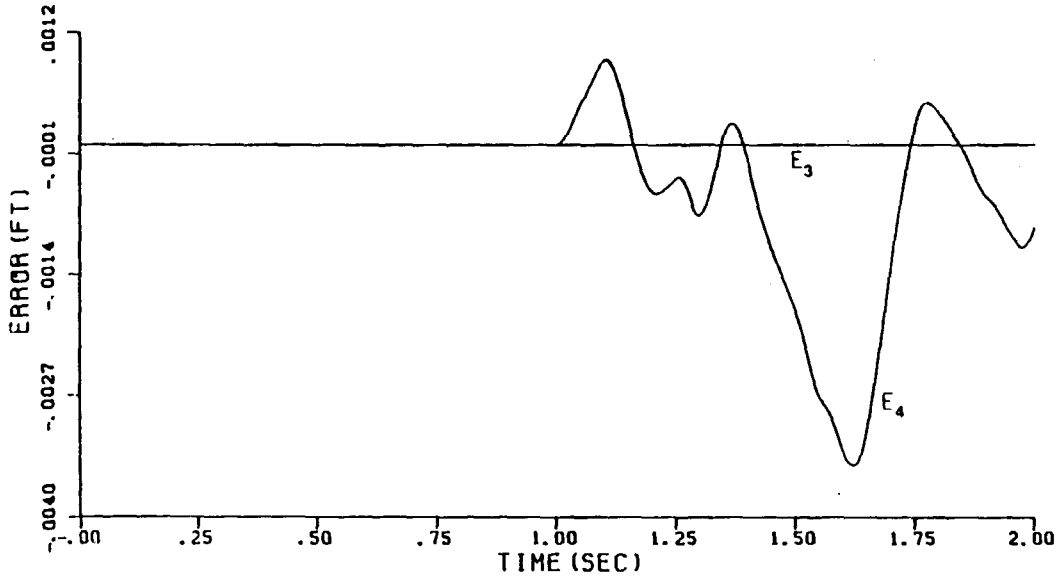

Figure 3-3: Detection Filter #1. No model mismatch.
Actuator 4 failure at T = 1 sec.

With no model mismatch, the detection filter #1 performed as expected, producing evident signatures at the output indicating the failure of actuator number 3 or 4. In the next chapter, the performance of this filter in the presence of model mismatch will be analyzed.

Chapter 4
Failure Detection with Model Mismatch

The best way of introducing the problem of failure detection in the presence of model mismatch, is by showing the results of the simulations of Detection Filter #1, introduced in the previous chapter, with mismatched evaluation models of the beam. Model mismatch occurs in two forms: **unmodeled dynamics** resulting from the truncation of the system model, and **parameter errors** in that portion of the system dynamics that is being modeled.

In the flexible beam, unmodeled dynamics take the form of unmodeled high frequency structural modes. Since the model of the flexible beam is essentially infinitely dimensioned, the design of the detection filter is based on a reduced order model of the beam. Then, those high frequency structural modes that have been truncated from the model are the unmodeled modes.

To test the performance of the detection filter in the presence of unmodeled modes, simulations are performed in which the evaluation model of the beam is of higher order than the model used in the filter design. For example, Detection Filter #1, based on a 7 mode model, is tested with an 8 mode evaluation model of the beam. Hence, in this simulation the eighth structural mode, with a frequency of 209.004 rad/sec., is the unmodeled mode. All the system modes, including the unmodeled one, are given zero initial conditions at $T = 0$ sec., and since the real physical beam has some damping, this is not an unrealistic assumption. Also, in order to highlight the effect of model mismatch, neither sensor noise nor disturbance is simulated throughout this thesis.

The result of the simulation of Detection Filter #1, with an 8 mode evaluation model of the system, and with failure of actuator 4 at T = 1 sec., is shown in Figure 4-1. The residual due to the unmodeled dynamics (the eighth structural mode) completely obscures the signature of the actuator failure (see also Fig. 3-3). Strikingly, this residual has a low frequency character rather than the frequency of the unmodeled bending mode.

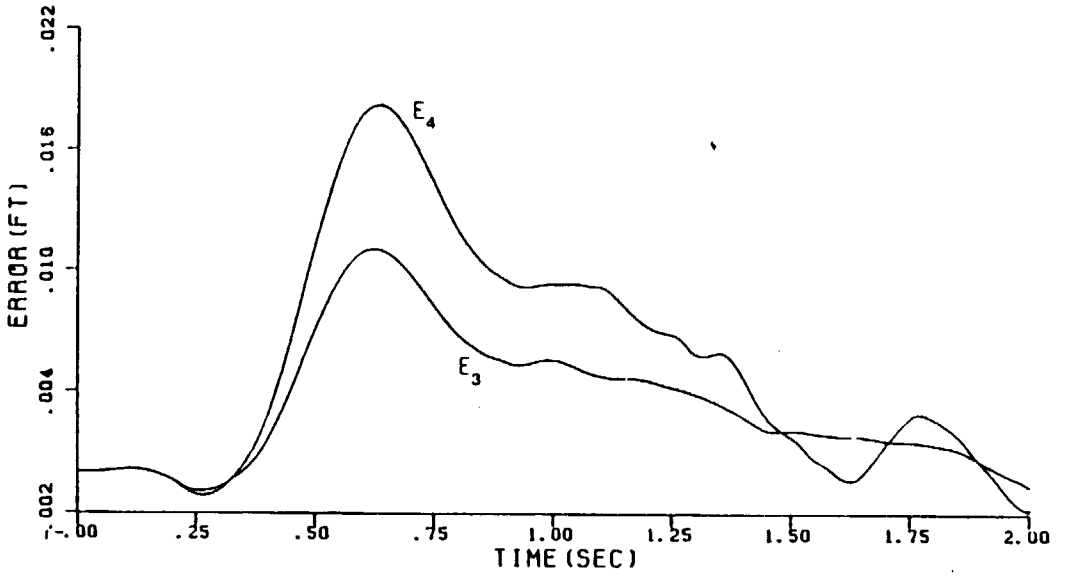

Figure 4-1: Detection Filter #1. Eighth Mode is Unmodeled. Actuator 4 Failure at T = 1 sec.

The parameter errors in the model of the flexible beam are the errors in the calculated values of the frequencies and shapes of the structural modes. That is, they are the errors in the figures of Table 3-I. Since the model frequencies and shapes depend on the physical characeristics of the beam, the errors in these quantities are correlated. However, when testing the performance of detection filters in the presence of parameter uncertainties percentage errors are introduced in the parameters of the evaluation model in a random manner with a uniform

distribution. For example, when considering parameter uncertainties of 5%, the percentage errors in the natural frequencies and shapes of the modes are uniformly distributed between -5% and +5%.

The errors in each of the matrices A, B and C, resulting from the errors in the knowledge of the modal frequencies and shapes, affect the performance of the detection filter in different ways. Therefore, in order to gain a better understanding of the problem, the detection filters are tested with parameter uncertainties in only one of the matrices A, B or C. In all cases, the detection filters are designed using the values of Table 3-I, and tested with parameter uncertainties by introducing errors in the matrices A, B and/or C of the evaluation model of the beam.

The result of the simulation of Detection Filter #1 with 0.05% parameter uncertainties in the system matrix A (modal frequencies), and with failure of actuator 4 at T = 1 sec., is shown in Fig. 4-2. Notice that the noise due to the parameter errors is larger than the failure signature, even though the level of parameter uncertainties is extremely low.

Figure 4-3 shows that the result of the simulation of Detection Filter #1 with 0.05% parameter uncertainties in the control matrix B, and with failure of actuator 4 at T = 1 sec.. The result of this simulation is even more surprising than the preceding ones. The residual due to errors smaller than 0.05% in the control matrix B, is of the same magnitude as the residual due to the complete failure of actuator 4 !

Finally, Fig. 4-4 shows the result of the simulation of Detection Filter #1 with 0.05% parameter uncertainties in the measurement matrix C, and with failure of actuator 4 at T = 1 sec.. It can be seen that the residual due to the parameter

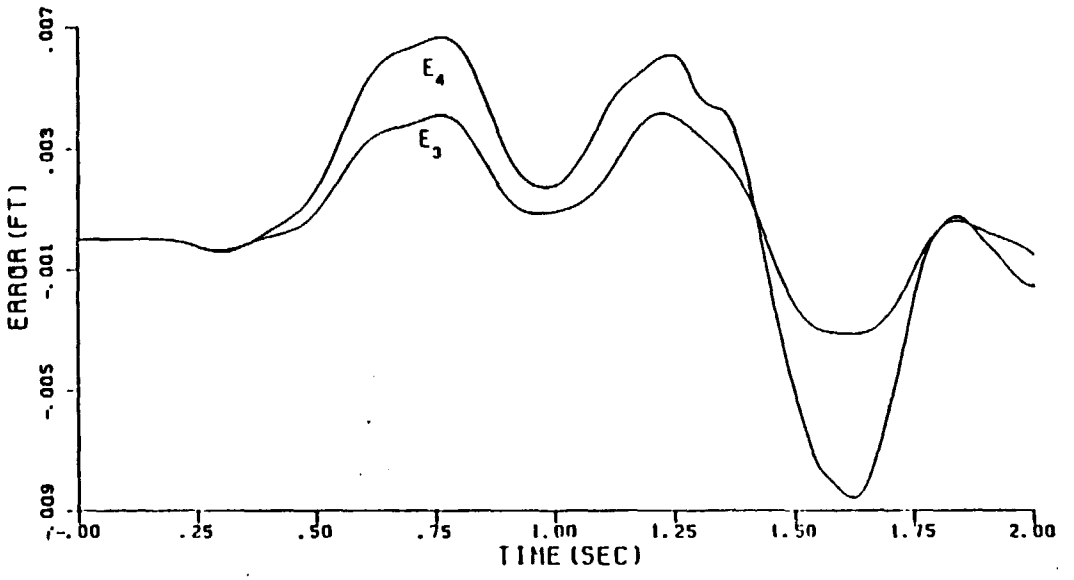

Figure 4-2: Detection Filter #1. Parameter Uncertainties in Matrix A = 0.05%. Actuator 4 Failure at T = 1 sec.

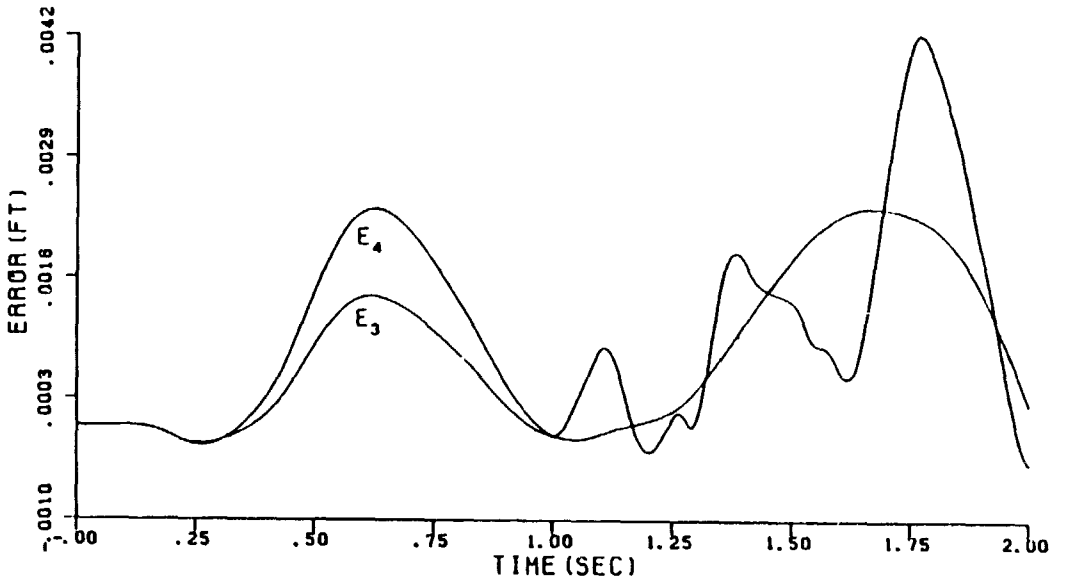

Figure 4-3: Detection Filter #1. Parameter Uncertainties in Matrix B = 0.05%. Actuator 4 Failure at T = 1 sec.

errors in matrix C, is two orders of magnitude larger than the failure signatures. In

addition, notice the very low frequency character of this residual. It seems so far that the errors in the measurement matrix C are the most critical ones.

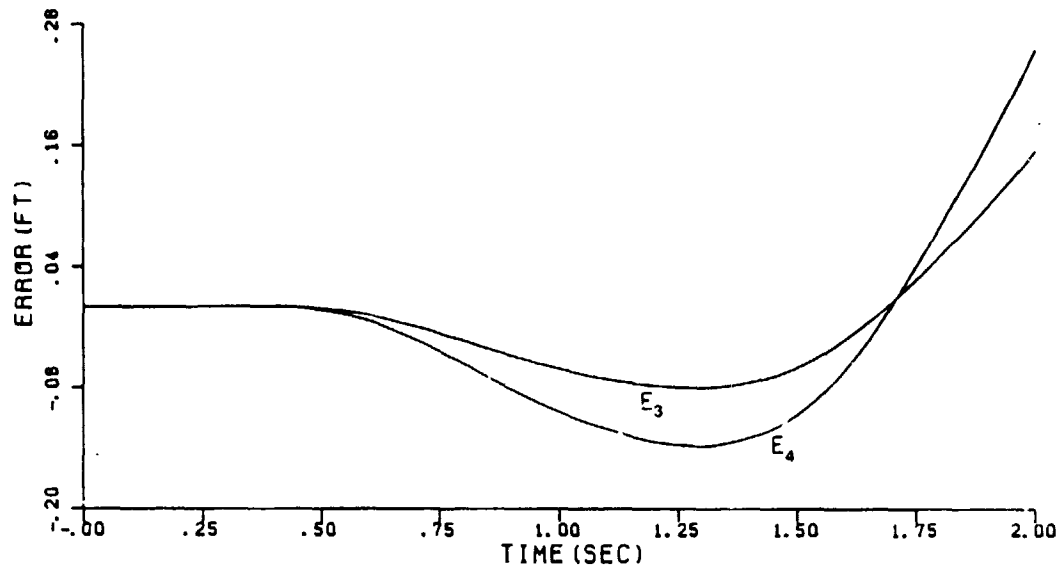

Figure 4-4: Detection Filter #1. Parameter Uncertainties in Matrix C = 0.05$^{c}_{c}$. Actuator 4 Failure at T = 1 sec.

Figures 4-1 through 4-4 dramatically illustrate the effects of model mismatch on the performance of the detection filter. Even with extremely low model uncertainties and high frequency unmodeled modes, the residual due to model errors makes the failure signature indistinguishable.

The objective in this chapter is to improve the visibility of the failure signature in the presence of model errors. To meet this objective, first the different dynamics associated with this problem are described. A frequency domain analysis that will lead to a more intelligent choice of the filter pole locations then follows. Finally, an approach to the design of robust detection filters based on low order models of the beam and output filtering, is presented.

4.1 Detection Filter Dynamics

In order to understand the reason for the poor results shown in Fig. 4-1 through 4-4, different aspects of the dynamics of detection filters are discussed in this section. Most of these results, however, are only valid when the plant is an undamped flexible structure, with a state model representation given by the matrices A, B and C described in Chapter 3.

4.1.1 Structural Mode Dynamics

The modal amplitude $\psi_i(t)$ of the *ith* mode, is given by equation (4.4) where the term to the right of the equal sign will be referred to as z_i. The block diagram corresponding to this equation is shown in Fig. 4-5

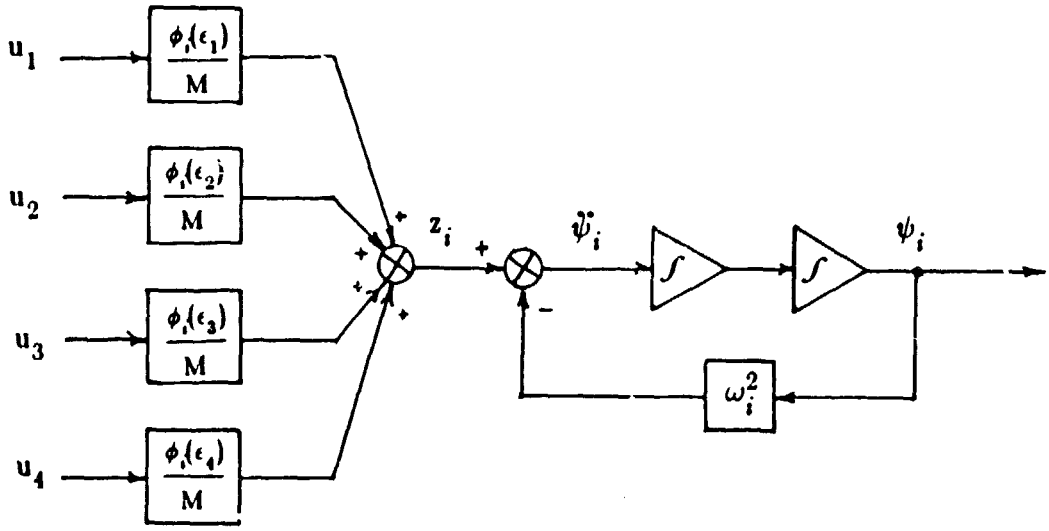

Figure 4-5: Structural Mode Dynamics

The transfer function from z_i to ψ_i is

$$T_i(s) = \frac{\psi_i(s)}{z_i(s)} = \frac{1}{s^2+\omega_i^2} \tag{4.1}$$

and the Bode plot of the frequency response $T_i(j\omega)$ is given in Fig. 4-6.

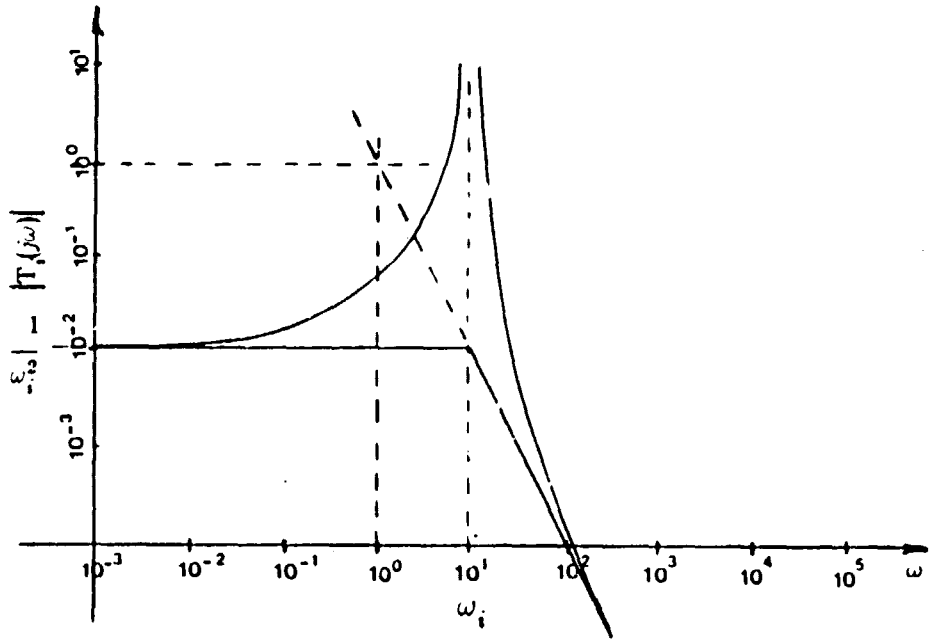

Figure 4-6: Modal Frequency Response

Note in Fig. 4-6, that the frequency response of the mode approaches $1/\omega_i^2$ as the frequency tends to zero.

4.1.2 Detection Space Dynamics

Given a detection filter configured to detect the failure event **f**, Beard showed that when event **f** occurs, the Laplace transform of the output error is:

$$\epsilon(s) = CA^u \mathbf{f}\ H(s)\ \eta(s) \tag{4.2}$$

$$H(s) = \frac{s^{\nu_f-u-1} + \alpha_{\nu_f-u-1}\ s^{\nu_f-u-2} + \ \ldots\ + \alpha_1}{s^{\nu_f} + p_{\nu_f}\ s^{\nu_f-1} + \ \ldots\ + p_1}$$

where the zeros of the denominator polynomial are the poles of the detection filter associated with the detection space $\underline{R}_f$, and the α_k's were defined in equation (2.19) .

From equation (4.2), it can be concluded that the transfer from $\eta(s)$ to $\epsilon(s)$ depends only on the dynamics associated with the detection space $\underline{R}_f$. This result is not surprising, since $\underline{R}_f$ is an invariant space and $\mathbf{f} \in \underline{R}_f$. Also note that while the designer has complete control over the denominator of H(s), by choosing the detection space poles, he cannot alter the numerator.

These results can be specialized to the problem of detecting the failure of an actuator in the flexible beam. It was found, for actuator failure events, that $u = 1$, $\nu_f = 2$ and $\mathbf{g} = \mathbf{f}$ (equivalently $\alpha_1 = 1$). In particular, for Detection Filter #1 (with all detection space poles at -10 rad/sec.) and complete failure of actuator 4 ($\eta(t) = u_4(t)$) equation (4.2) becomes

$$\epsilon(s) = CA\mathbf{b}_4 \; H_4(s) \; u_4(s) \tag{4.3}$$

where

$$H_4(s) = \frac{1}{s^2 + 20\,s + 100}$$

Moreover, since the transformed output error is

$$\mathbf{E}(s) = R\,\epsilon(s) = R\,CA\mathbf{b}_4 \; H_4(s)\,u_4(s)$$

and

$$R\,CAb_4 = \begin{bmatrix} 0 \\ 1 \end{bmatrix}$$

then

$$E_4(s) = H_4(s)\, u_4(s) \tag{4.4}$$

The Bode plot of the frequency response $H_4(j\omega)$, corresponding to Detection Filter #1, is given in Fig. 4-7.

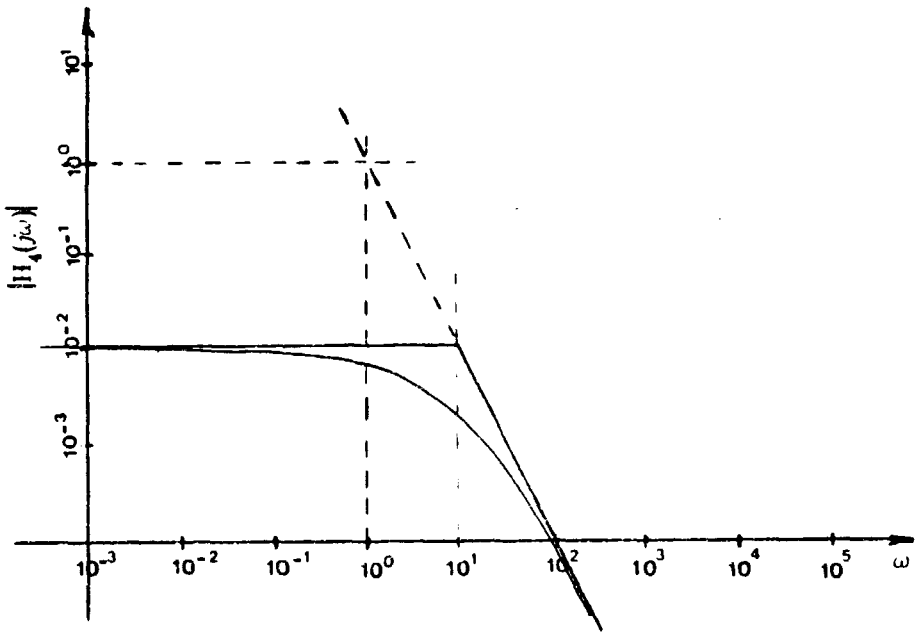

Figure 4-7: Detection Space Transfer

4.1.3 Model Error Dynamics

In this subsection, models for the different types of model mismatch are developed. These models are the basis for the frequency response analysis performed in the next section, that will help explain the very large residuals

produced by "very small" modeling errors.

In all the following cases of model mismatch, the state and output equations of the filter are the same as before, and for convenience are repeated here:

$$\dot{\hat{\mathbf{x}}}(t) = \mathrm{A}\,\hat{\mathbf{x}}(t) + \mathrm{B}\,\mathbf{u}_c(t) + \mathrm{D}\,[\,\mathbf{y}(t) - \hat{\mathbf{y}}(t)\,] \tag{4.5}$$

$$\hat{\mathbf{y}}(t) = \mathrm{C}\,\hat{\mathbf{x}}(t)$$

where the matrices A, B and C were defined in the previous chapter for N modes. First, the case in which the system has more than N modes (this will always be the case for flexible structures) is analyzed. Then, three cases are analyzed in which only one of the matrices A, B or C contain errors and the other two are exact. Finally, the real situation in which the three matrices contain errors is considered.

4.1.3.1 Unmodeled Modes

Suppose that N is the number of structural modes that are modeled in the design of the detection filter. Then, the state and output equations for the beam can be written as

$$\begin{bmatrix} \dot{\mathbf{x}} \\ \dot{\mathbf{x}}_u \end{bmatrix} = \begin{bmatrix} \mathrm{A} & 0 \\ 0 & \mathrm{A}_u \end{bmatrix} \begin{bmatrix} \mathbf{x} \\ \mathbf{x}_u \end{bmatrix} + \begin{bmatrix} \mathrm{B} \\ \mathrm{B}_u \end{bmatrix} \mathbf{u}$$

$$\mathbf{y} = \begin{bmatrix} \mathrm{C} & \mathrm{C}_u \end{bmatrix} \begin{bmatrix} \mathbf{x} \\ \mathbf{x}_u \end{bmatrix}$$

where the matrices A, B and C correspond to the modeled part of the system

dynamics, and A_u, B_u and C_u correspond to the unmodeled part. The state and output equations for the filter are exactly the same as before (Equation (4.5)). Therefore, the new state and output error equations are:

$$\dot{\mathbf{e}}(t) = (A - DC)\,\mathbf{e}(t) - DC_u\,\mathbf{x}_u(t)$$
$$\epsilon(t) = C\,\mathbf{e}(t) + C_u\,\mathbf{x}_u(t) \tag{4.6}$$

where

$$\dot{\mathbf{x}}_u(t) = A_u\,\mathbf{x}_u(t) + B_u\,\mathbf{u}(t)$$

The poles of the filter are still given by the eigenvalues of (A - DC), and therefore, the presence of unmodeled modes does not affect the stability of the filter. They do, however, impair the detecton capabilities of the filter, by generating a residual that obscures the failure signature.

For the sake of clarity, equation (4.6) is written as

$$\dot{\mathbf{e}}(t) = (A - DC)\;\mathbf{e}(t) - D\sum_{i=N+1}^{\infty} \mathbf{c}_i\,\psi_i(t) \tag{4.7}$$

where

$$\mathbf{c}_i = \begin{bmatrix} \phi_i(\epsilon_1) \\ \phi_i(\epsilon_2) \\ \phi_i(\epsilon_3) \\ \phi_i(\epsilon_4) \end{bmatrix}$$

and where $\psi_i(t)$ is the amplitude of an unmodeled mode.

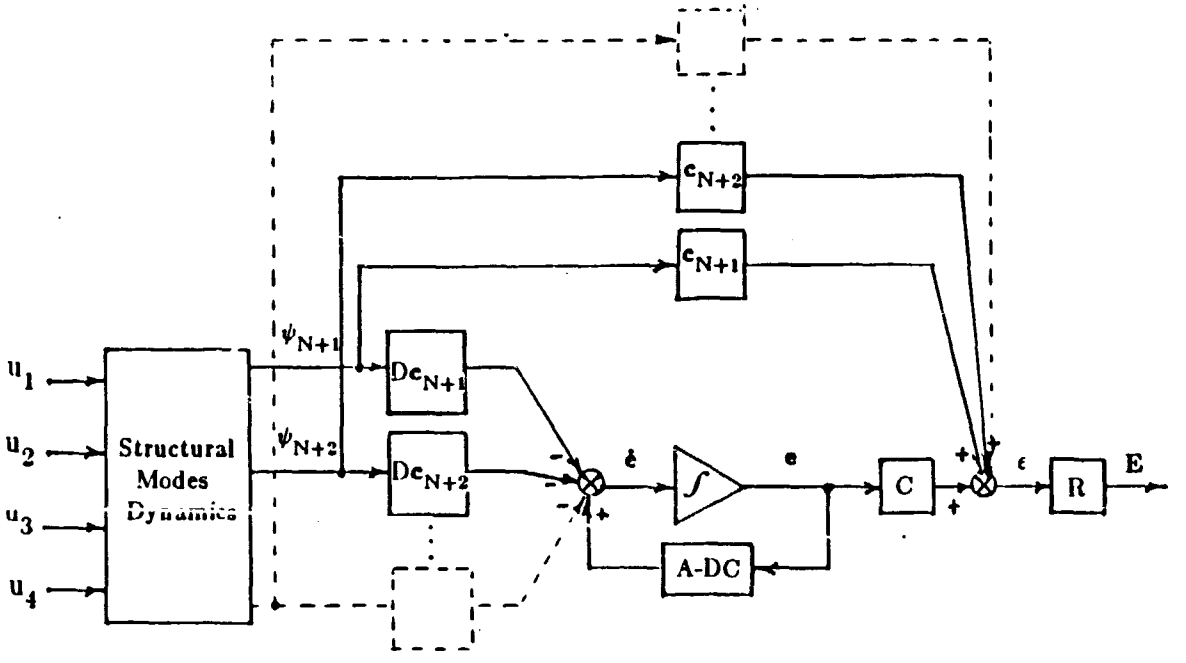

Figure 4-8: Unmodeled Modes Error Dynamics

Figure 4-8 shows a block diagram representation of equation (4.7). The actuators drive the unmodeled modes in the same way shown in the block diagram of Fig. 4-5. The unmodeled modes amplitudes ψ_{N+1}, ψ_{N+2}, . . . ,then generate an output residual through two different paths: a direct path through the vectors $\mathbf{c}_i$, and an indirect path by driving the state error equations through the "control vector" $\mathbf{Dc}_i$. Note that while the designer has no control over the direct path , he has "some" control on the indirect path by adjusting the filter pole locations with the gain matrix D. However, since D must be a detector gain, and is in both the feedback loop (A - DC) and the control vector $\mathbf{Dc}_i$, this is not a trivial problem.

4.1.3.2 Parameter Errors in A

The parameters of the system matrix A are the modal natural frequencies. The true modal frequencies are called ω_i^*, and the true system matrix is called A^*.

Hence, if ω_i and A are the modal frequencies and the system matrix used in the filter design, define:

$$\Delta\omega_i^2 = \omega_i^{*2} - \omega_i^2 \tag{4.8}$$

$$\Delta A = A^* - A$$

and, therefore,

$$\Delta A = \begin{bmatrix} 0 & 0 & 0 & 0 & \cdots & 0 & 0 \\ \Delta\omega_1^2 & \cdot & \cdot & \cdot & & \cdot & \cdot \\ 0 & \cdot & 0 & \cdot & & \cdot & \cdot \\ \cdot & \cdot & \Delta\omega_2^2 & \cdot & & \cdot & \cdot \\ \cdot & \cdot & 0 & \cdot & & \cdot & \cdot \\ \cdot & \cdot & \cdot & \cdot & & \cdot & \cdot \\ \cdot & \cdot & \cdot & \cdot & & \cdot & \cdot \\ \cdot & \cdot & \cdot & \cdot & & \cdot & \cdot \\ \cdot & \cdot & \cdot & \cdot & & 0 & \cdot \\ 0 & 0 & 0 & 0 & \cdots & \Delta\omega_N^2 & 0 \end{bmatrix}$$

Hence, the state and output equations for the system are now:

$$\dot{\mathbf{x}}(t) = (A + \Delta A)\,\mathbf{x}(t) + B\,\mathbf{u}(t)$$

$$\mathbf{y}(t) = C\,\mathbf{x}(t) \tag{4.9}$$

Combining these equations with the equations of the filter (Eq. (4.5)), the new state and output error equations are:

$$\dot{\mathbf{e}}(t) = (\mathrm{A} - \mathrm{DC})\,\mathbf{e}(t) + \Delta\mathrm{A}\,\mathbf{x}(t)$$

$$\epsilon(t) = \mathrm{C}\,\mathbf{e}(t) \tag{4.10}$$

These equations can also be written as:

$$\dot{\mathbf{e}}(t) = (\mathrm{A} - \mathrm{DC})\,\mathbf{e}(t) + \sum_{i=1}^{N} \Delta\mathbf{a}_i\,\psi_i(t)$$

$$\epsilon(t) = \mathrm{C}\,\mathbf{e}(t) \tag{4.11}$$

where

$$\Delta\mathbf{a}_i = \Delta\omega_i^2\ \hat{\mathbf{e}}_{N(2\times i)} = \begin{bmatrix} 0 \\ \cdot \\ \cdot \\ \cdot \\ 0 \\ \Delta\omega_i^2 \\ 0 \\ \cdot \\ \cdot \\ \cdot \\ 0 \end{bmatrix}$$

The block diagram representing the equation (4.11) is illustrated in Fig. 4-9.

From Eq. (4.11) or Fig. 4-9, notice that the modal amplitudes ψ_i drive the state error through the "control vector" $\Delta\mathbf{a}_i$, thus generating a residual at the output. This error model is similar to the error model for actuator failures, but with ψ_i and $\Delta\mathbf{a}_i$ in place of u_i and $\mathbf{b}_i$.

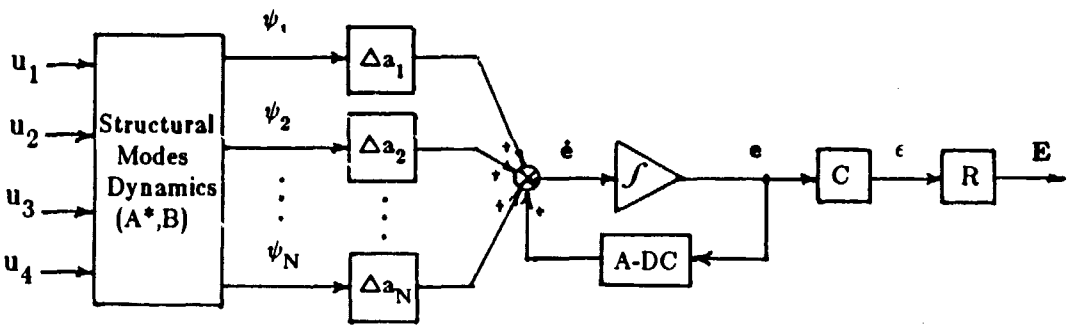

Figure 4-9: Error Dynamics for Model Error in A

4.1.3.3 Parameter Errors in B

The parameters of the control matrix B are the values of the mode shapes at the actuator locations. The true control matrix is B^*, and the control matrix used in the filter design is B. Define the difference between these two matrices as:

$$\Delta B = B^* - B$$

where

$$\Delta B = [\, \Delta \mathbf{b}_1 \;\; \Delta \mathbf{b}_2 \;\; \Delta \mathbf{b}_3 \;\; \Delta \mathbf{b}_4 \,]$$

Therefore, the system state and output equations are now:

$$\dot{\mathbf{x}}(t) = A\, \mathbf{x}(t) + (B + \Delta B)\, \mathbf{u}(t) \qquad (4.12)$$

$$\mathbf{y}(t) = \mathrm{C}\,\mathbf{x}(t)$$

and, combining them with the filter equations, get the new state and output error equations:

$$\begin{aligned} \dot{\mathbf{e}}(t) &= (\mathrm{A} - \mathrm{DC})\,\mathbf{e}(t) + \sum_{i=1}^{4} \Delta\mathbf{b}_i\,\mathrm{u}_i \\ \epsilon(t) &= \mathrm{C}\,\mathbf{e}(t) \end{aligned} \tag{4.13}$$

These equations are represented in a block diagram form in Fig. 4-10.

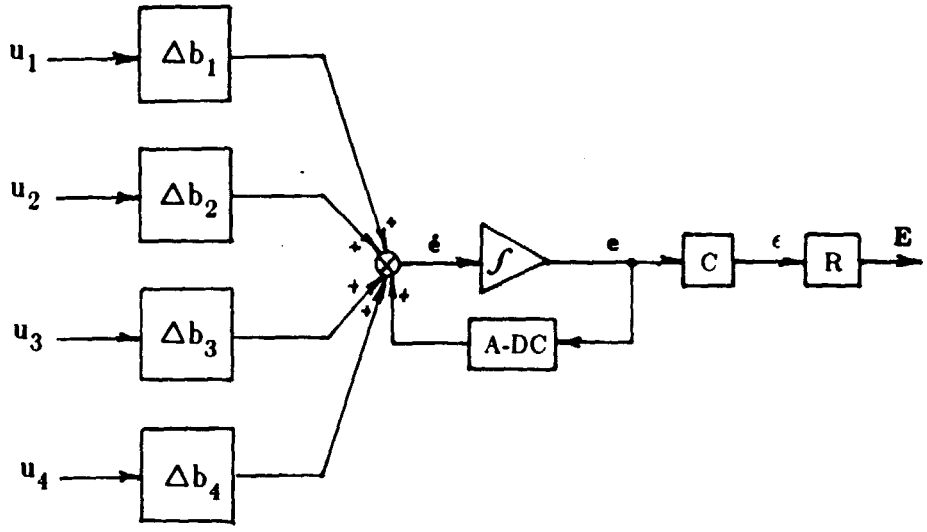

Figure 4-10: Error Dynamics for Model Error in B.

From Eq. (4.13) and Fig. 4-10, it can be noted that this error model is the same as the error model for actuator failures but with $\Delta\mathbf{b}_i$ instead of $\mathbf{b}_i$.

4.1.3.4 Parameter Errors in C

The parameters of the measurement matrix C are the values of the mode shapes at the sensor locations. Define C^* as the true measurement matrix. The difference between C^* and C (the measurement matrix used in the filter design), is defined as:

$$\Delta C = C^* - C$$

where

$$\Delta C = [\, \Delta C_1 \;\; \Delta C_2 \;\; . \;\; . \;\; . \;\; \Delta C_N]$$

Then, the state and output system equations are:

$$\dot{\mathbf{x}}(t) = A\,\mathbf{x}(t) + B\,\mathbf{u}(t) \tag{4.14}$$

$$\mathbf{y}(t) = (\, C + \Delta C \,)\,\mathbf{x}(t)$$

and the new state and output error equations are:

$$\dot{\mathbf{e}}(t) = (A - DC)\,\mathbf{e}(t) - D \sum_{i=1}^{N} \Delta \mathbf{c}_i\, \psi_i(t) \tag{4.15}$$

$$\epsilon(t) = C\,\mathbf{e}(t) + \sum_{i=1}^{N} \Delta \mathbf{c}_i\, \psi_i(t)$$

In Fig. 4-11, the block diagram representation of Eq. 4-15 is shown. It is important to note that this error model is similar to the error model for unmodeled modes (Fig. 4-8). The main difference is that while the state error in Eq. (4.15) is driven by the amplitude of the **modeled** structural modes, the state error in Eq. (4.7) is

driven by the amplitude of the **unmodeled** ones. The other difference is in the vector multiplying the modal amplitudes: in Eq. (4.15) this vector is $\Delta \mathbf{C}_i$, and in Eq. (4.7) is $\mathbf{C}_i$.

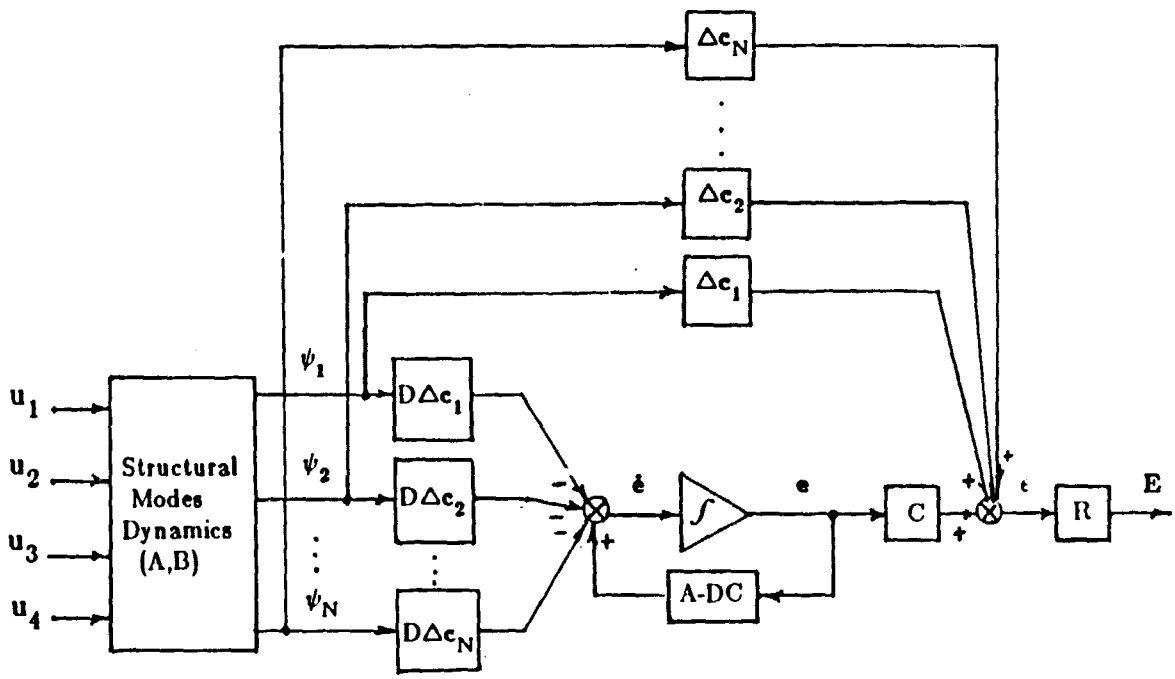

Figure 4-11: Error Dynamics for Model Error in C

4.1.3.5 Parameter Errors in A, B and C

In the real problem, all the matrices A, B and C contain errors. This problem can be analyzed by dividing it into the three cases explained in the three previous subsections, and then adding the output residuals obtained in each case. However, in order for the superposition principle to apply, a modification must be introduced when dividing the problem into the three cases illustrated in Figures 4-9, 4-10 and 4-11: the modal amplitudes ψ_i in Fig. 4-9 and 4-11 must be generated by the **true** beam model, with the true system matrix $\mathbf{A}^*$ and the true control matrix $\mathbf{B}^*$ instead of the matrices A and B used in the filter design.

The modal amplitudes obtained with $\mathbf{A}^*$ and $\mathbf{B}^*$, however, are not different in

character than the ones obtained with A and B (for practical values of parameter errors). Moreover, the reasons for the extremely large residuals when there are parameter errors in the model, lie on the transfers from the modal amplitudes ψ_i to the output $\epsilon(t)$ in Fig. 4-9 and Fig. 4-11, and on the transfers from the control inputs u_j to the output $\epsilon(t)$ in Fig. 4-10. Therefore, the problem of parameter errors in the matrices A, B and C can be analyzed by dividing the problem into three cases in which only one of the matrices contains errors and the other two are exact. This is the approach taken in this thesis.

4.2 Frequency Response Analysis

The reasons for the poor performance exhibited by Detecton Filter #1 in the presence of model mismatch, can be explained by conducting a frequency response analysis, based on the error models developed in the previous section.

From Eq. (4.1), it can be concluded that the higher the natural frequency of the structural mode, the lower the amplitude transfer at low frequencies. Therefore, since the unmodeled mode (the eight structural mode) is a very high frequency mode, its amplitude has very small low frequency components, and most of its energy is at its natural frequency. However, Fig. 4-1 shows, very surprisingly, that the unmodeled mode produced a residual with a low frequency character rather than the high frequency of the unmodeled bending mode.

The reason for this residual behavior can be explained in terms of the frequency response functions for the transfer from the amplitude of the eight mode ψ_8 to the residuals E_3 and E_4 (see Fig. 4-8). These frequency response functions are shown in Fig. 4-12, where the extremely high amplitude transfer at low frequencies can be noted. This very large gain at low frequencies amplifies the

small low frequency components of the unmodeled mode excitation, giving the residuals of Fig. 4-1 a low frequency character.

A simple calculation can show that the low frequency gains in Fig. 4-12 result in an unfavorable signal to noise ratio. This calculation is only an approximation and is based on the assumption that actuator 4, the one that fails at T = 1 sec., is the only active actuator. Under this assumption, the low frequency gain for the transfer from u_4 to ψ_8 can be computed as:

$$\frac{|\psi_8|}{|u_4|} = \frac{b_8}{\omega_8^2} = \frac{1.102}{43683} = 2.522 \times 10^{-5} \qquad \text{for } \omega \approx 0$$

where $b_8 = \phi_8(\epsilon_4)$ / M (see Fig. 4-5). The low frequency gain for the transfer from ψ_8 to E_4 can be obtained from Fig. 4-12:

$$\frac{|E_4|}{|\psi_8|} = 2070 \qquad \text{for } \omega \approx 0$$

Therefore, the ratio $|E_4|$ / $|u_4|$ is calculated as:

$$H_n = \frac{|E_4|}{|u_4|} = 2.522 \times 10^{-5} \times 2070 = 0.052 \qquad \text{for } \omega \approx 0$$

This ratio corresponds to the noise present at the residual E_4, due to the unmodeled mode. The ratio corresponding to the signature produced by the failure of actuator 4 is, from equations (4.3) and (4.4):

$$H_s = \frac{|E_4|}{|u_4|} = 0.01 \qquad \text{for } \omega \approx 0$$

Therefore, the low frequency signal to noise ratio at E_4 is $H_s/H_n = 1/5.2$. This unfavorable signal to noise ratio explains why low frequency noise obscured completely the failure signature in Fig. 4-1.

In the real experiment, the four actuators are active. In this case, it is reasonable to expect the modal amplitude ψ_8 to be larger than the one resulting from only one actuator. Consequently, a larger noise at E_4 is also expected. The failure signature, however, remains the same because it depends only on actuator 4. Therefore, it is likely in the real experiment, for the signal to noise ratio to be worse than 1/5.2.

The results shown in Fig. 4-12 were very unexpected. A detection filter is a linear observer whose gain matrix D has the additional constraint, besides making the filter stable, of restricting the output error due to a particular failure to a single line in the output space. The typical behavior of a linear observer is: 1) to follow the measurement noise when its frequency lies inside the bandwidth of the filter, and 2) not to respond to the measurement noise when its frequency is higher than the filter bandwidth, thus resulting in large residuals. Translated into the frequency domain, this means that the frequency response of the transfer from the measurement noise to the residual is expected to be very small within the bandwidth of the filter, and then grow to a certain value at higher frequencies. Detection Filter #1 behaved as expected at frequencies higher than 10 rad/sec by responding moderately to the unmodeled mode noise. However, it behaved quite differently than expected at low frequencies, by actually amplifying the unmodeled mode noise, as can be seen in Fig. 4-12. It seems that the directionality constraint

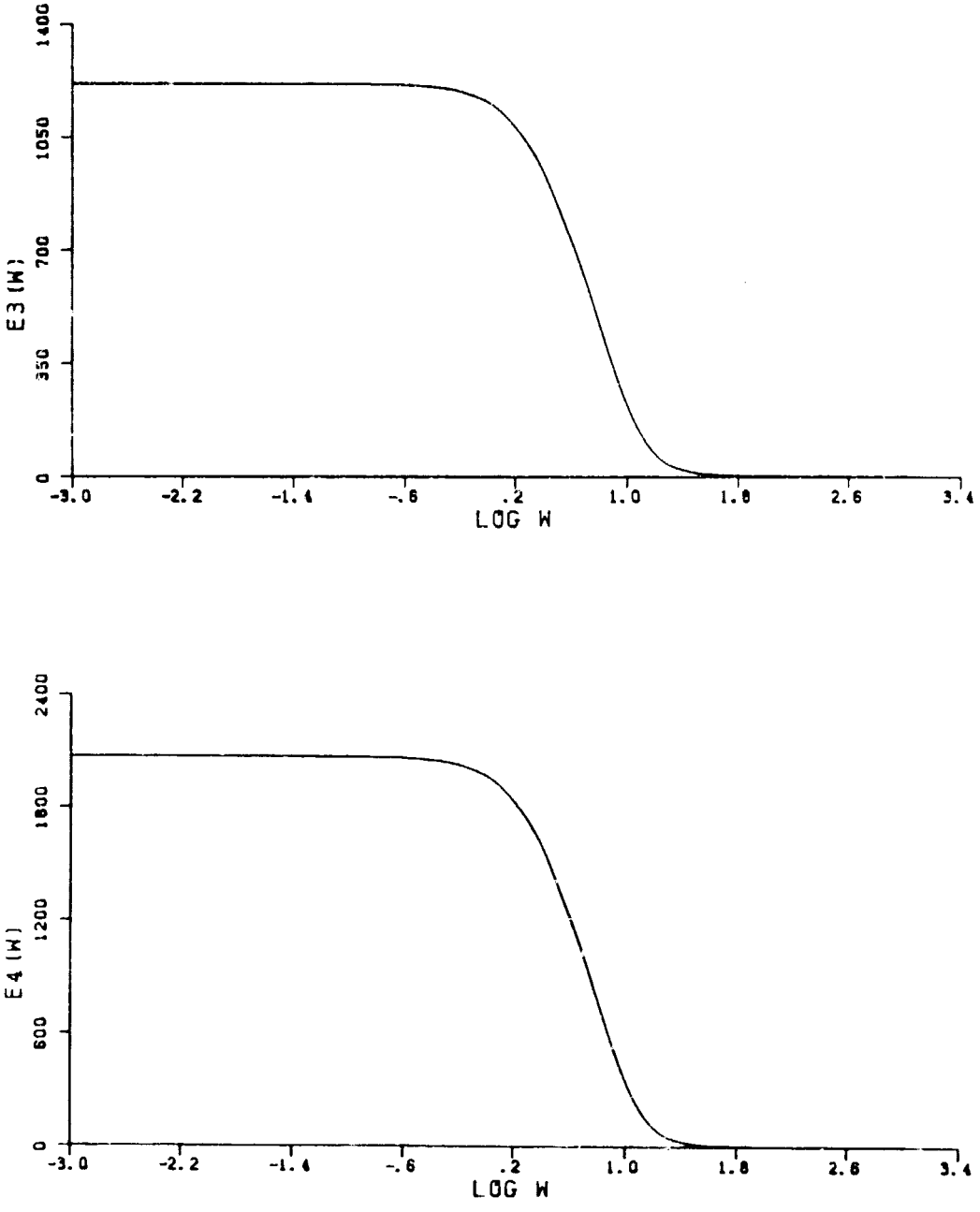

Figure 4-12: Detection Filter #1. Unmodeled Mode Transfer

combined with the dynamics of the flexible beam, resulted in a detection filter that is a very poor observer when all of its poles are placed at -10 rad/sec.

The results of testing Detection Filter #1 with 0.05% parameter uncertainties in system matrix A, can be seen in Fig. 4-2. Note that the residual that obscures the failure signature has the frequency of the first bending mode. The error dynamics for the case of parameter errors in A is shown in Fig. 4-9. The vectors $\Delta\mathbf{a}_1$ and $\Delta\mathbf{a}_2$ are zero because they correspond to the rigid modes, whose frequencies are known to be exactly zero. Of the bending modes, the first one, with a frequency of 11 rad/sec, comes the closest to lying within the bandwidth of the filter. Therefore, since the contributions from the higher bending modes are filtered out, the residuals have the frequency of the first bending mode. Figure 4-13 shows the frequency response of the transfer from ψ_3 to the residuals E_3 and E_4.

When testing Detection Filter #1 with parameter uncertainties, the most surprising result was obtained when considering parameter errors in matrix B. The residuals produced by parameter errors smaller than 0.05% in the control matrix B, were of the same magnitude as the signature resulting from the complete failure of actuator 4 (See Fig. 4-3).

As can be seen in Fig. 4-10, the reason for these large residuals must lie in the transfers from the control imputs u_i to the residuals E_3 and E_4. The frequency response functions for the transfer from the control u_4 to the residuals E_3 and E_4 are shown in Fig. 4-14. The values of these functions at low frequency are 0.0065 for E_3 and 0.011 for E_4. Therefore, since the low frequency gain corresponding to failure of actuator 4 is 0.01, the residuals and the failure signature are of the same magnitude.

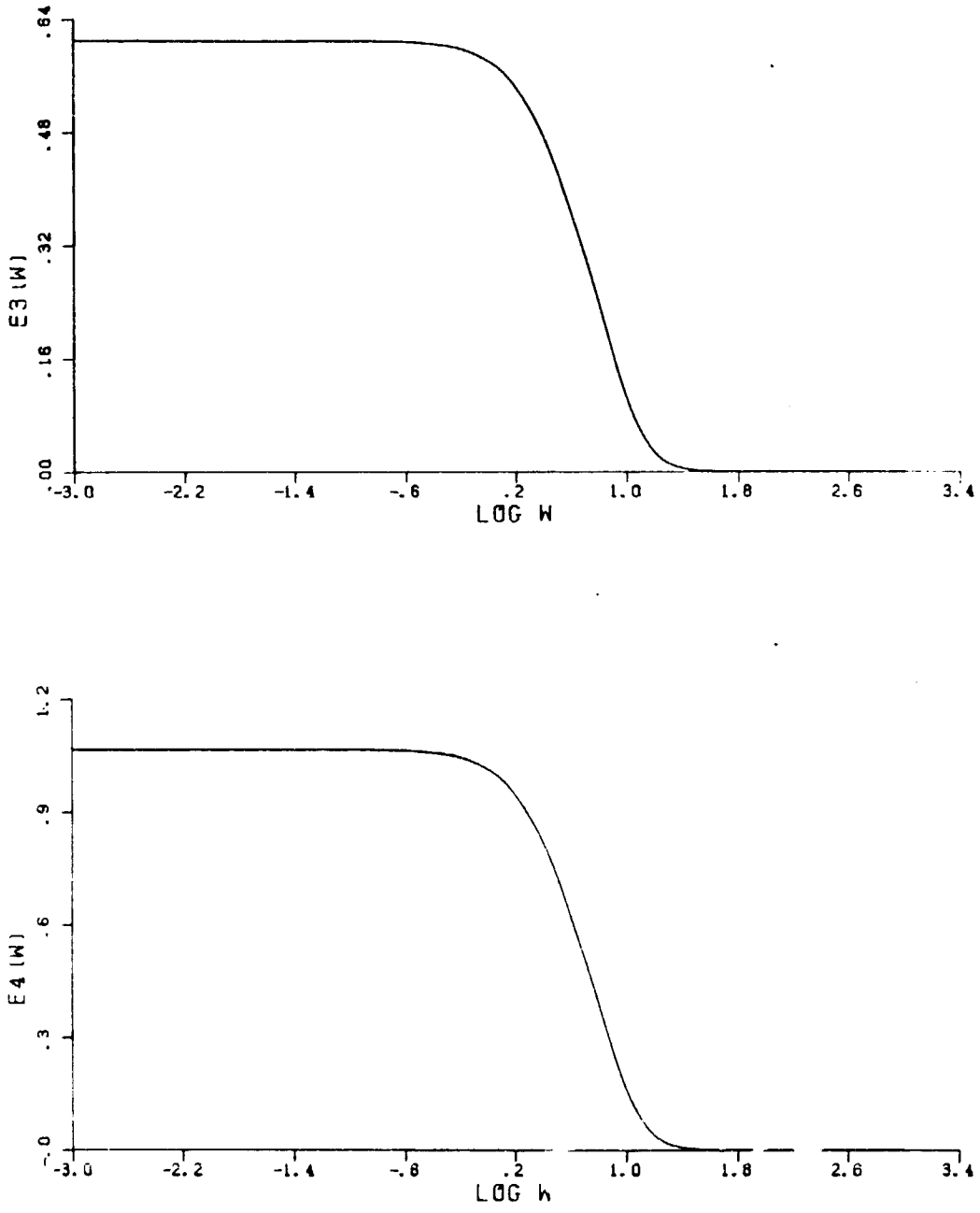

Figure 4-13: Detection Filter #1. Parameter Errors in A = 0.05%. Transfer from ψ_3 to E_3 and E_4.

It is interesting to note that even though the elements of the vector $\Delta \mathbf{b}_4$ are smaller than 0.05% of the respective elements in $\mathbf{b}_4$, the amplitude transfer from u_4 to E_4 is actually a little larger with $\Delta \mathbf{b}_4$ than with $\mathbf{b}_4$ as the control vector in Fig. 4-10. However, this would not be the case if $\Delta \mathbf{b}_4$ lay in the same direction in the state space as $\mathbf{b}_4$. For example, if the error in each element of $\mathbf{b}_4$ were +0.05%, then $\Delta \mathbf{b}_4 = 0.0005 \times \mathbf{b}_4$ and the gain corresponding to $\Delta \mathbf{b}_4$ would be 0.05% of the gain corresponding to $\mathbf{b}_4$ (i.e., $0.0005 \times 0.01 = 5 \times 10^{-6}$).

Since the dynamics of both detection spaces are the same, then the large low frequency gains that result when $\Delta \mathbf{b}_4$ does not lie in the same direction as $\mathbf{b}_4$ must be due to the dynamics of the completion spaces.

The test of Detection Filter #1 with 0.05% parameter uncertainties in the measurement matrix C, produced the results shown in Fig. 4-4. The residuals have a very low frequency character and appear to be unbounded.

The error model for the case of parameter errors in C, is shown in Fig. 4-11. As mentioned earlier, it is similar to the error model for unmodeled modes. Figure 4-15 shows the frequency response functions for the transfer from the modal amplitude ψ_1 to the residuals E_3 and E_4. The low frequency gains are almost three orders of magnitude smaller than those corresponding to the transfer from the unmodeled mode ψ_8 to the residuals E_3 and E_4. The reason for this is that the vector $\Delta \mathbf{c}_1$ is much smaller than the vector $\mathbf{c}_8$.

The beam is being driven by the actuators in an open loop manner. Therefore, the amplitude of the rigid modes ψ_1 and ψ_2, since their poles are at the origin, start to increase and become unbounded. That is, the beam moves away from the reference and starts to rotate. Therefore, even though the low frequency transfer from ψ_1 and ψ_2 to $\mathbf{E}$ is relatively small, since the modal amplitudes ψ_1 and

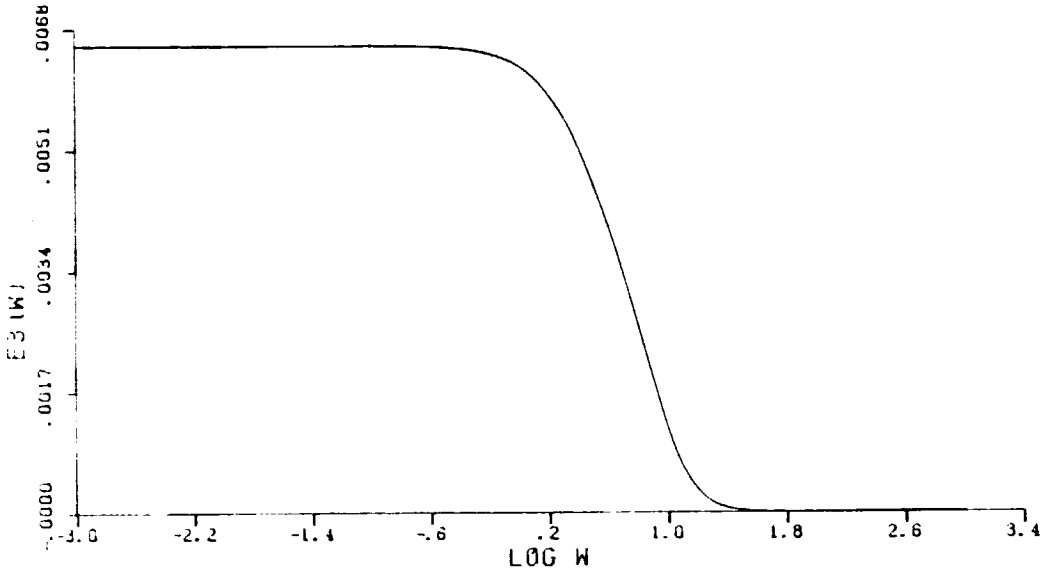

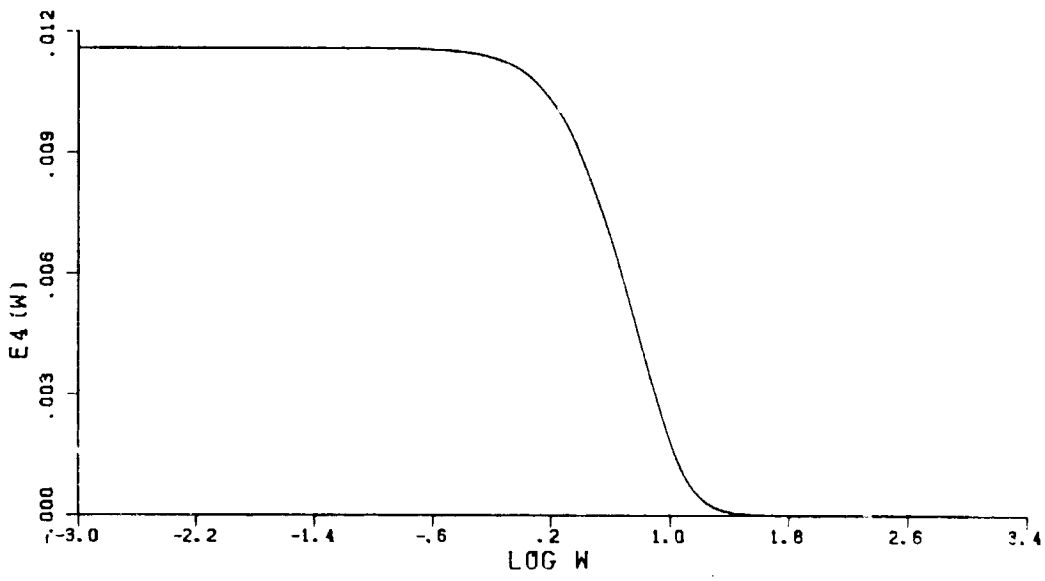

Figure 4-14: Detection Filter #1. Parameter Errors in B = 0.05%.
Transfer from u_4 to E_3 and E_4.

ψ_2 are growing with no bounds, eventually ψ_1 and ψ_2 become large enough to generate residuals that obscure the failure signature. This explains the very low frequency and the unbounded nature of the residuals in Fig. 4-4.

To summarize, the reasons for the poor performance of Detection Filter #1 in the presence of model mismatch were explained in terms of frequency response functions (Fig. 4-12 through 4-15). It was found that these frequency responses had features that were very unexpected, like very large low frequency gains.

It is believed that the "strange" transfer properties of Detection Filter #1 are the result of applying the directionality constraints to the dynamics of flexible structures. The question now is whether a different choice of filter pole locations would improve these transfer properties and the performance of the filter.

It is reasonable to expect that by increasing the bandwidth of the filter, by moving the filter poles further to the left in the s - plane, the filter's ability to track the measurement vector $\mathbf{y}(t)$ will improve, thus resulting in smaller error residuals. This would be true for both detection space and completion space poles. However, since moving the detection space poles to the left also reduces the size of the failure signature (Eq. (4.2)), it is not clear whether this would result in a better signal to noise ratio. Conversely, since the failure signature does not depend on the completion space poles, moving these poles to the left could result in a better signal to noise ratio.

To test this hypothesis, a detection filter was designed with the same detection space poles, but with the completion space poles moved to -100 rad/sec.

Detection Filter #2:

# of modes = 7

failure events = Actuators 3 and 4

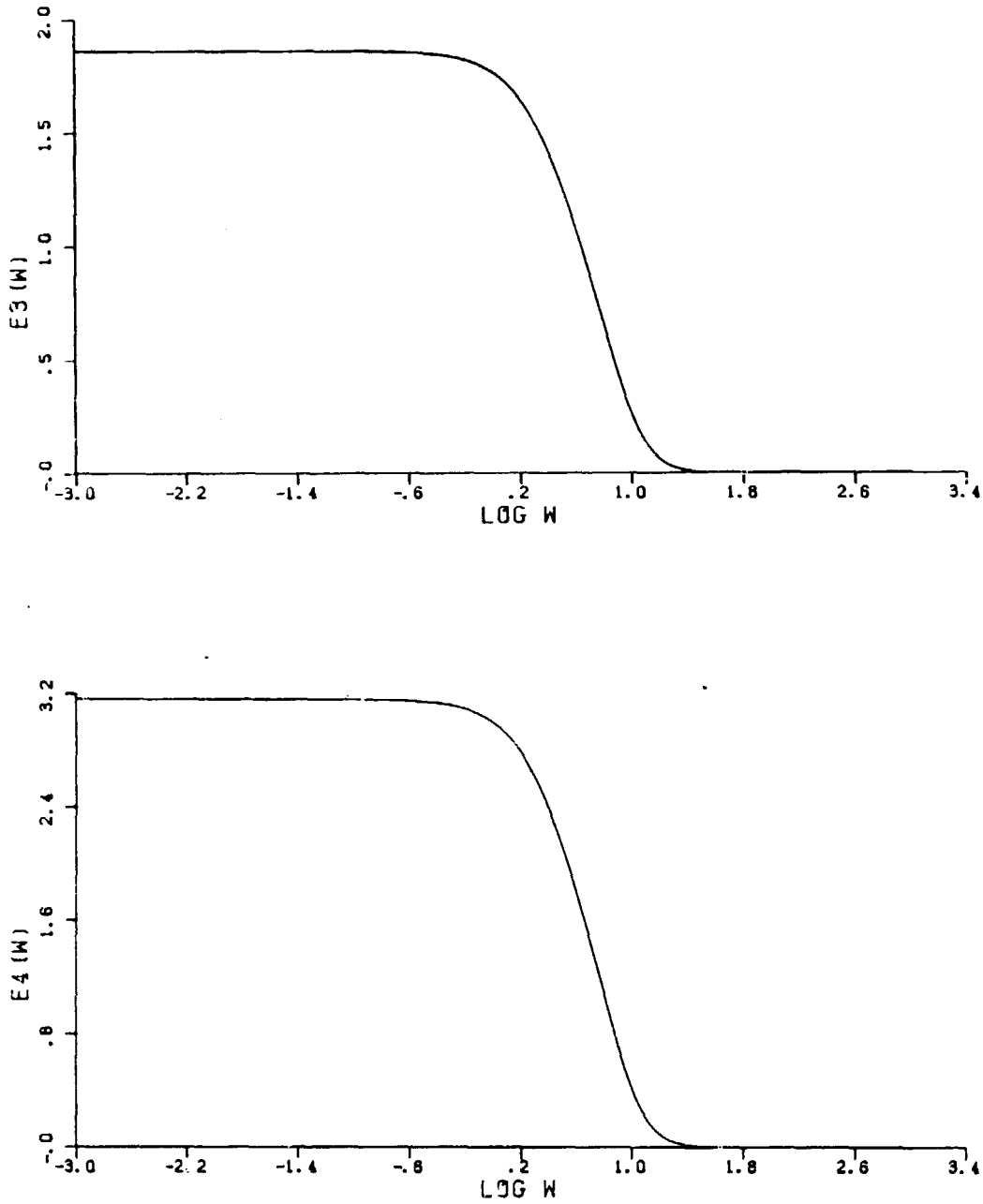

Figure 4-15: Detection Filter #1. Parameter Errors in C = 0.05%.
Transfer from ψ_1 to E_3 and E_4.

Poles:

4 detection space poles at -10 rad/sec

10 completion space poles at -100 rad/sec

Since the location of the detection space poles was not changed, the signatures for the failure of actuators 3 and 4 remained the same as before, and are shown in Fig. 3-2 and 3-3.

For the remainder of this section, Detection Filter #2 will be subject to the same frequency response analysis and will be simulated under the same conditions as Detection Filter #1.

Figure 4-16 shows the frequency response functions for the transfer from the unmodeled mode ψ_8 to the residuals E_3 and E_4, for Detection Filter #2. Note the dramatic decrease in the low frequency gain.

The improved transfer properties of Detection Filter #2 suggest that it should perform much better than Filter #1 in the presence of unmodeled dynamics. This is shown to be the case in Fig. 4-17, where Detection Filter #2 is tested in the presence of the unmodeled eight mode. The residuals no longer have a low frequency character, and the frequency of the bending mode is evident. More importantly, the signature of the failure of actuator 4 at 1 sec. is clearly visible.

Figure 4-18 shows that there has also been a dramatic improvement in the transfer corresponding to the case of parameter errors in

The results of the simulation of Detection Filter #2 with 0.05% parameter uncertainties in A, are shown in Fig. 4-19. The large improvements in the transfer properties are reflected in these results, where the failure signature now is clearly visible. The bias in the residuals has vanished and the frequency of the first

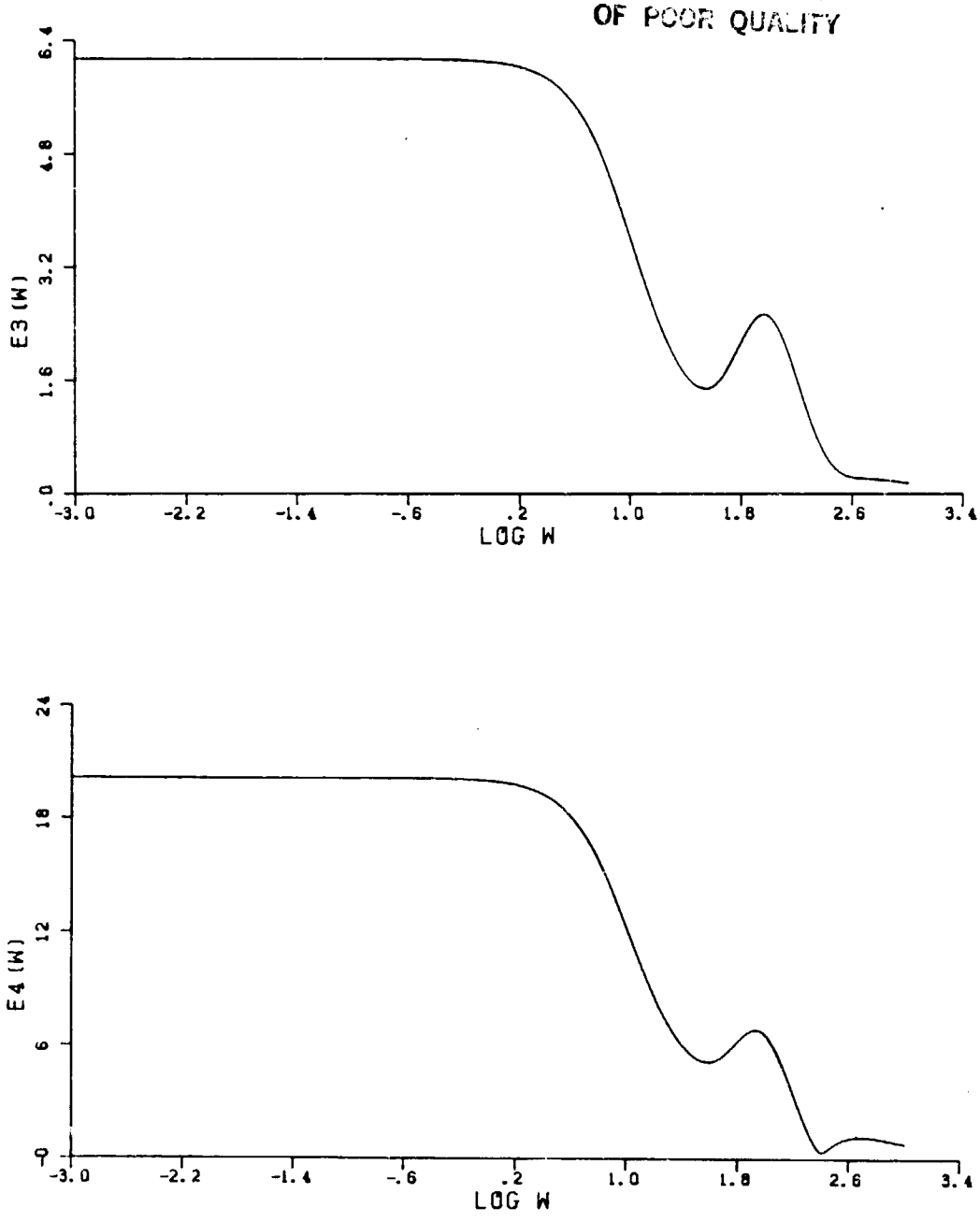

Figure 4-16: Detection Filter #2. Unmodeled Mode Transfer

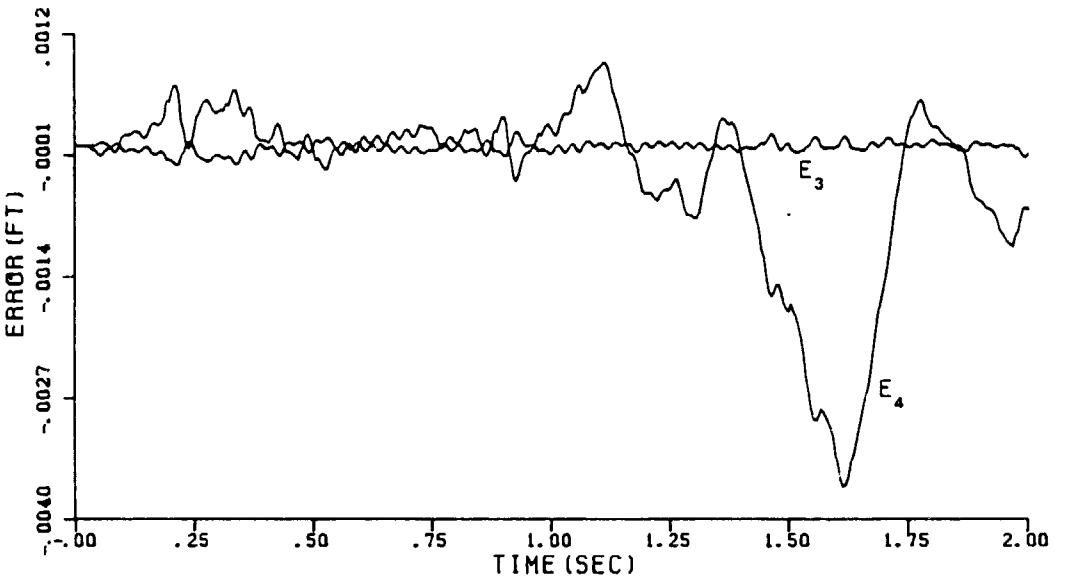

Figure 4-17: Detection Filter #2. Eighth Mode is Unmodeled. Actuator 4 Failure at T = 1 sec.

bending mode is barely noticeable. Now, the frequency of the second bending mode becomes evident.

Notice that the errors in the modal frequencies of the third, fourth and fifth bending modes do not produce any noticeable effects in the residuals. The reason for this desirable result is that the frequencies of these bending modes lie outside the bandwidth of the filter, and therefore, they are filtered out. Since the uncertainty in the knowledge of the modal frequencies increases the higher these frequencies are, this result is very important.

Figure 4-20 shows the residuals produced by the simulation of Detection Filter #2 with 1% parameter uncertainty in matrix A. The failure signature is completely obscured by the residuals, and therefore, it can be concluded that the improved filter cannot perform adequately with uncertainties equal or larger than 1% in the knowledge of the modal frequencies.

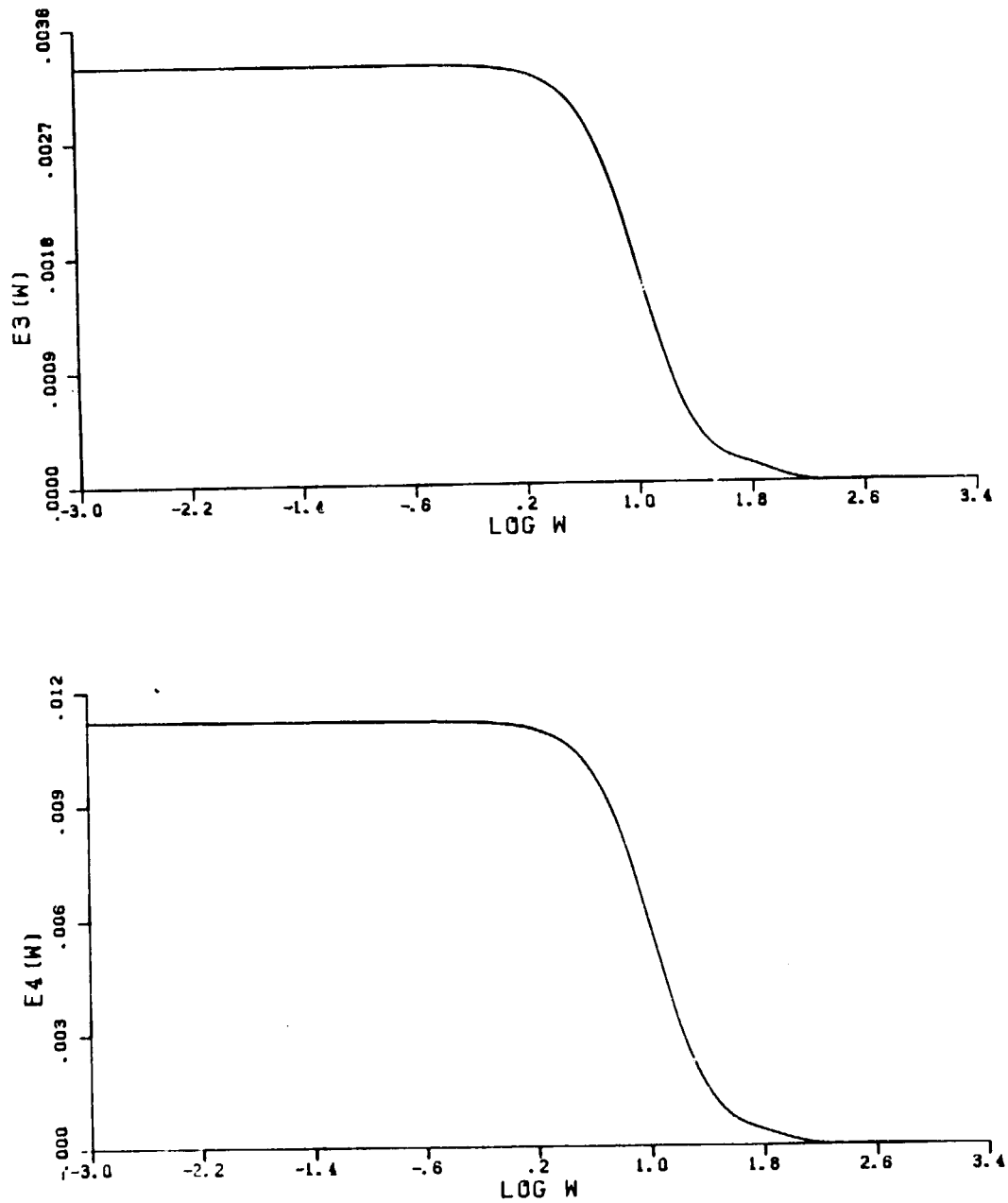

Figure 4-18: Detection Filter #2. Parameter Errors in A = $0.05\tilde{c}$. Transfer from ψ_3 to E_3 and E_4.

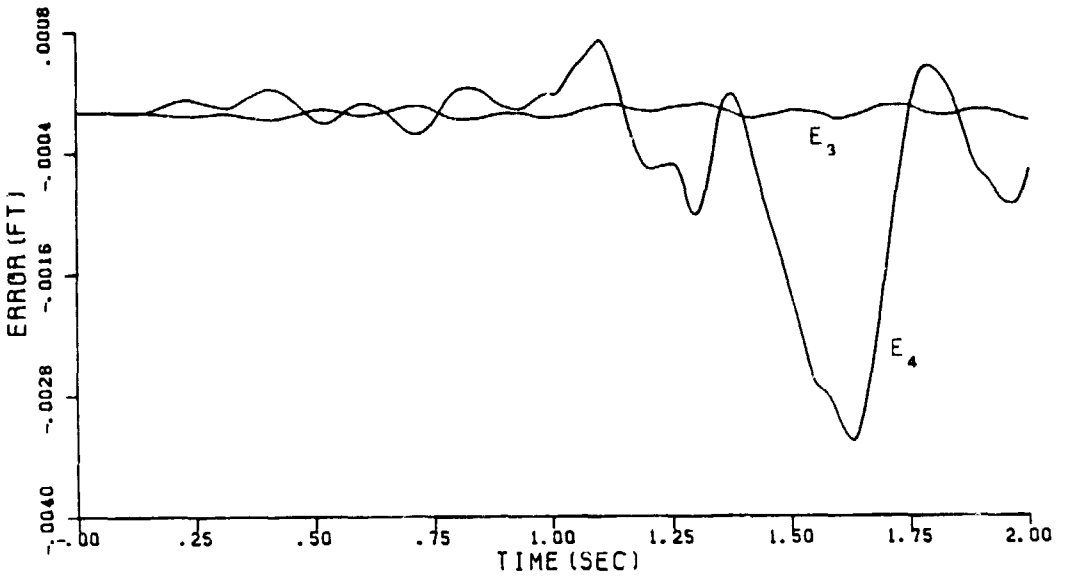

Figure 4-19: Detection Filter #2. Parameter Errors in Matrix A = 0.05%. Actuator 4 Failure at T = 1 sec.

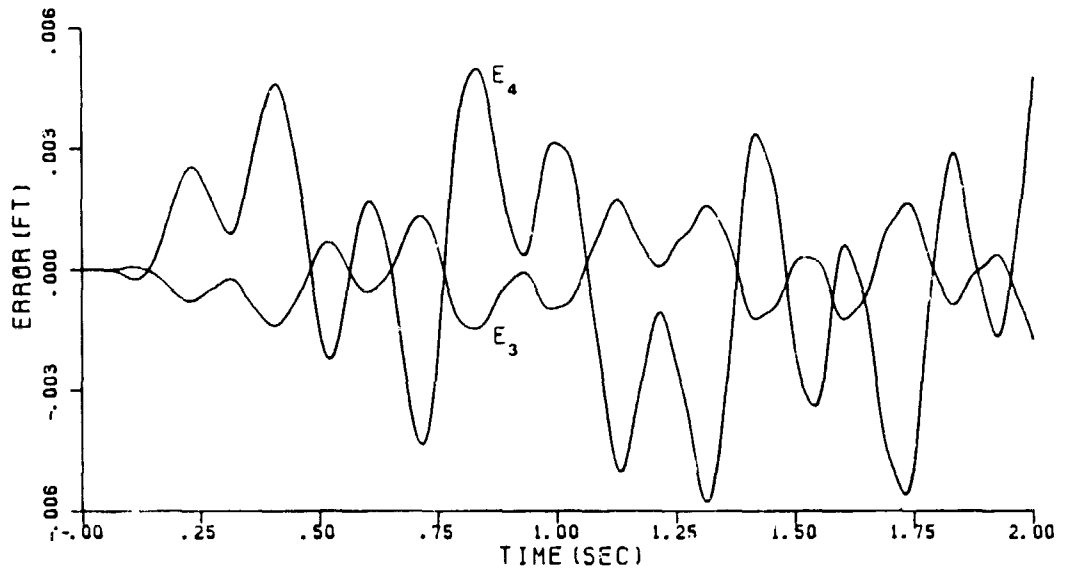

Figure 4-20: Detection Filter #2. Parameter Errors in Matrix A = 1%. Actuator 4 Failure at T = 1 sec.

Detection Filter #2 also showed a remarkable improvement in performance when tested in the presence of parameter uncertainties in B. The frequency response functions related to this case are shown in Fig. 4-21. The low frequency gains are two orders of magnitude smaller than the gain corresponding to Detection Filter #1.

The results of the simulation of Detection Filter #2 with 0.05% parameter uncertainties in B, can be seen in Fig. 4-22. The improvement is remarkable. The residuals due to model mismatch are barely noticeable. However, the improved filter is still not good enough to detect failures in the presence of more realistic levels of parameter uncertainties. The filter was tested with 5% parameter uncertainties in B, and the signature was completely obscured by the residual (Fig. 4-23).

Finally, Detection Filter #2 was tested with parameter uncertainties in the measurement matrix C. Its transfer properties are shown in Fig. 4-24, where a large improvement can also be noted. The simulation, shown in Fig. 4-25 gave much better results as well. However, the improvements were not large enough to make the failure signature clearly visible.

To summarize, dramatic improvements have been accomplished by moving the completion space poles further to the left in the s - plane. The largest improvements were obtained in the performance of the filter in the presence of unmodeled modes and parameter errors in B. The improved filter is able to detect failures with almost 5% parameter uncertainties in B.

Even though the improvements in the performance of the filter with model errors in A and C were also remarkable, the filter would not tolerate parameter errors in A of up to 1%, and in the case of system matrix C, the improvements

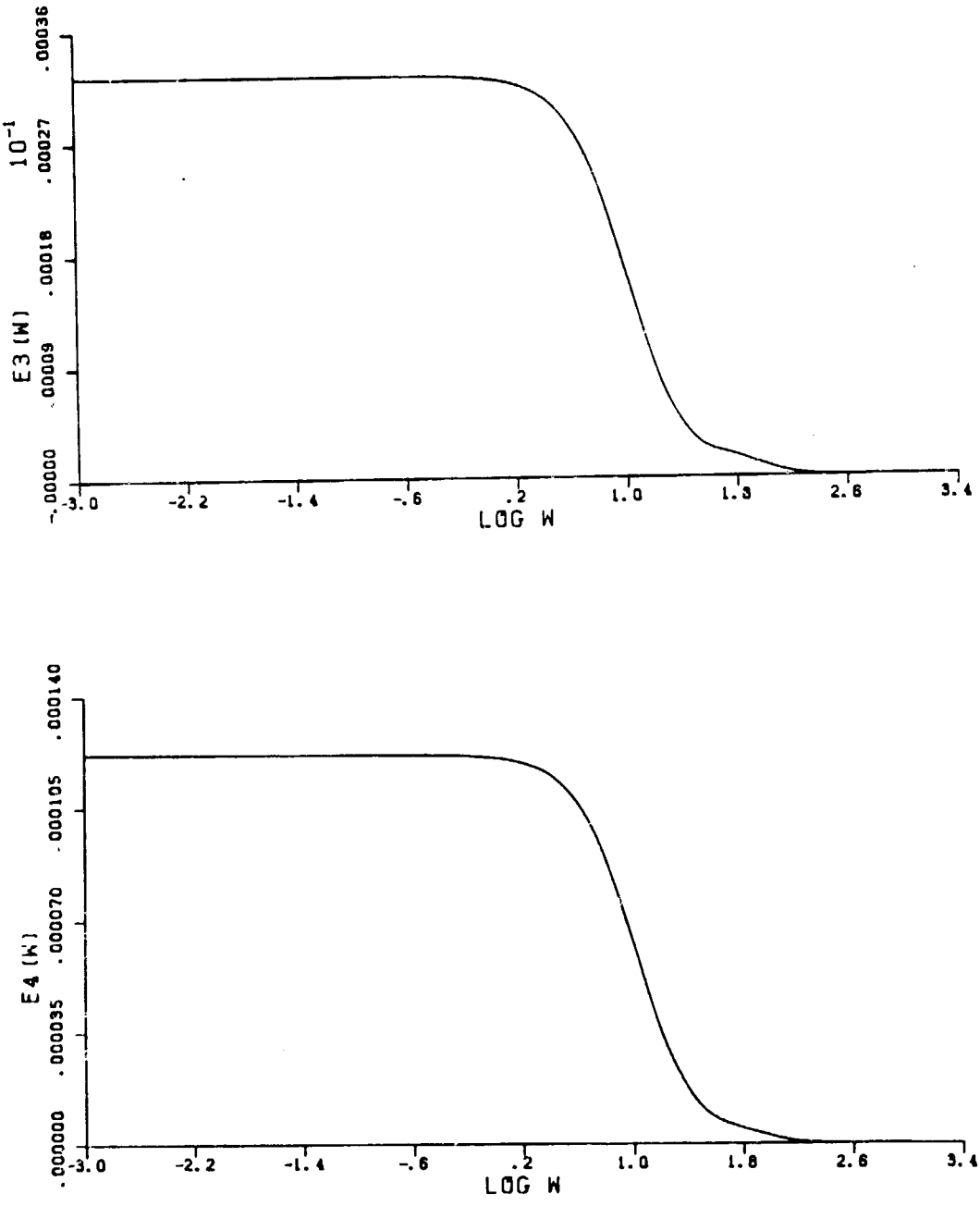

Figure 4-21: Detection Filter #2. Parameter Errors in B = 0.05%. Transfer from u_4 to E_3 and E_4.

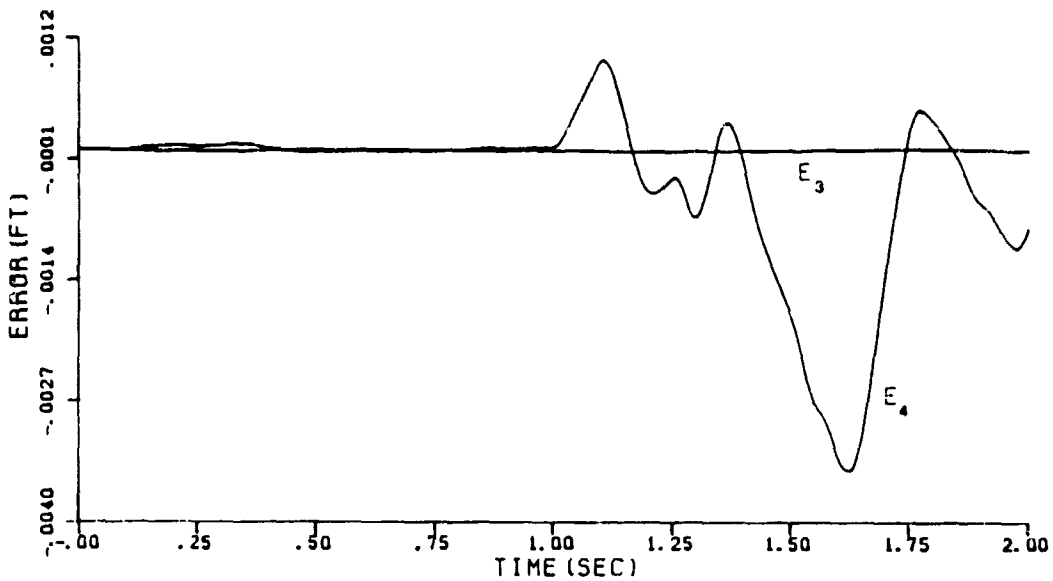

Figure 4-22: Detection Filter #2. Parameter Errors in Matrix B = 0.05%. Actuator 4 Failure at T = 1 sec.

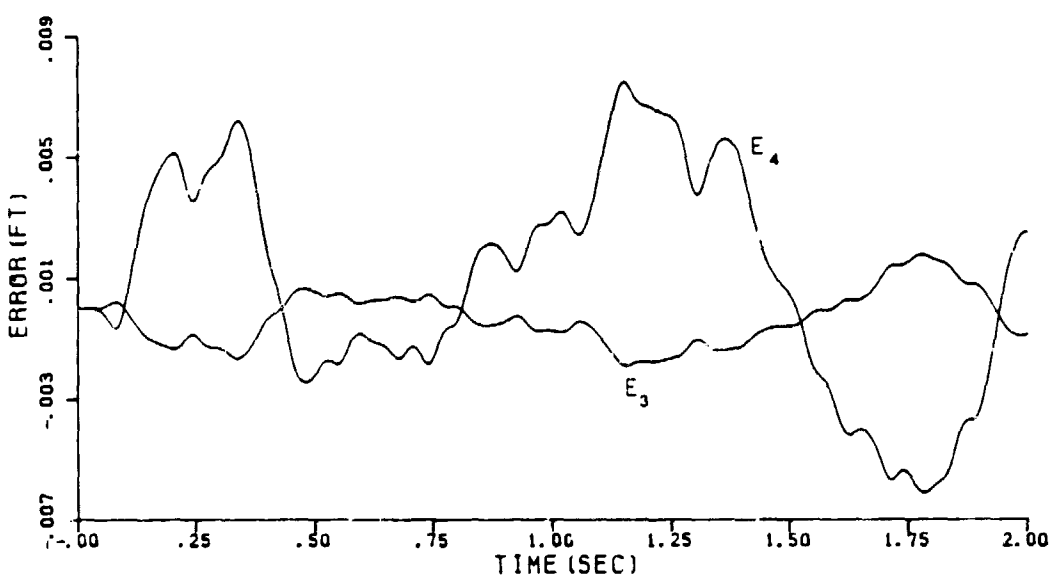

Figure 4-23: Detection Filter #2. Parameter Errors in Matrix B = 5%. Actuator 4 Failure at T = 1 sec.

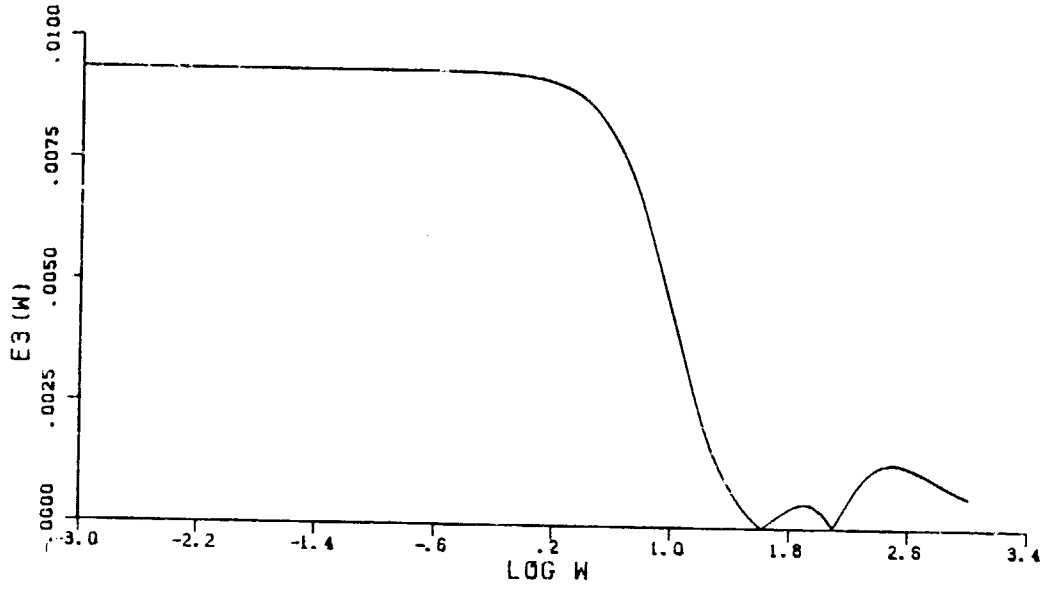

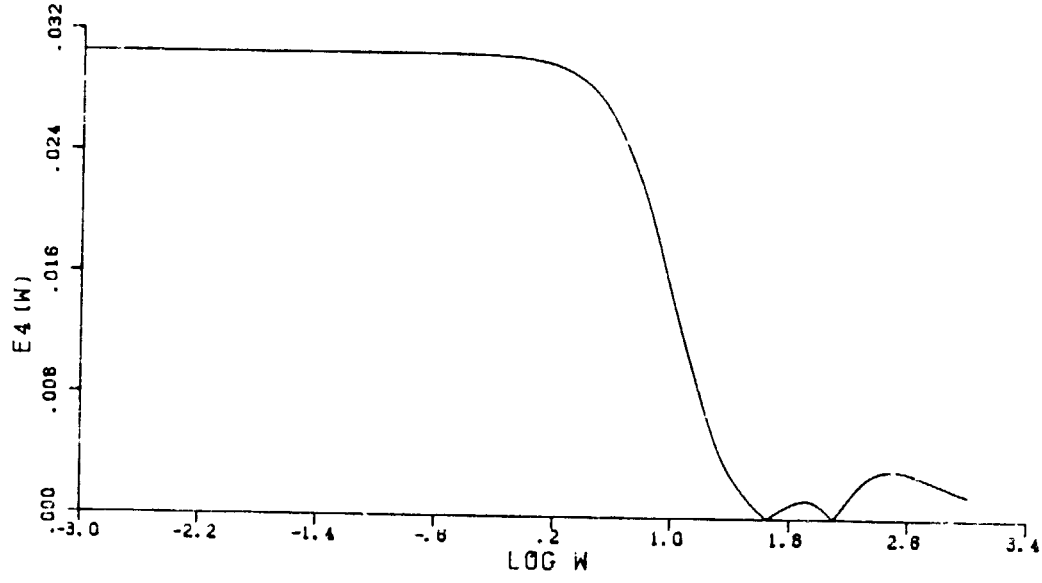

Figure 4-24: Detection Filter #2. Parameter Errors in C = 0.05%. Transfer from ψ_3 to E_3 and E_4.

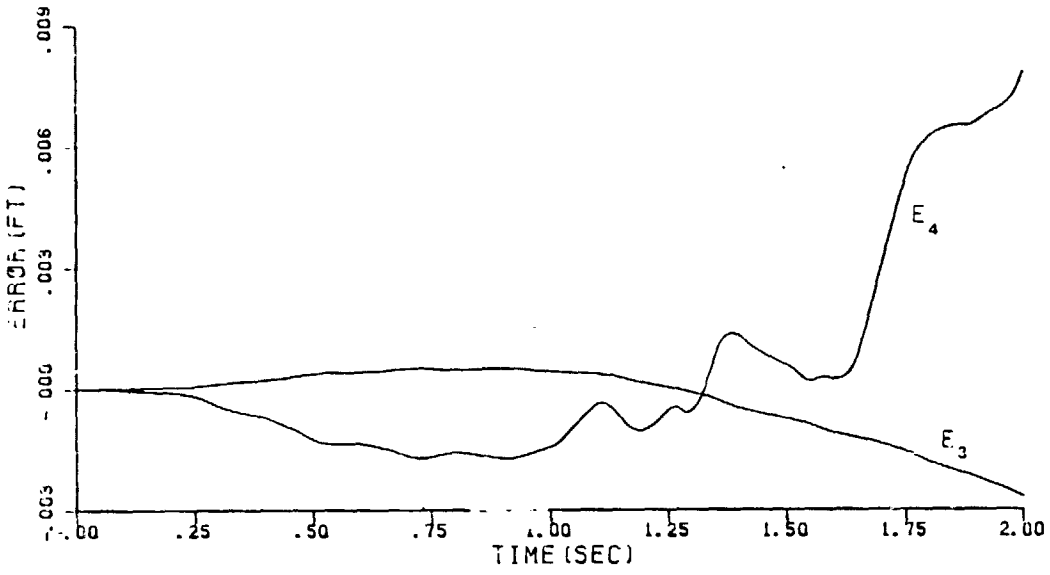

Figure 4-25: Detection Filter #2. Parameter Errors in C = 0.05%.
Actuator 4 Failure at T = 1 sec.

were not enough to allow successful detection with 0.05% parameter uncertainties.

However, the reasons for this disappointing performance may lie in part on the somewhat unrealistic conditions under which the filter was tested. In the case of parameter errors in A, the state error was driven mainly by the very large components of the modal amplitudes at their natural frequencies resulting from the lack of damping in the beam. The real beam, however, has some damping and therefore these components would be considerably smaller. In addition, all the modal amplitudes are kept small by the action of the control system during its nominal operation. In the case of parameter errors in C, the state error was driven by the unbounded amplitudes of the rigid modes corresponding to the drifting and rotation of the beam. In the real problem, however, the control system would prevent the beam from drifting and rotating.

It is also worth noting that the performance of the detection filter with

parameter errors in A could be improved by filtering the output. Figure 4-20 shows that the error residuals have a very large component at the frequency of the second bending mode (31.36 rad/sec.). Therefore, since the bandwidth of the failure signature is 10 rad/sec., the performance of Detection Filter #2 could be improved by filtering E_3 and E_4 with a bandwidth of 10 rad/sec. .

Finally, something should be said about the placement of the detecton space poles. Unlike the case of the completion space poles, the choice of the locations of the detection space poles strongly depends on the frequency content of the control signals. It is clear that moving these poles to the left in the s - plane reduces the residuals due to model mismatch and reduces the failure signature as well. However, whether the signal to noise ratio improves or not will depend, among other things, on the frequency content of the control inputs. The same is true when considering the damping associated with these poles. Therefore, the choice of the location of the detection space poles should be made on the basis of more realistic simulations which include the control system along with the disturbances of the beam. Moreover, a consideration to be taken into account when choosing these poles is the response time of the detection filter.

4.3 Reduced Order Detection Filters

In Chapter 3, it was shown that detection filters based on a model of the beam with more than 4 structural modes (the number of sensors) could not be configured to detect more than three actuator failure events. Moreover, the design of these filters was made very difficult by the presence of completion spaces, and the specification of the filter poles did not result in a unique gain matrix D. Another disadvantage of these filters, as shown by Detecton Filters #1 and #2,

was their very complex dynamics. Their robust properties varied dramatically with the location of the completion space poles, and even the improved filter (Detection Filter #2) could not tolerate realistic levels of parameter uncertainties.

This section analyzes the design and performance of detection filters based on a model of the beam containing as many structural modes as the number of displacement sensors p, and with all of its poles placed in the same location. It will be shown that these filters do not have the disadvantages mentioned above. Also, ways of coping with the larger number of unmodeled modes will be discussed, along with the effects of using a reduced order model upon the detection and identification capabilities of the filter.

4.3.1 Detection Filters with N = p

Let's consider the design of a detection filter based on a model of the beam with p structural modes, where p is the number of independent displacement measurements. That is,

$$N = p = \#\text{ of sensors} = \text{rank } C$$

Define the p × p matrix M as:

$$M = [\, \mathbf{c}_1 \;\; \mathbf{c}_2 \;\; \cdots \;\; \mathbf{c}_p \,]$$

where $\mathbf{c}_i$ is the column of matrix C corresponding to the amplitude of the *ith* structural mode. It will be assumed that rank M = p, and therefore, M is nonsingular. If this is not the case, the number of sensors used in the detection filter should be reduced until rank M = p.

In order to simplify both the filter design and the analysis that will follow, a transformation is performed on the measurement vector **y**:

$$\mathbf{y}^+ = M^{-1}\ \mathbf{y}$$

then,

$$\mathbf{y}^+ = M^{-1}\, C\, \mathbf{x}$$

and

$$\mathbf{y}^+ = C^+\, \mathbf{x}$$

where

$$C^+ = M^{-1}\, C = \begin{bmatrix} 1 & 0 & 0 & 0 & \cdots & 0 & 0 \\ 0 & 0 & 1 & 0 & \cdots & \cdot & 0 \\ \cdot & \cdot & 0 & 0 & \cdots & \cdot & 0 \\ \cdot & \cdot & \cdot & \cdot & & \cdot & \cdot \\ \cdot & \cdot & \cdot & \cdot & & \cdot & \cdot \\ \cdot & \cdot & \cdot & \cdot & & \cdot & \cdot \\ \cdot & \cdot & \cdot & \cdot & & 0 & 0 \\ 0 & 0 & 0 & 0 & \cdots & 1 & 0 \end{bmatrix}$$

From the structure of C^+, it is easy to verify that

$$\mathbf{y}^{+} = \begin{bmatrix} \psi_1 \\ \psi_2 \\ \cdot \\ \cdot \\ \cdot \\ \psi_N \end{bmatrix} \tag{4.16}$$

Figure 4-26 shows the new block diagram of the failure detection filter which incorporates the measurement transformation M^{-1}. Notice that the detection filter now uses the transformed measurement matrix C^{+}. Also, it is easy to show that:

$$D = D^{+} M^{-1}$$

$$\epsilon = M \epsilon^{+}$$

The state and output error equations corresponding to the failure of the *jth* actuator are:

$$\dot{\mathbf{e}}(t) = (A - D^{+} C^{+}) \mathbf{e}(t) + \mathbf{b}_j \eta(t) \tag{4.17}$$

$$\epsilon^{+}(t) = C^{+} \mathbf{e}(t)$$

where the vector $\mathbf{b}_j$ has the structure:

$$\mathbf{b}_j^{T} = \begin{bmatrix} 0 & b_{j1} & 0 & b_{j2} & \cdots & 0 & b_{jN} \end{bmatrix} \tag{4.18}$$

Theorem 4.1 :

The gain matrix D^{+} that is a detector gain for **all** actuator failure events $\mathbf{b}_j$, and that assigns the filter poles as given by the roots of the equation

$$0 = (s^{2} + 2 \xi \omega_F s + \omega_F^2)^N$$

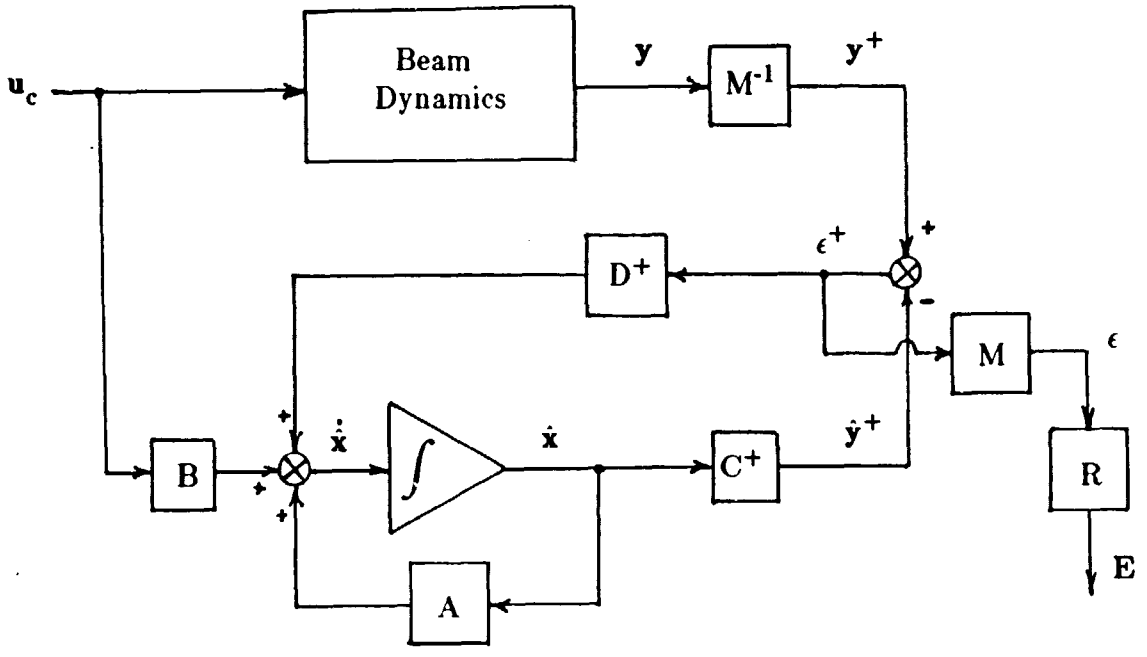

Figure 4-26: The Failure Detection Filter with Output Vector Transformation

is unique and given by:

$$D^+ = \begin{bmatrix} d_1^+ & 0 & \cdots & 0 \\ 0 & d_2^+ & & 0 \\ \vdots & 0 & \ddots & \vdots \\ \vdots & \vdots & & 0 \\ 0 & 0 & \cdots & d_N^+ \end{bmatrix} \tag{4.19}$$

where

$$\mathbf{d}_i^+ = \begin{bmatrix} 2\xi\omega_F \\ \\ (\omega_F^2 - \omega_i^2) \end{bmatrix}$$

Proof:

First, calculate the matrix $(A - D^+ C^+)$ as:

$$A - D^+C^+ = \begin{bmatrix} P & & & 0 \\ & P & & \\ & & \ddots & \\ 0 & & & P \end{bmatrix} \qquad (4.20)$$

where the 2×2 matrix P is:

$$P = \begin{bmatrix} -2\xi\omega_F & 1 \\ \\ -\omega_F^2 & 0 \end{bmatrix}$$

The poles of the filter are given by the roots of the characteristic equation of the matrix $(A - D^+ C^+)$. That is, the roots of the equation

$$0 = \det(s\, I - A + D^+ C^+)$$

Since the matrix $(A - D^+ C^+)$ is block diagonal, using a result from linear algebra get:

$$\det(s\,I - A + D^{+}\,C^{+}) = (\det(s\,I - P))^{N} = (s^2 + 2\xi\omega_F\,s + \omega_F^2)^{N}$$

Therefore, the poles of the filter are given by the roots of the equation

$$0 = (s^2 + 2\xi\omega_F\,s + \omega_F^2)^{N}$$

as stated in the theorem.

To prove that the gain matrix D^{+} given in (4.19) is a detector gain for all actuator failure events, the transfer function vector $\mathbf{T}_j(s)$ defined as

$$\epsilon^{+}(s) = \mathbf{T}_j(s)\,\eta(s) \tag{4.21}$$

$$\mathbf{T}_j(s) = C^{+}\,(s\,I - A + D^{+}\,C^{+})^{-1}\,\mathbf{b}_j$$

is calculated. It is easy to show that

$$(s\,I - A + D^{+}\,C^{+})^{-1} = \begin{bmatrix} Q & & & \\ & Q & & 0 \\ & & \ddots & \\ & 0 & & \\ & & & Q \end{bmatrix}$$

where

$$Q = (s\,I - P)^{-1} = \frac{1}{s^2 + 2\xi\omega_F\,s + \omega_F^2} \times \begin{bmatrix} s & 1 \\ -\omega_F^2 & s + 2\xi\omega_F \end{bmatrix}$$

Then, by premultiplying by C^{+} and postmultiplying by $\mathbf{b}_j$ obtain:

$$\mathbf{T}_j(s) = \frac{1}{s^2 + 2\xi\omega_F\, s + \omega_F^2} \times \begin{bmatrix} b_{j1} \\ b_{j2} \\ \vdots \\ b_{jN} \end{bmatrix}$$

where $b_{j1}, b_{j2}, \ldots, b_{jN}$ are the elements of the event vector $\mathbf{b}_j$ in (4.18). Finally, by defining the vector $\mathbf{b}_j^+$as:

$$\mathbf{b}_j^+ = \begin{bmatrix} b_{j1} \\ b_{j2} \\ \vdots \\ b_{jN} \end{bmatrix} \tag{4.22}$$

equation (4.21) can be written

$$\epsilon^+(s) = \mathbf{b}_j^+ \frac{\eta(s)}{s^2 + 2\xi\omega_F\, s + \omega_F^2} \tag{4.23}$$

Then, it can be concluded that when the *jth* actuator fails, the output error ϵ^+ remains in the single direction given by the vector $\mathbf{b}_j^+$. Therefore, since the event vector $\mathbf{b}_j$ represents **any** actuator failure, the matrix D^+ in (4.19) is a detector gain for **all** actuator failure events, and the proof is complete. ∇

As it was shown in Theorem 4.1, the design of the detection filters being considered in this section is trivial. The gain matrix D, in the filter implementation without the transformation, (Fig. 2-1), can be obtained as $D = D^{+} M^{-1}$. This gain matrix D is a detector gain for all actuator failure events as well, and the output error ϵ remains in the direction CAb_j when the *jth* actuator fails.

So far, two important advantages of detection filters with N = p over higher order filters have been shown: 1) these filters can be configured to detect **all** actuator failure events, and 2) the filter design is trivial. Now, their performance in the presence of model mismatch will be analyzed.

A detection filter with N = p = 4 was designed using Theorem 4.1 with all of its poles placed at -10 rad/sec (i.e., $\omega_F = 10$ rad/sec and $\xi = 1$). This detection filter was named Detection Filter #3.

Detection Filter #3:

# of modes = # of sensors = 4

failure events: all actuator failures

Poles: 8 detection space poles at -10 rad/sec

To be able to compare the performance of this filter with the performance of Detection Filters #1 and #2, the output ϵ is transformed with the pseudo inverse matrix R to detect only failures of actuators 3 and 4, as was done with the previous filters. That is, the matrix R in Fig. 4-26 is the pseudo inverse of the matrix CF:

$$R = [(CF)^T CF]^{-1} (CF)^T \tag{4.24}$$

where

$$CF = [CAb_3 \quad CAb_4]$$

Since the detection space poles of Detection Filter #3 are the same as in Filters #1 and #2, and since the transfer function from u_4 to E_4 (for complete failure of actuator 4) is still given by Eq.(4.4), the failure signature produced by the complete failure of actuator 4 is exactly the same as in Fig. 3-3.

It is easy to see that Detection Filter #3 is going to perform much better in the presence of parameter errors in control matrix B than Filters #2 and #1. The vectors $\Delta\mathbf{b}_j$ in Fig. 4-10 have the same structure as the actuator failure events $\mathbf{b}_j$ in (4.18). Therefore, the vectors $\Delta\mathbf{b}_j$ generate unidirectional error residuals governed by Eq. (4.3) with $\Delta\mathbf{b}_j$ and u_j in place of $\mathbf{b}_4$ and u_4. This means that the error residual generated by $\Delta\mathbf{b}_j$, when compared with the signature produced by $\mathbf{b}_j$, is of the same order as the percentage errors in $\mathbf{b}_j$. In other words, there is no direction-dependent amplification of $\Delta\mathbf{b}_j$ as in Filters #1 and #2.

Figure 4-27 shows the frequency response functions for the transfer from u_4 to the residuals E_3 and E_4, corresponding to 0.05% parameter errors in B. The low frequency gains are two orders of magnitude smaller than the gains for Detection Filter #2 shown in Fig. 4-14. Therefore, Detection Filter #3 will perform much better in the presence of parameter errors in B than Filters #1 and #2.

It is also reasonable to expect Detection Filter #3 to perform better in the presence of parameter errors in system matrix A, for the same reasons it performed better with parameter errors in B. The vector $\Delta\mathbf{a}_j$ in Fig. 4-9 also have the same structure as the actuator failure events $\mathbf{b}_j$, and therefore also generate unidirectional output through the dynamics of the detection spaces.

Figure 4-28 shows the response function of the transfer from the unmodeled eighth mode to the residuals E_3 and E_4. The low frequency gains are one order of magnitude smaller than for Detection Filter #2 in Fig. 4-16. Therefore, Detection

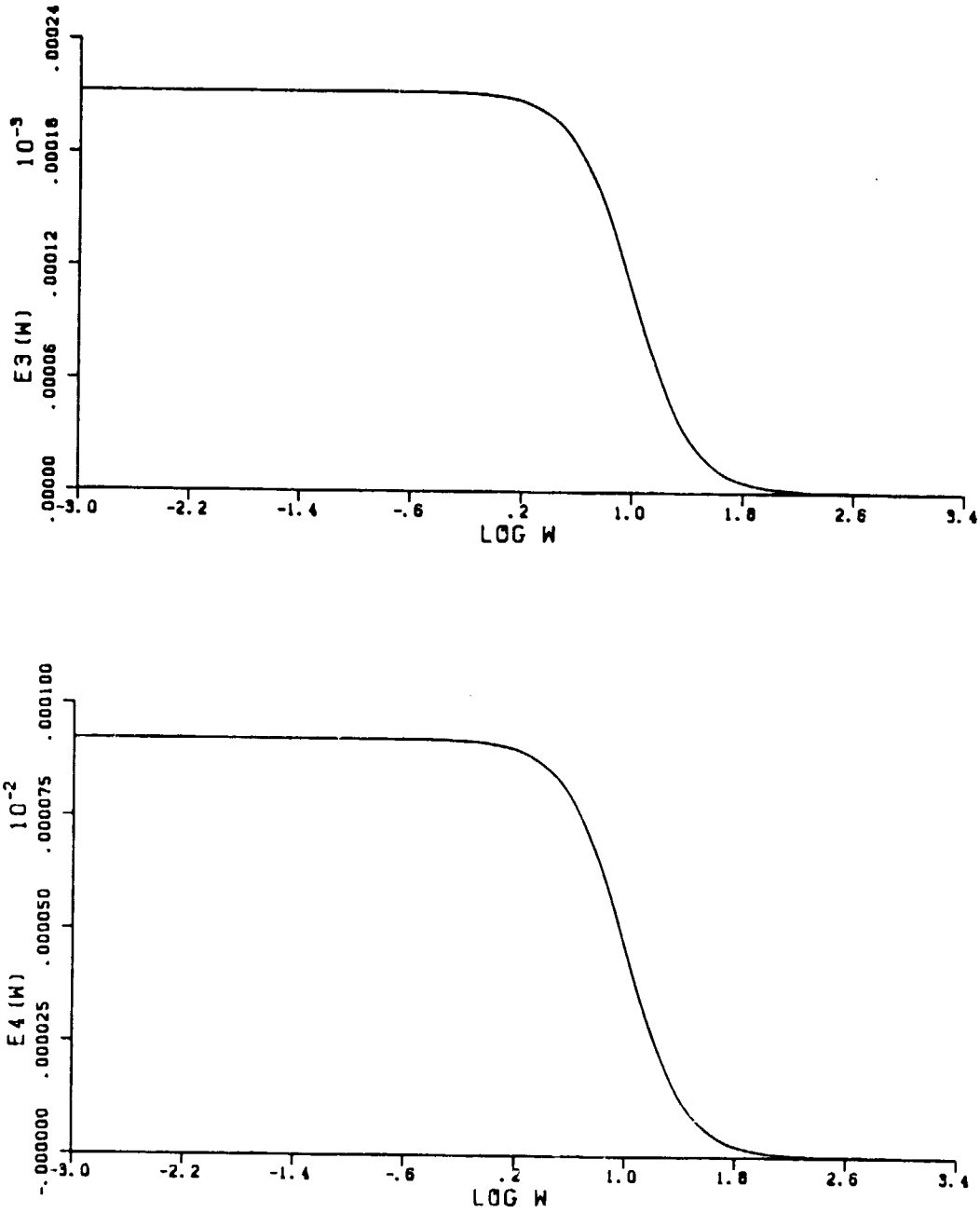

Figure 4-27: Detection Filter #3. Parameter Errors in B = 0.05%. Transfer from u_4 to E_3 and E_4. R = Pseudo Inverse.

Filter #3 will perform better in the presence of the unmodeled eighth mode than Filter #2. But, on the other hand, the fifth, sixth and seventh structural modes are unmodeled in Detection Filter #3, while they are modeled in Filter #2. In addition, these unmodeled modes have smaller natural frequencies than the eighth mode, and therefore, they are more excited. Hence, the problem of unmodeled modes is more serious in Detection Filter #3 than in Detection Filter #2.

Part of the problem of unmodeled dynamics in Detection Filter #3 can be solved by output filtering. Since the natural frequencies of the unmodeled modes are higher than the bandwidth of the filter (i.e., 10 rad/sec), by filtering the output error ϵ with a bandwidth of 10 rad/sec, the large components of the error residuals, due to the natural frequencies of the unmodeled modes passing through the direct path in Fig. 4-8, can be eliminated without affecting the failure signature. Therefore, the elements of the output error vector $\mathbf{E}$ were filtered by second order filters with bandwidths of 10 rad/sec. .

Figure 4-29 shows the results of the simulation of Detection Filter #3 with no model mismatch, with failure of actuator 4 at $T = 1$ sec. and with output filtering. Note that the failure signature is smaller than the failure signature produced with no output filtering in Fig. 3-3. This difference could have been avoided by choosing a slightly wider bandwidth for the output filters.

Detection Filter #3 was then tested in the presence of unmodeled dynamics. Figure 4-30 shows the results of the simulation of Detection Filter #3 with an 8 mode evaluation model of the beam, with failure of actuator 4 at $T = 1$ sec. and with output filtering. The error residuals due to the four unmodeled modes (the fifth, sixth seventh and eighth structural modes) completely obscure the failure signature. From the low frequency character of these error residuals, it can be concluded that the output filter was successful in eliminating the high frequency

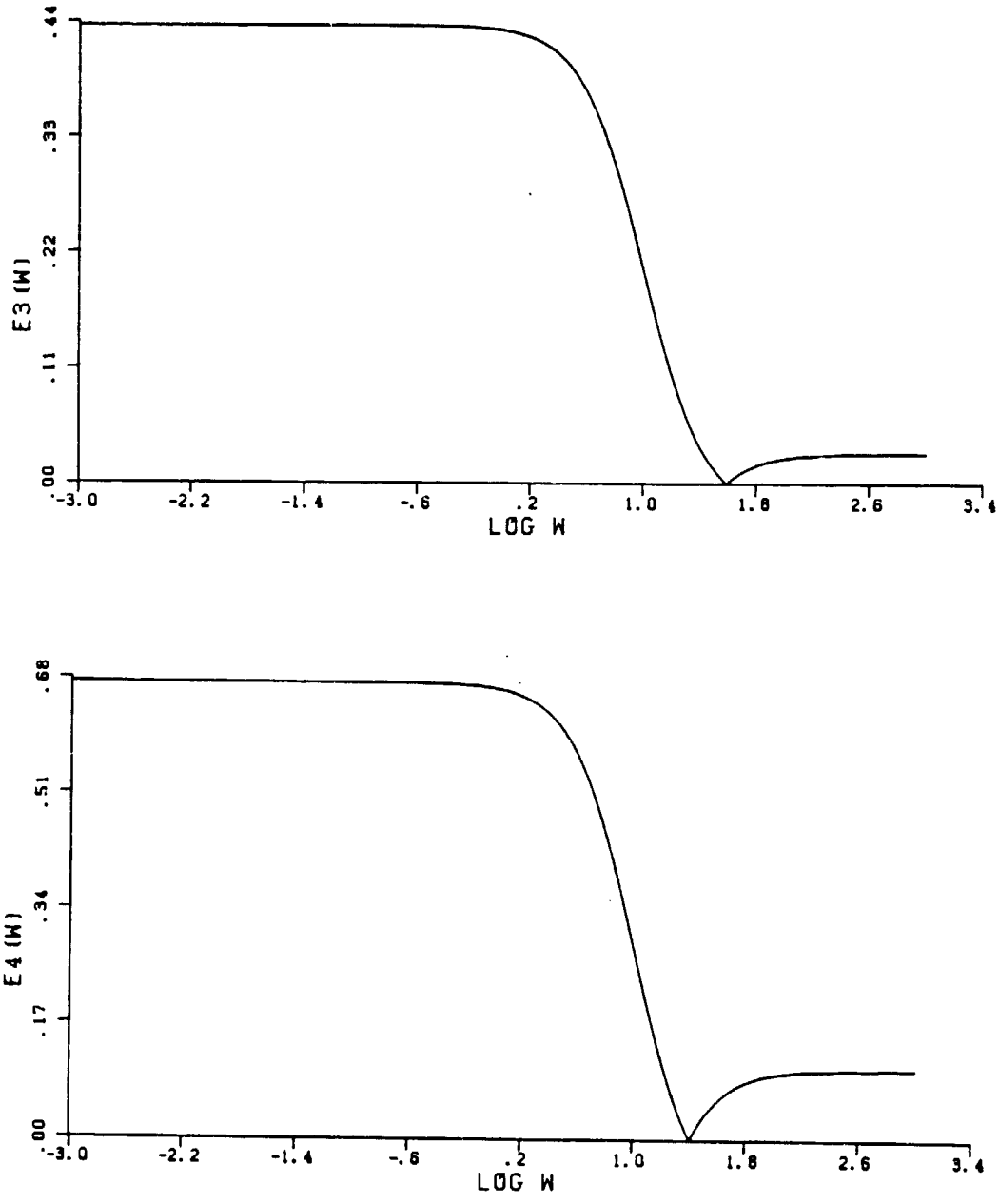

Figure 4-28: Detection Filter #3. Unmodeled Eighth Mode Transfer.
R = Pseudo Inverse

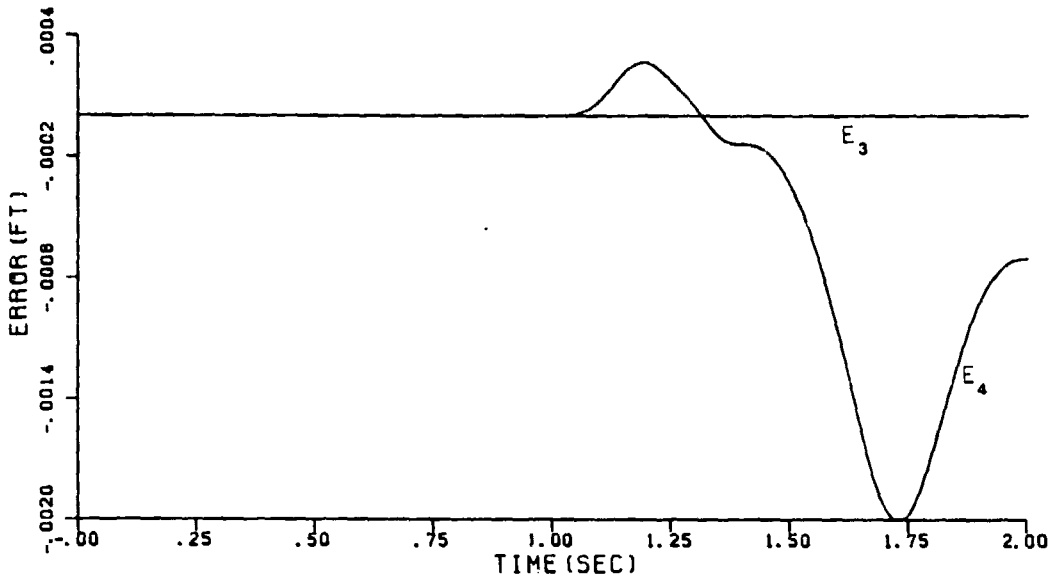

Figure 4-29: Detection Filter #3. No Model Mismatch. Actuator 4 Failure at T = 1 sec. . R = Pseudo Inverse. Output Filtering.

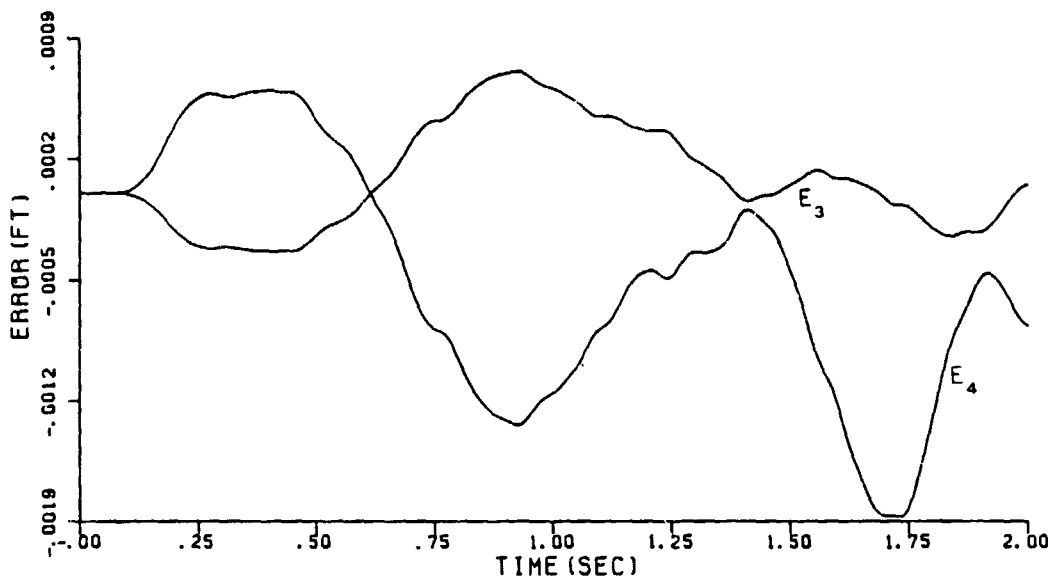

Figure 4-30: Detection Filter #3. Four Unmodeled Modes. Actuator 4 Failure at T = 1 sec. . R = Pseudo Inverse. Output Filtering.

components corresponding to the modal frequencies passing through the direct path. Then, the large error residuals are due to the low frequency components of the unmodeled mode amplitudes that lie within the bandwidth of the filter, and therefore, cannot be filtered out without affecting the failure signature.

In the next two sections, ways of improving the performance of Detection Filter #3 in the presence of unmodeled modes will be introduced.

4.3.2 Improved Output Transformation

An impressive improvement in the performance of Detection Filter #3 in the presence of model mismatch can be obtained by simply using a different output transformation R. But before introducing the new transformation, an analysis of the dynamics of the detection filter described in Theorem 4.1 is in order.

To simplify the analysis, only one unmodeled mode will be considered: the eighth structural mode. Then, the state and output error equations are

$$\begin{aligned} \dot{\mathbf{e}}(t) &= (A - D^+ C^+) \mathbf{e}(t) - D^+ \mathbf{c}_8^+ \psi_8(t) \\ \epsilon^+(t) &= C^+ \mathbf{e}(t) + \mathbf{c}_8^+ \psi_8(t) \\ \epsilon(t) &= M \epsilon^+(t) \end{aligned} \tag{4.25}$$

where

$$\mathbf{c}_8^+ = M^{-1} \mathbf{c}_8$$

and $\mathbf{c}_8$ is the column of the measurement matrix C corresponding to the amplitude of the eighth structural mode. Due to the structure of matrices A, D^+ and C^+, Eq.((4.25)) can be written as:

$$\dot{\mathbf{e}}_i = (A_i - \mathbf{d}_i^+ \mathbf{c}^T)\,\mathbf{e}_i - \mathbf{d}_i^+ c_{8i}\,\psi_8 \qquad (4.26)$$

$$\epsilon_i^+ = \mathbf{c}^T \mathbf{e}_i + c_{8i}\,\psi_8 \qquad i = 1, 2, \ldots N$$

where

$$\mathbf{e}_i = \begin{bmatrix} (\psi_i - \hat{\psi}_i) \\ \\ (\dot{\psi}_i - \hat{\dot{\psi}}_i) \end{bmatrix}$$

$$\mathbf{c}^T = [\,1 \quad 0\,]$$

$$A_i = \begin{bmatrix} 0 & 1 \\ \\ -\omega_i^2 & 0 \end{bmatrix}$$

and where $\mathbf{d}_i^+$ was defined in (4.19), c_{8i} is the *ith* element of the vector $\mathbf{c}_8^+$ and ϵ_i^+ is the *ith* element of the output error vector ϵ^+. The two elements of the vector $\mathbf{e}_i$ are the errors in the estimate of the amplitude of the *ith* structural mode and the error in the estimate of its rate of change. The block diagram corresponding to Eq. (4.26) is shown in Fig. 4-31.

From Eq. (4.26) and Fig. 4-31, it can be concluded that the error dynamics of the detection filter described in Theorem 4.1 are decoupled. That is, the detection filter estimates the modal amplitude ψ and its rate of change $\dot{\psi}$ for each structural mode separately. This decoupling is achieved in the following way. First, since the number of modes is equal to the number of independent displacement measurements, it is possible to calculate the modal amplitudes by transforming the measurement vector $\mathbf{y}$ to $\mathbf{y}^+$ as can be seen in (4.16). Second, the structure of the

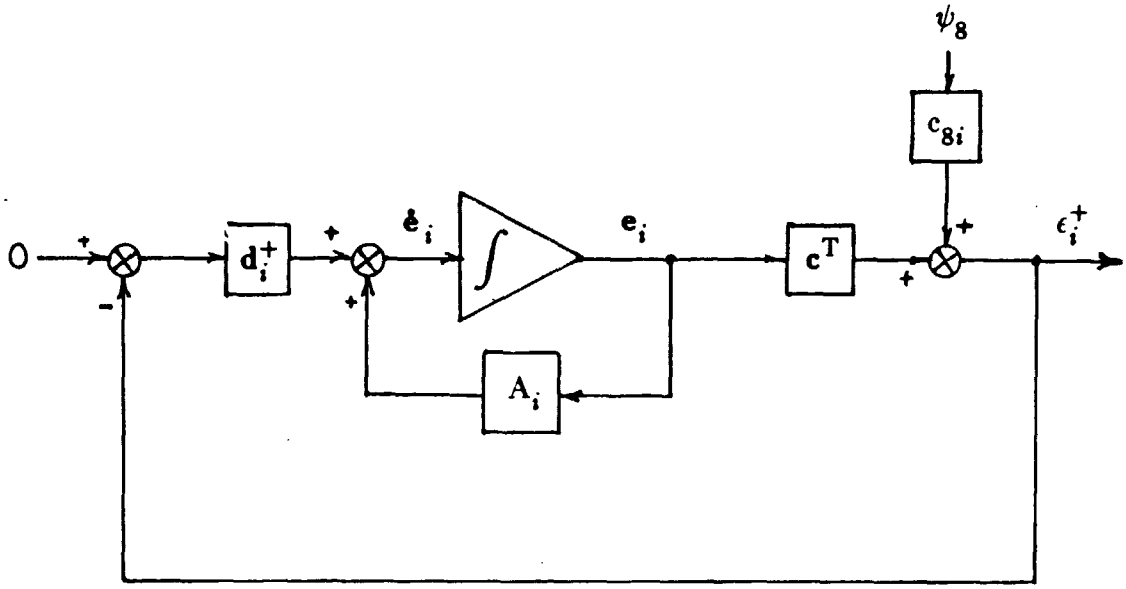

Figure 4-31: Decoupled Dynamics of Detection Filters with N = p.

gain matrix D^+ in (4.19) applies the residual ψ_i - $\bar{\psi}_i$ to the corresponding *ith* mode (see Figure 4-26).

The decoupled dynamics of the detection filter described in Theorem 4.1 are very easy to analyze. As can be seen in Fig. 4-31, the unmodeled modes can be treated as disturbances in the decoupled loops corresponding to each of the modeled modes. Then, the transfer from ψ_8 to ϵ_i^+can be easily obtained as:

$$\frac{\epsilon_i^+(s)}{c_{8i}\,\psi_8(s)} = \frac{s^2 + \omega_i^2}{s^2 + 2\xi\,\omega_F\,s + \omega_F^2} \tag{4.27}$$

This transfer function is called the Disturbance Transfer. Figure 4-32 shows th' Bode plots of the disturbance transfer for two modal frequencies, one larger than the bandwidth of the filter ω_F and the other smaller. Note that for $\omega_i > \omega_F$ there

is actually an amplification of the unmodeled mode noise within the bandwidth of the filter, while for $\omega_i < \omega_F$ there is an attenuation.

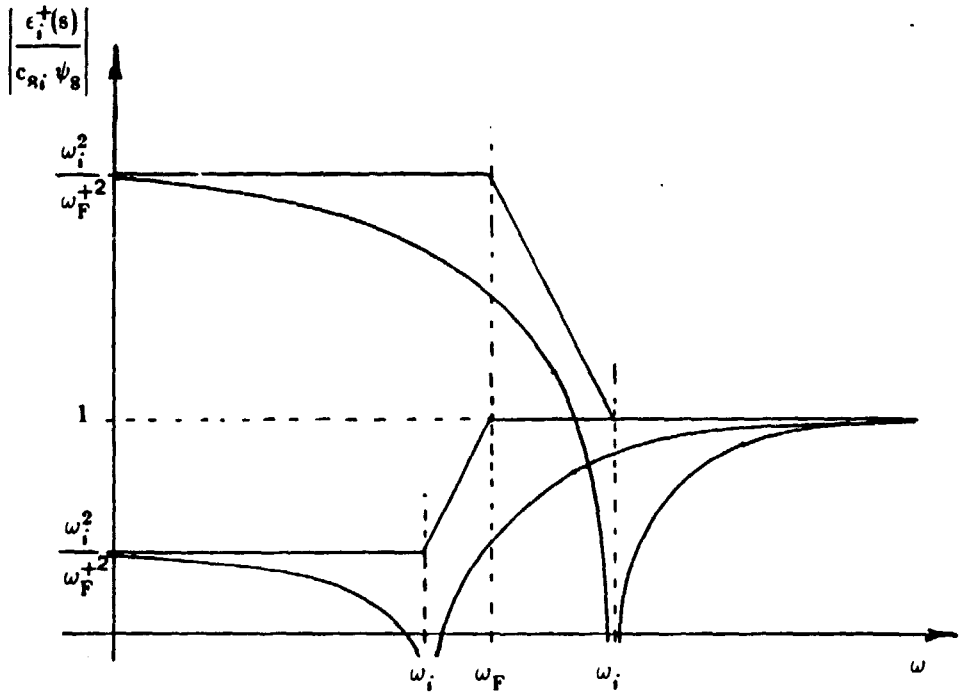

Figure 4-32: Frequency Response of the Disturbance Transfer.

There are four structural modes modeled into Detection Filter #3, two rigid modes and two bending modes. The rigid modes, with modal frequencies of 0 rad/sec., totally reject the unmodeled mode disturbance at low frequencies, because the low frequency gain of the disturbance transfer is zero. On the other hand, the bending modes with modal frequencies of 11.4 and 31.4 rad/sec. have disturbance transfers with low frequency gains of 1.3 and 9.8 respectively. Therefore, the large error residuals in Fig. 4-30 are due to the bending modes. Specifically, the presence of the unmodeled modes generates neglectable low frequency errors in the residuals ϵ_1^+ and ϵ_2^+ corresponding to the rigid modes, significant low frequency errors in the residual ϵ_3^+ corresponding to the first bending mode and very large low frequency

errors in the residual ϵ_4^+ corresponding to the second bending mode.

The output error vector ϵ is calculated from ϵ^+ as $\epsilon = M\,\epsilon^+$. Therefore, the large residuals ϵ_3^+ and ϵ_4^+ produced by the unmodeled modes generate large unidirectional errors in the directions of $\mathbf{c}_3$ and $\mathbf{c}_4$, respectively, in the output space of ϵ. Hence, by choosing a different output transformation R, the errors in the directions $\mathbf{c}_3$ and $\mathbf{c}_4$ can be separated in such a way that they no longer affect the failure signature. The improved output transformation that achieves this separation is:

$$R = [\, CA\mathbf{b}_3 \quad CA\mathbf{b}_4 \quad \mathbf{c}_3 \quad \mathbf{c}_4 \,]^{-1} \tag{4.28}$$

and the new transformed output error vector $\mathbf{E}$ is:

$$\mathbf{E} = R\,\epsilon = \begin{bmatrix} E_3 \\ E_4 \\ E_{b1} \\ E_{b2} \end{bmatrix}$$

where E_3 and E_4 contain the failure signatures of actuators 3 and 4 respectively, and E_{b1} and E_{b2} only contain the error residuals due to the unmodeled modes, and correspond to the first and second bending mode respectively (actually $E_{b1} = \epsilon_3^+$ and $E_{b2} = \epsilon_4^+$).

Figure 4-33 shows the frequency response functions for the transfer from the unmodeled eighth mode ψ_8 to the residuals E_3 and E_4 obtained using the improved transformation R in (4.28), for Detection Filter #3 with no output filtering. These

response functions show a remarkable improvement when compared with the response functions in Fig. 4-28 obtained using the pseudo inverse as the output transformation. Note that the low frequency gains are actually zero. It is important to stress that these gains are zero because the low frequency gains of the disturbance transfers of the rigid modes are zero. That is, the zero low frequency gains in Fig. 4-33 are not particular to the unmodeled eighth mode, but they will occur in the transfers of all the unmodeled modes.

The use of the improved output transformation solves the problem of the unmodeled modes only at low frequencies within the bandwidth of the filter. Output filtering is still needed to eliminate the high frequency components of the residuals that lie outside the bandwidth of the filter. Detection Filter#3 with output filtering and with the improved transformation was then tested in the presence of four unmodeled modes and failure of actuator 4 at T = 1 sec.. Figure 4-34 shows the result of this simulation which was done under exactly the same conditions as the simulation in Fig. 4-30, but with a different output transformation. The improvement is remarkable. The low frequency components of the residuals have been totally eliminated and the failure signature is now clearly visible. The small error residuals consist mainly of a high frequency component at the frequency of the first unmodeled mode (i.e., 61.25 rad/sec.), that was not filtered out completely by the output filter. This high frequency component can be reduced further by increasing the order of the output filter.

As mentioned earlier in this chapter, the state and output error equations with parameter errors in matrix C have the same structure as the error equations with unmodeled modes (see Fig. 4-11). Then, it is easy to see that the use of the improved output transformation produces transfers from ψ_i to the residuals E_3 and E_4 with zero low frequency gains. Therefore, the use of the improved output

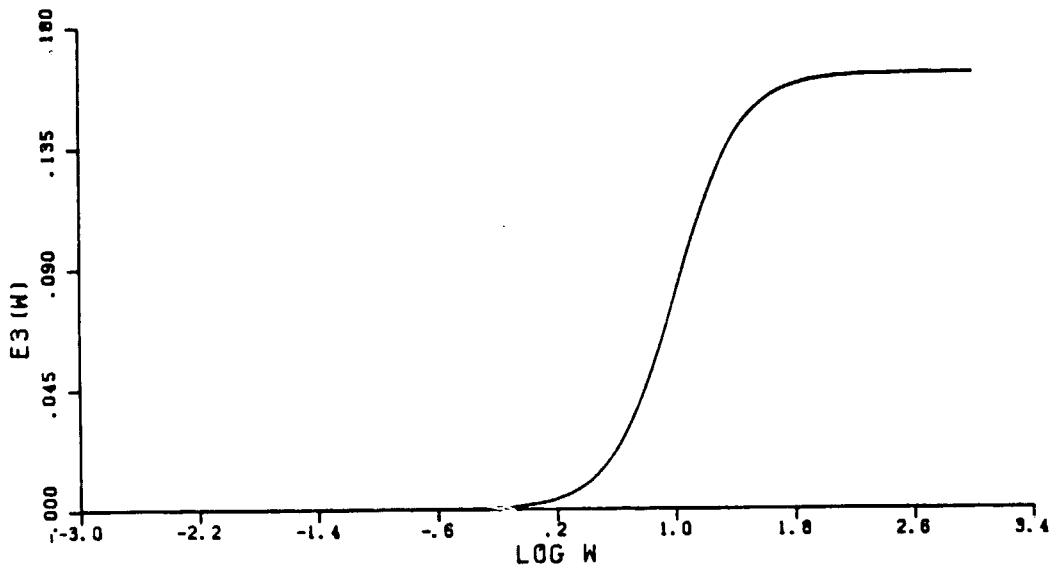

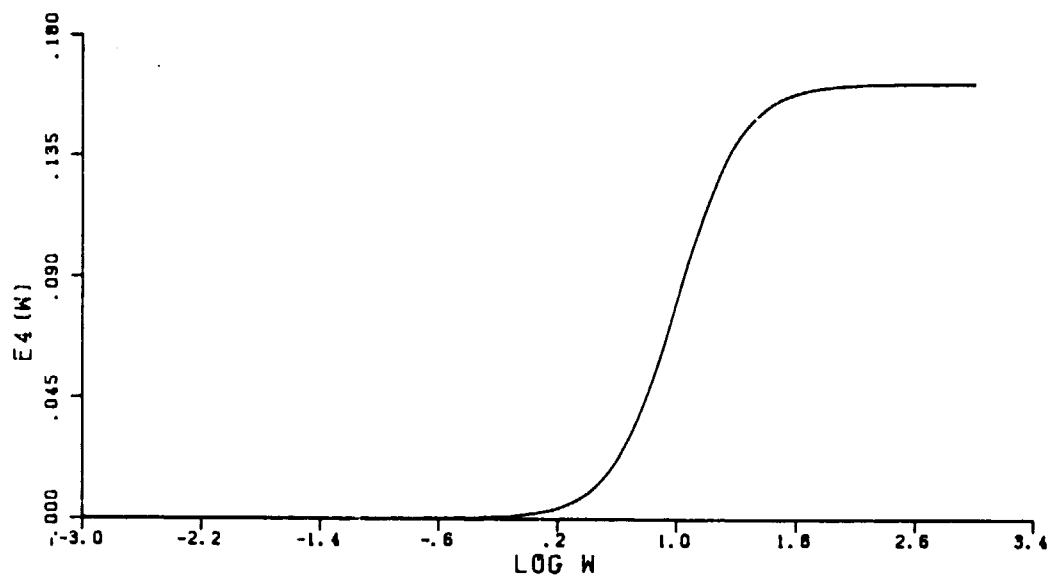

Figure 4-33: Detection Filter #3. Unmodeled Eighth Mode Transfer.
R = Improved Transformation.

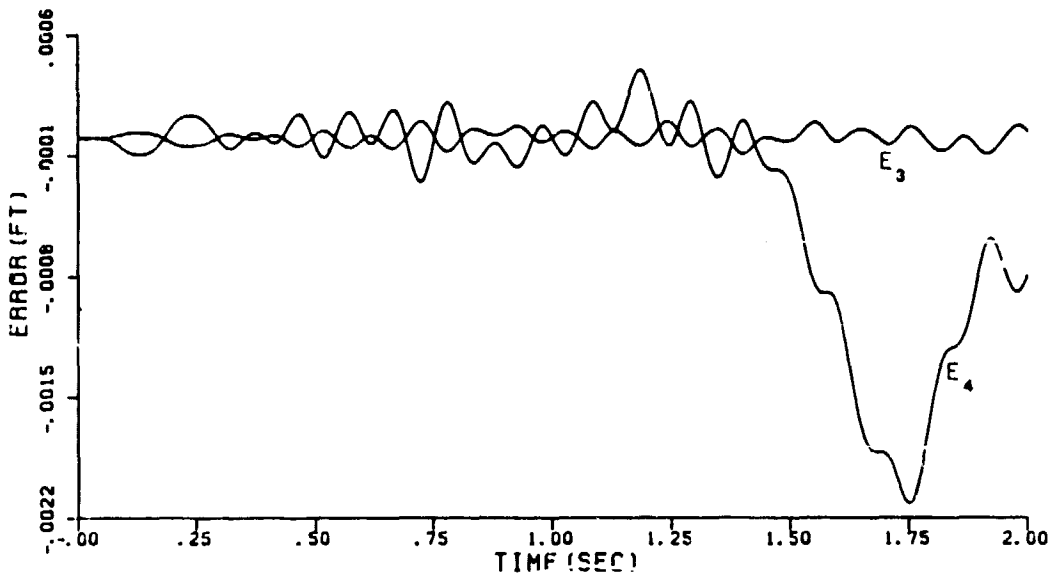

Figure 4-34: Detection Filter #3. Four Unmodeled Modes. Actuator 4 Failure at T = 1 sec.. R = Improved Transformation. Output Filtering.

transformation also produces remarkable improvements in the performance of the filter in the presence of parameter errors in C.

The parameter errors in the system matrix A consist only of the errors in the frequencies of the two bending modes. From Fig. 4-9 and Fig. 4-21, it can be seen that these errors affect only the loops corresponding to the bending modes, and therefore, only generate errors in the residuals ϵ_3^+ and ϵ_4^+. Then, for the same reasons explained before, the improved transformation totally separates these errors from the failure signature. That is, the transfers from ψ_i to E_3 and E_4 are zero at all frequencies, and therefore, the errors in the frequency of the two bending modes generate absolutely no errors in the residuals E_3 and E_4.

In the previous section, it was shown that Detection Filter #3 represented a large improvement in the performance in the presence of parameter errors in B. The new output transformation, however, only introduces a minor improvement.

With this transformation, only the errors in B corresponding to the modal shapes of the rigid modes generate errors in the residuals E_3 and E_4. It is important to note that the shapes of the rigid modes are usually very well known. Therefore, the results shown in Figures 4-35 and 4-36 with 5% and 10% parameter errors in B are too pessimistic.

Detection Filter #3, with output filtering and with the improved output transformation, was then tested in the presence of all types of model mismatch and with actuator 4 failure time at T = 1 sec.. Figure 4-35 shows the results of the simulation with four unmodeled modes and with 5% parameter uncertainties in all the matrices A, B and C. Figure 4-36 shows the results of the same simulation but with 10% parameter uncertainties in A, B and C. In both cases the failure signature is clearly visible, and therefore, for the first time in this thesis it is possible to detect and identify the failure of actuator 3 and 4 under realistic conditions.

The use of the new output transformation results in very large improvements in the performance of the filter in the presence of model mismatch. For this reason, in the rest of this section, the new output transformation will be analyzed a little further, and a new way of reading the detection information from the output error will be introduced.

During nominal operation the error residuals due to model mismatch lie mainly in a plane spanned by the vectors $\mathbf{c}_3$ and $\mathbf{c}_4$, as was shown earlier in this section. Then, when failure of actuator 3 or 4 occurs, the error residuals lie in the space spanned by the vectors $CA\mathbf{b}_3$, $\mathbf{c}_3$ and $\mathbf{c}_4$ or $CA\mathbf{b}_4$, $\mathbf{c}_3$ and $\mathbf{c}_4$ respectively. So, there are actually three output error spaces associated with this detection problem, one space corresponding to the nominal operation and two spaces corresponding to the failure of actuators 3 and 4. The improved output transformation produces

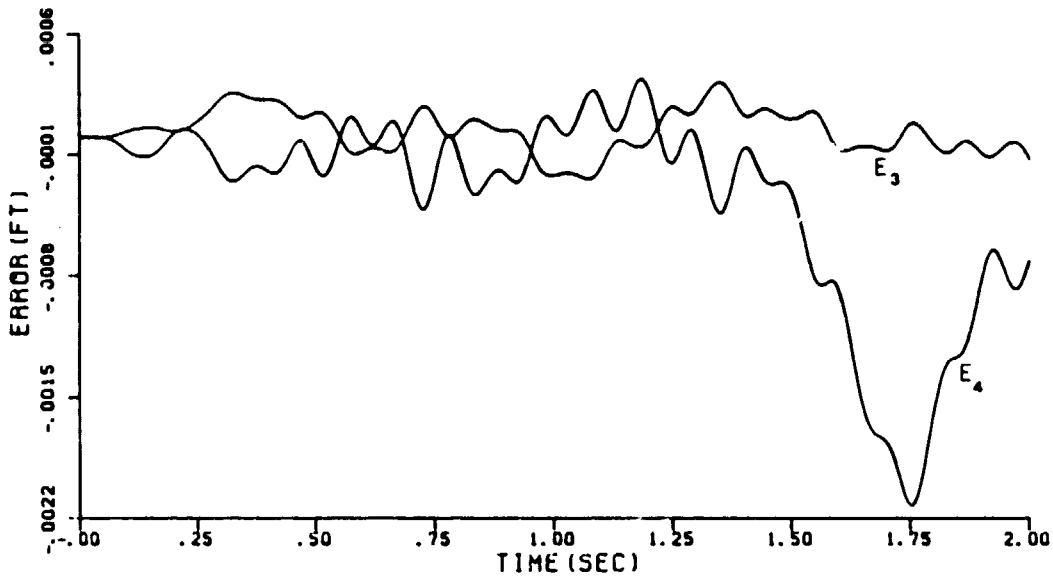

Figure 4-35: Detection Filter #3. Four Unmodeled Modes. Parameter Errors in A, B and C = 5%. Actuator 4 Failure at T = 1 sec.. R = Improved Transformation. Output Filtering.

excellent results because it is able to distinguish between these three spaces. During nominal operation, it generates large error residuals in E_{b_1} and E_{b_2}. and when actuator 3 or 4 fails, it generates large error residuals in E_3, E_{b_1} and E_{b_2} or E_4, E_{b_1} and E_{b_2} respectively. Therefore, the residuals E_3 and E_4 can detect and identify the failure of actuator 3 and 4 in the presence of model mismatch.

Detection Filter #3, as mentioned earlier in this section, produces unidirectional output with any actuator failure event. However, the improved transformation in (4.28) cannot be configured to detect more than two actuator failure events since two directions of the transformation have to be dedicated to suppress the effects of model mismatch. Therefore, Detection Filter #3 requires two improved output transformations in order to detect and identify the four actuator failure events. For example, one transformation can be configured to

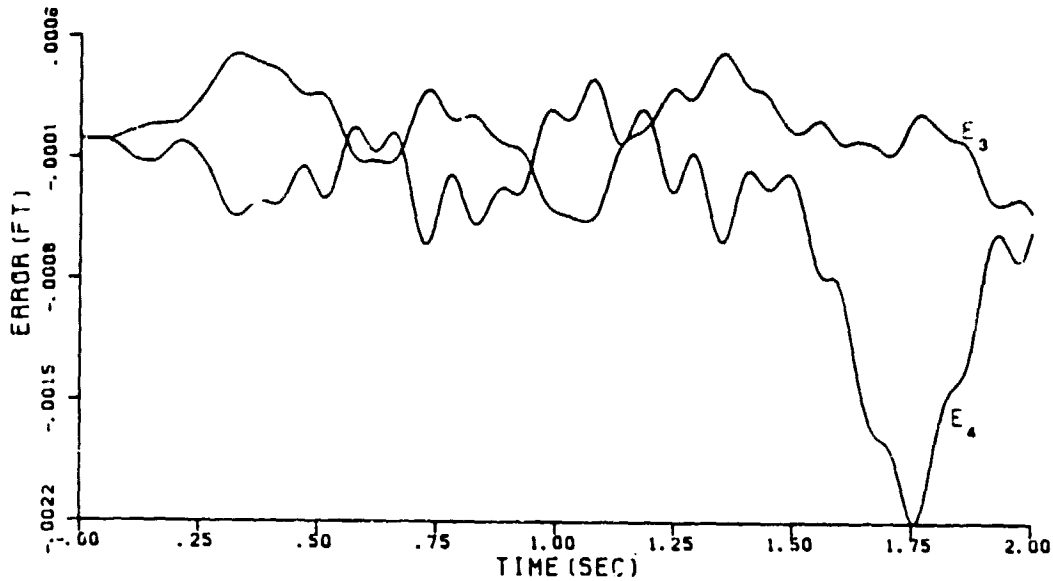

Figure 4-36: Detection Filter #3. Four Unmodeled Modes. Parameter Errors in A, B and C = 10%. Actuator 4 Failure at T = 1 sec.. R = Improved Transformation. Output Filtering.

detect failure of actuators 1 and 2, and the other transformation can be configured to detect failure of actuators 3 and 4. Then, when actuator 1 fails, the residual E_1 will grow while E_2 will remain zero in the first transformation, and the residuals E_3 and E_4 in the second transformation will both grow. Thus, the growth of three residuals are needed to identify the failed actuator. This is a very undesirable result because it complicates the decision algorithms and also increases the possibilities of incorrect identifications.

A new way of reading the output error information that can identify the failure of any number of actuators, will now be explained. Even though this new way has some interesting advantages when compared with the output transformation, the main reason it is introduced here is to help gain more insight into the detection filter problem.

The new approach, used in conjunction with output filtering, is illustrated in Fig. 4-37. Note that the output error ϵ^+ is used instead of ϵ, the reasons for this becoming clear later. Each component of the vector ϵ^+ is filtered with a bandwidth of 10 rad/sec. to eliminate the high frequency components produced by model mismatch (the output filters have to be identical to preserve the unidirectionality of ϵ^+ when a failure occurs). The filtered output error will be called $\mathbf{v}$. When the *jth* actuator fails, the output error $\mathbf{v}$ remains in the single direction given by the vector $\mathbf{b}_j^+$in (4.22).

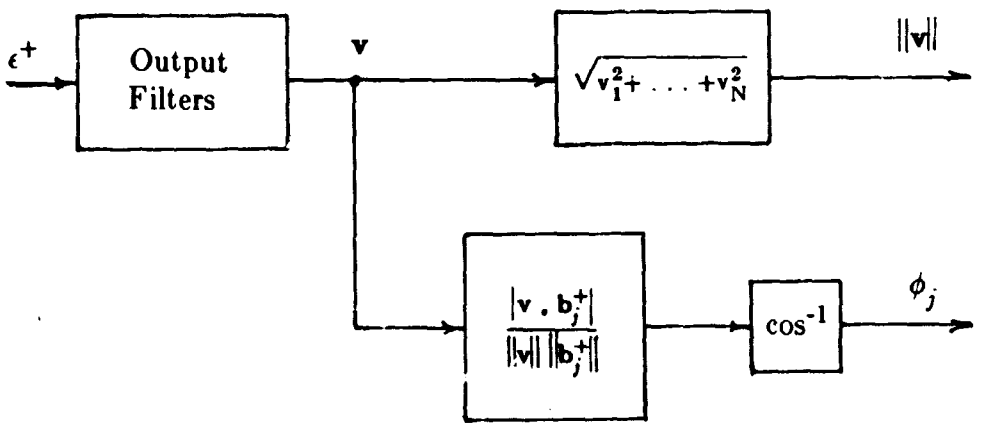

Figure 4-37: New Output Error Processing

The new approach, unlike the transformations used so far, treats the detection and identification problems separately. Detection is based on the norm of the output error vector $\mathbf{v}$. During nominal operation, the detection residual $\|\mathbf{v}\|$ is zero, if there is no model mismatch, and when a failure occurs, it becomes significantly nonzero. Therefore, by looking at the detection residual $\|\mathbf{v}\|$, the failure of any actuator (actually any component) can be detected. To identify

which component has failed, p directionality residuals are generated that represent the angles from 0 to 90 degress between the output error vector **v** and the output directions $\mathbf{b}_j^+$ for $j = 1, 2 \ldots p$, corresponding to each actuator failure. During nominal operation, these residuals have no significance, and therefore, are not computed. When the *jth* actuator fails, the output error **v** remains in the direction of vector $\mathbf{b}_j^+$ and therefore the directionality residual ϕ_j is zero while the other directionality residuals have a nonzero value between 0 and 90 degrees. Hence, the actuator that failed is the one corresponding to the directionality residual that was zero (or closest to zero in the presence of model mismatch).

In an operational system, the directionality residuals should be computed only when the detection residual becomes larger than a certain tolerance indicating that a component has failed. In this thesis, however, since the interest is to analyze the character of the residuals without actually making any decisions, the directionality residuals will be computed starting at T = 1 sec., which is the time at which the failure occurs.

As mentioned earlier in this section, the presence of unmodeled modes generates large low frequency errors in the residuals ϵ_3^+ and ϵ_4^+ corresponding to the bending modes while generating negligible errors in the residuals ϵ_1^+ and ϵ_2^+. ϵ_3^+ and ϵ_4^+ can be eliminated by only using ϵ_1^+ and ϵ_2^+ and the components of $\mathbf{b}_j^+$ corresponding to the rigid modes, b_{j1}^+ and b_{j2}^+, in the computation of the detection and directionality residuals. But, since ϵ_3^+ and ϵ_4^+ are no longer needed in the residual generation, there is no need for the detection filter to estimate the amplitudes and amplitude rates of the bending modes and therefore, the states of the detection filter corresponding to the bending modes can be eliminated. Hence, the detection filter in the configuration shown in Fig. 4-26 will have only the four states corresponding to the rigid modes. However, the measurement transformation

matrix M must remain the same (4 × 4 nonsingular matrix) and therefore, the mode shapes of the first two bending modes are still needed in the design of this filter.

A Detection Filter designed in this way is characterized as having 4 modeled modes and 2 detection and identification modes. Such a filter, then, has 4 states: the number of detection and identification modes times two. A detection filter with these characteristics was designed and was named Detection Filter #4.

Detection Filter #4:

# of modeled modes = 4

# of detection and identification modes = 2 (4 states)

Poles: 4 detection space poles at -10rad/sec.

Detection Filter #4 uses the errors in the estimates of the rigid modes amplitudes produced by the failure of an actuator to detect and identify the failed actuator.

All the detection filters will be tested with output filtering, as shown in Fig. 4-37, even in the case of no model mismatch, for the rest of this section.

Figures 4-38 and 4-39 show the results of the simulations of Detection Filter #4 with no model mismatch and with failure of actuators 1 and 4, respectively, at T = 1 sec..

In both cases, the actuator failures create clearly evident signatures in the detection residuals. Also, in both cases, the directionality residuals corresponding to the failed actuators remain at zero while the other directionality residuals become clearly greater than zero.

However, these simulations show a big difference in the "ability" of Detection

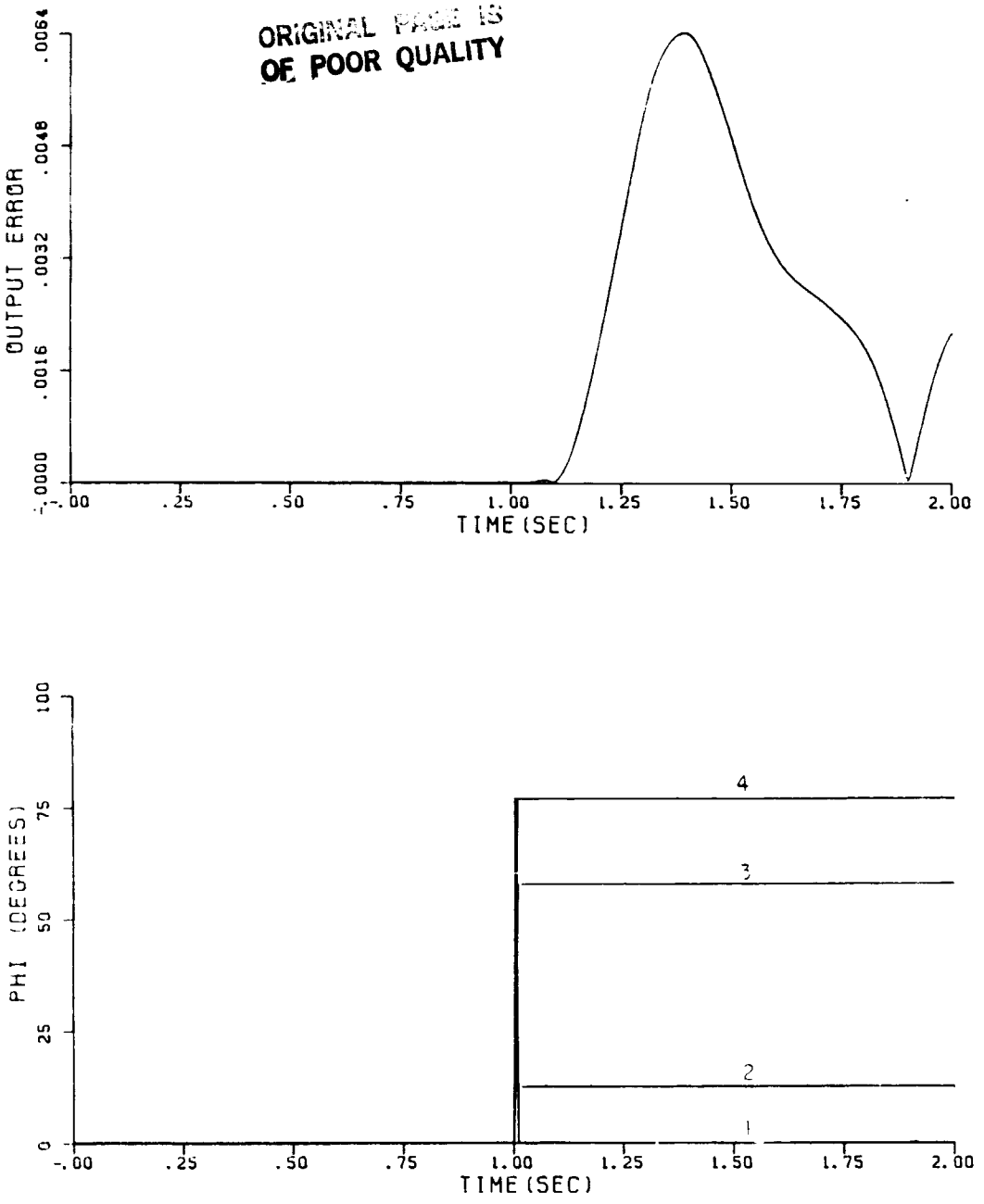

Figure 4-38: Detection Filter #4. No Model Mismatch. Actuator 1 Failure at T = 1 sec.. Output Filtering.

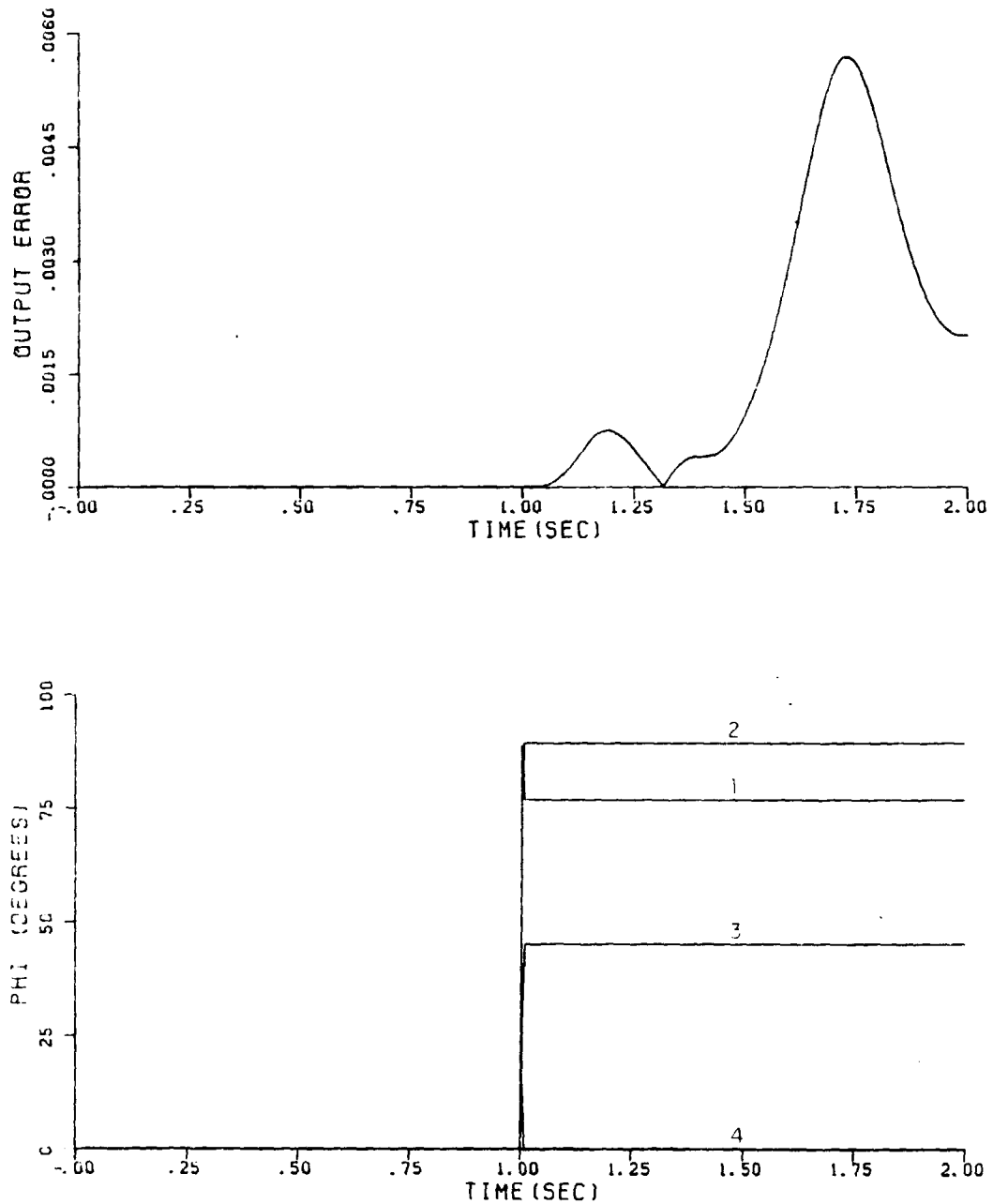

Figure 4-39: Detection Filter #4. No Model Mismatch. Actuator 4 Failure at T = 1 sec.. Output Filtering.

Filter #4 to identify correctly the actuator that failed in the presence of model mismatch. It is intuitively clear that the ability of the detection filter to identify correctly the failure of the *jth* actuator in the presence of model mismatch is related to the smallest of the angular distances between the output direction corresponding to actuator *j* failure and the output directions corresponding to the other actuator failures. If this angle is large, it will take a large error residual due to model mismatch to "rotate" the output error in order to result in an incorrect or undetermined identification. If this angle is small, the opposite happens. From now on, this angle will be referred to as the "phase margin for actuator *j*." The phase margin for actuator 1 is 12 degrees while for actuator 4 is 44 degrees. Therefore, the ability of Detection Filter #4 to identify correctly the failure of actuator 1 in the presence of model mismatch, is much smaller than its ability to identify correctly the failure of actuator 4.

The physical interpretation of the phase margin is very clear. The phase margin for actuator 1 corresponds to the angular distance between the failure direction of actuator 1 and the failure direction of actuator 2, as can be seen in Fig. 4-38. These two actuators are placed next to each other, with a separation of 2 feet, at the end of the beam (Fig. 3-1). The control effects of each of the actuators upon the rigid mode corresponding to the displacement of the beam, are identical. Therefore, what differentiates the failure of actuator 1 from the failure of actuator 2, is the difference in the control of these actuators upon the rigid mode corresponding to rotation. Since they are placed close together at the end of the beam, they both have very similar influence on the rotation of the beam. Therefore, since the effect upon the rotation and displacement of the beam due to a control being applied to actuator 1 is very similar to the effect due to the same control being applied to actuator 2, it is very difficult to distinguish between the

failures of those two actuators from the amplitudes of the rigid modes.

On the other hand, since actuator 4 is 3.5 feet away from the closest actuator, actuator 3, and since this actuator is at the center of the beam, the difference in the control of these actuators upon the rotation and translation of the beam, is much larger. This accounts for the large phase margin for actuator 4.

Detection Filter #4 was then tested in the presence of four unmodeled modes. Figure 4-40 shows the results corresponding to the failure of actuator 1 and Fig. 4-41 shows the results corresponding to the failure of actuator 4. In both cases, the failure signatures in the detection residuals were much larger than the noise due to model mismatch. The dominant component in the noise has the frequency of the first unmodeled mode that was not completely eliminated by the output filter, as was the case for Detection Filter #3 in Fig. 4-34. The analysis of the directionality residuals is a little more involved. Whenever the failure signature is smaller than the noise due to model mismatch, the output error is dominated by the noise, and therefore, it is no longer unidirectional thus producing the large rapid vertical oscillations. Hence, the directionality residuals are significant only when the failure signature, in the detection residual, is larger than the background noise, and even in this case it is not guaranteed that the directionality residuals will identify correctly the failed actuator. For example, in the case of failure of actuator 1, the failure can be correctly, but marginally, identified for a very short period of time, even though the failure signature is much larger than the noise during most of the failure interval. On the other hand, the failure of actuator 4 can be clearly identified whenever the failure signature becomes a little larger than the noise.

The poor performance of Detection Filter #4 when trying to identify the failure of actuator 1, was not due to large model mismatch noise, but rather due to the small phase margin for actuator 1. In fact, the noise was much smaller than

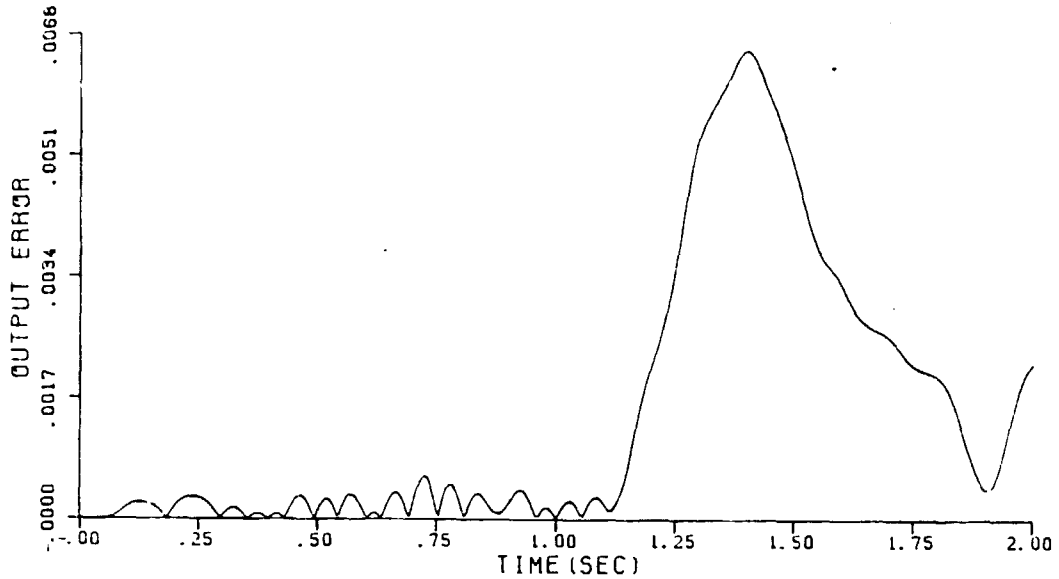

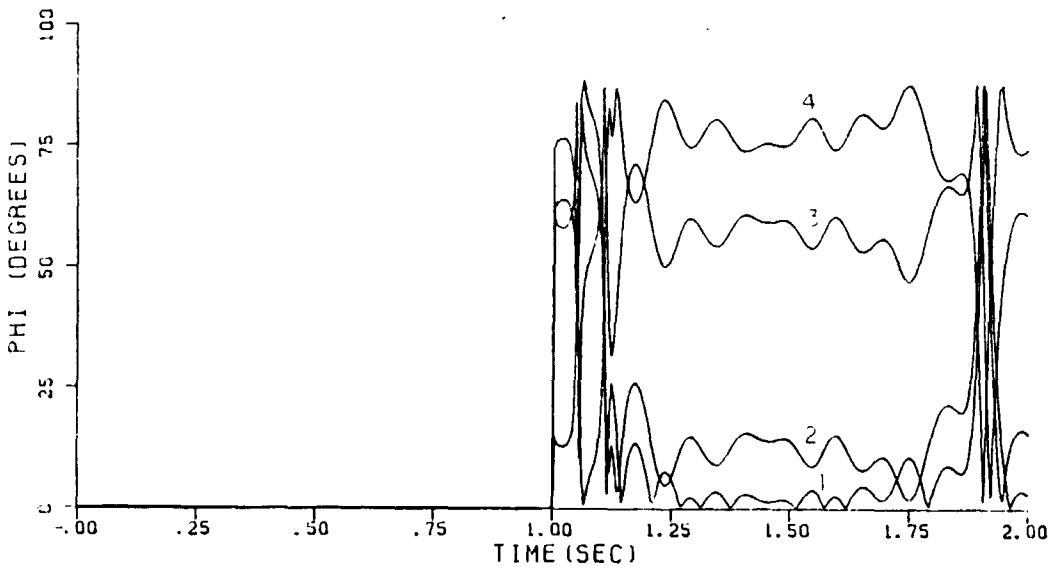

Figure 4-40: Detection Filter #4. Four Unmodeled Modes. Actuator 1 Failure at T = 1 sec.. Output Filtering.

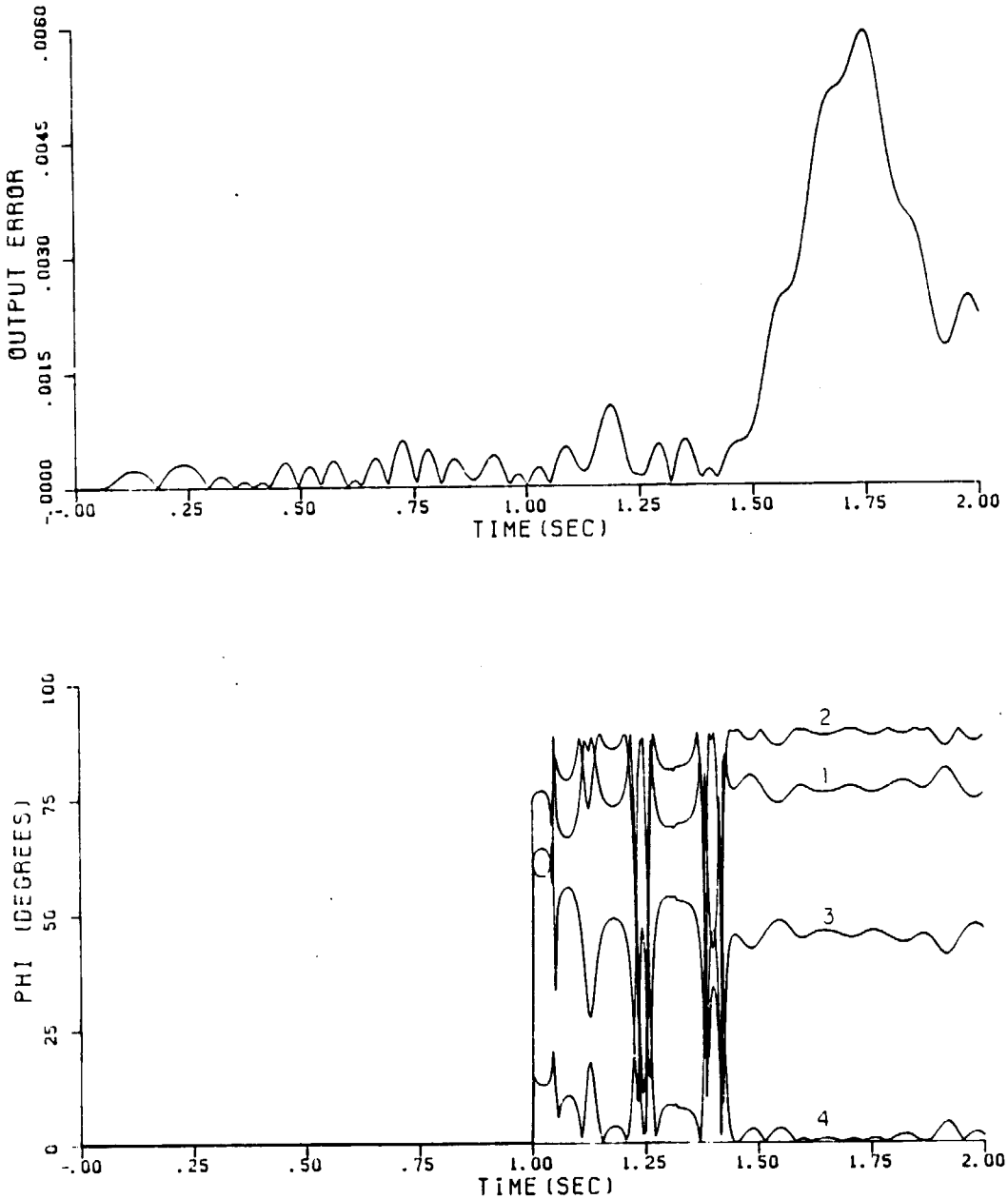

Figure 4-41: Detection Filter #4. Four Unmodeled Modes. Actuator 4 Failure at T = 1 sec.. Output Filtering.

the failure signature, allowing a very clear detection of the failure. One way of solving this problem is to increase the orders of the output filters in order to reduce the noise even further. Another solution, is to increase the phase margin for actuator 1 by augmenting the number of detection and identification modes. However, keep in mind that the estimation of the higher frequency modes are more affected by noise, and that was the reason for eliminating them in the design of Detection Filter #4. Therefore, this approach will be successful only if the improvement resulting from the larger phase margin is greater than the increase in noise due to model mismatch. To test this solution, Detection Filter #5 was designed with 4 modeled modes and 3 detection and identification modes.

Detection Filter #5:

# of modeled modes = 4

# of detection and identification modes = 3 (6 states)

#Poles: 6 detection space poles at -10rad/sec..

Detection Filter #5 uses the two rigid modes and the first bending mode in the process of detecting and identifying an actuator failure. Figure 4-42 shows the results of testing Detection Filter #5 with no model mismatch and with failure of actuator 1 at T = 1 sec.. Note that by incorporating the bending mode, the phase margin for actuator 1 increased from 12 to 37 degrees.

Detection Filter #5 was then tested with four unmodeled modes and failure of actuator 1 at T = 1 sec.. The results of this simulation are shown in Fig. 4-43. The failure signature is still clearly evident in the detection residual and the result of adding a bending mode to the filter only produced a very small increase in the low frequency components of the noise. The larger phase margin, combined with a very low increase in noise, resulted in directionality residuals that clearly identify

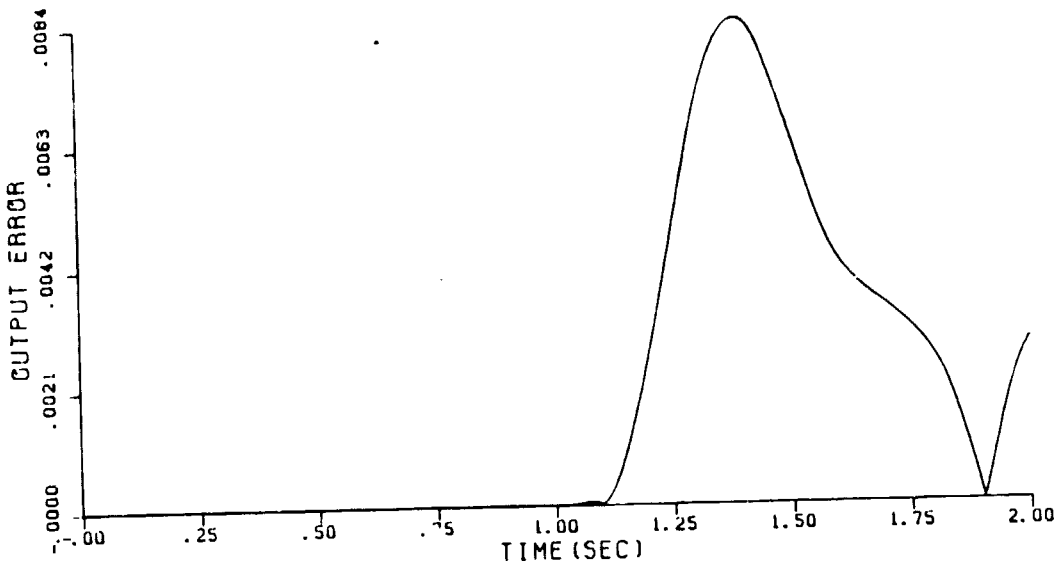

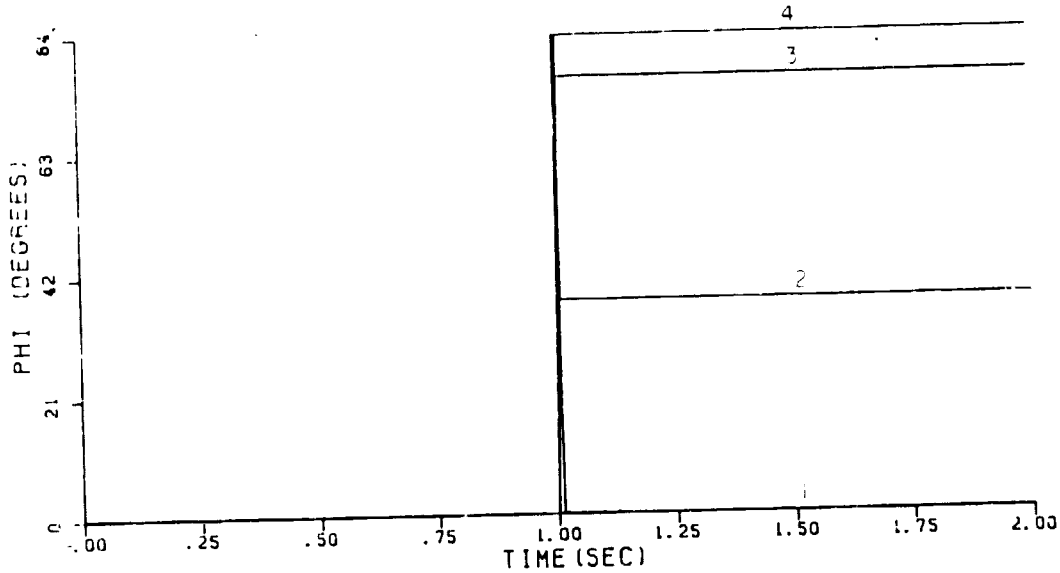

Figure 4-42: Detection Filter #5. No Unmodeled Modes. Actuator 1 Failure at T = 1 sec.. Output Filtering

the failure of actuator 1. Therefore, it can be concluded that the addition of the bending mode to the filter was sucessful in improving the identification capabilities of the filter.

To clarify what has been explained so far, the second bending mode will be added to the filter. Then, the resulting filter is Detection Filter #3 and the only difference is in the processing of the output error. Figure 4-44 shows the results of the simulation of Detection Filter #3 with no model mismatch and actuator 1 failure at T = 1 sec.. The phase margin increased to 70 degrees, twice the phase margin of Detection Filter #5. Figure 4-45 shows the same simulation but with four unmodeled modes. The detection capabilities of the filter have been greatly impaired by the presence of large low frequency error residuals due to model mismatch. As explained earlier in this section, the large low frequency residuals are due to the large low frequency gain of the disturbance transfer corresponding to the second bending mode. However, note that the detection residual can still be generated from the rigid modes only, as was done in Detection Filter #4, while using the four modes in the calculation of the directionality residuals. In such a case, the advantage of the very low noise of the rigid modes in the detection of the failures, is combined with the advantage of the larger phase margin of the higher order filter in the identification of the failure. The results of the directionality residuals may be a little misleading. These residuals correctly indicate the failure of actuator 1. However, since the noise due to model mismatch is very slowly varying, it is not clear whether the residuals would continue to indicate correctly the failure of actuator 1 if the simulation was continued beyond 2 seconds.

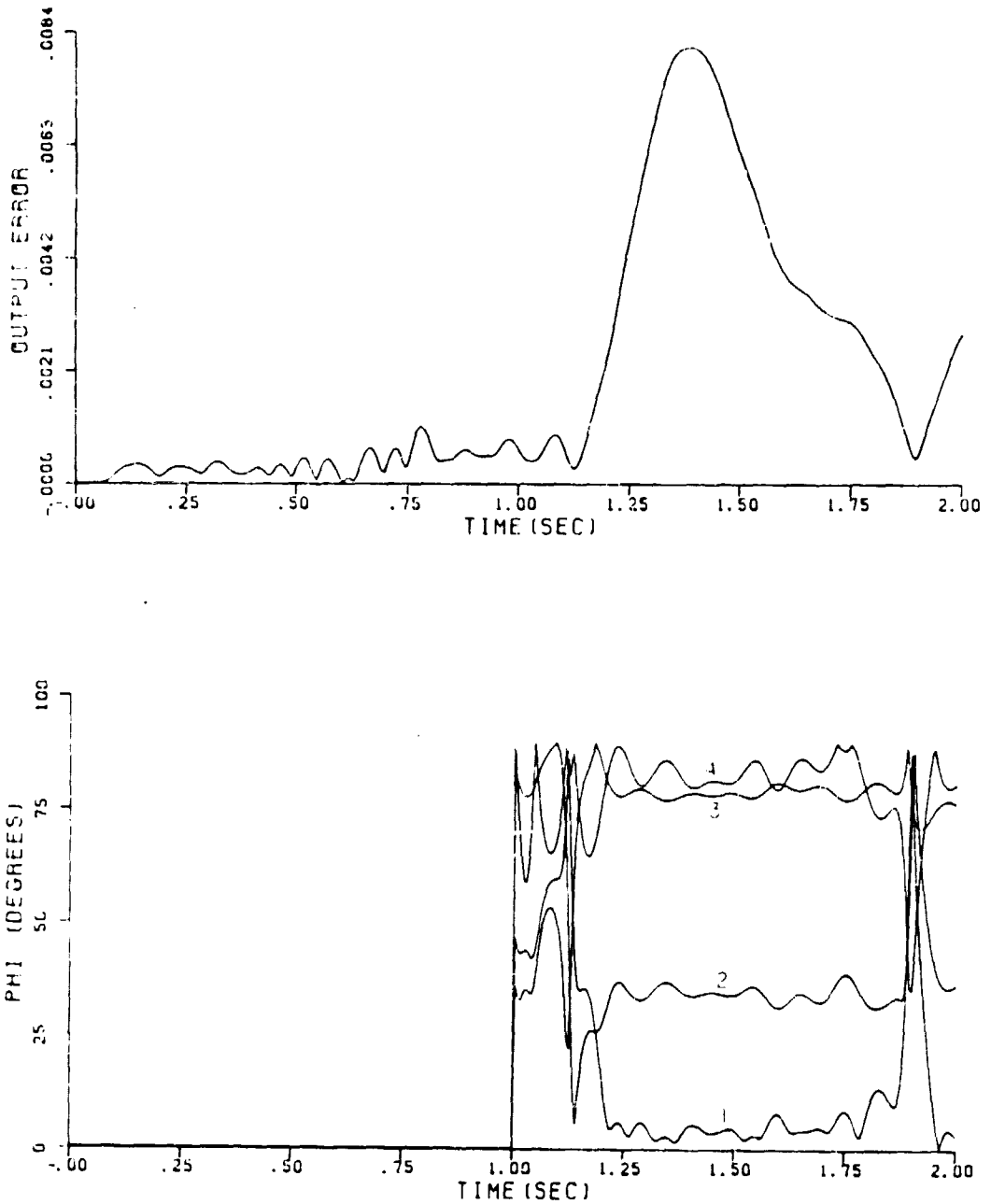

Figure 4-43: Detection Filter #5. Four Unmodeled Modes. Actuator 1 Failure at T = 1 sec.. Output Filtering.

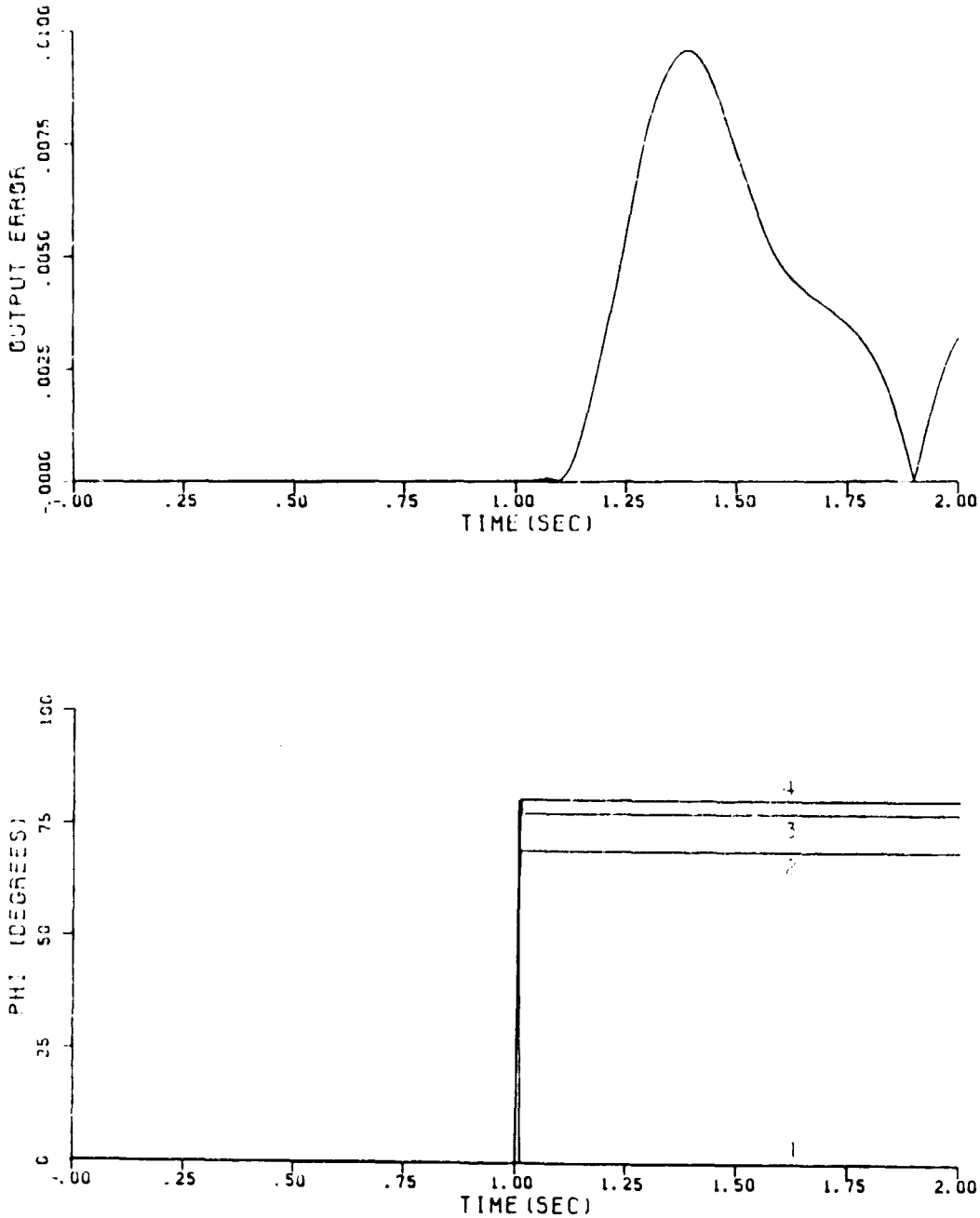

Figure 4-44: Detection Filter #3. No Model Mismatch. Actuator 1 Failure at T = 1 sec.. Output Filtering.

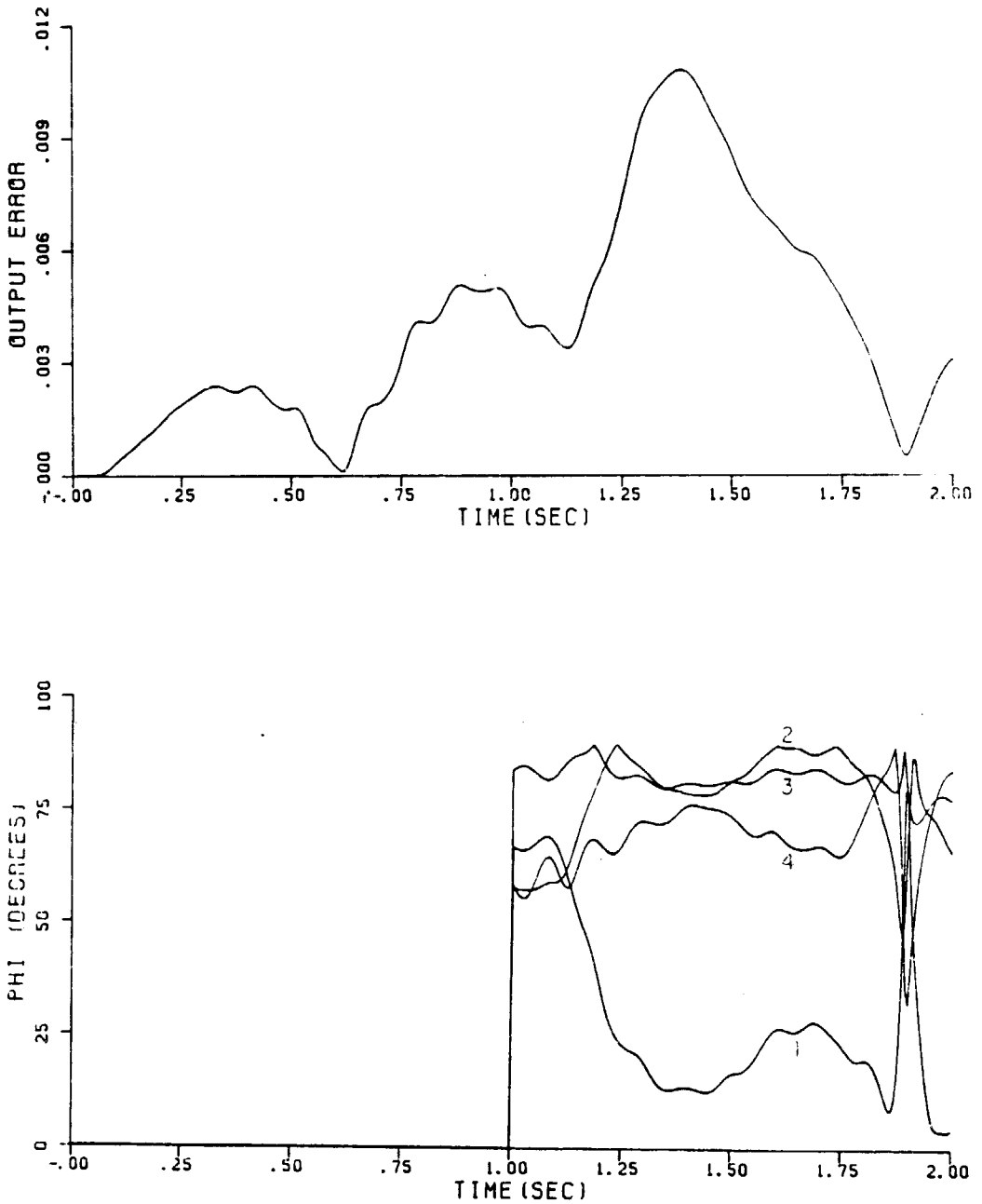

Figure 4-45: Detection Filter #3. Four Unmodeled Modes. Actuator 1 Failure at T = 1 sec.. Output Filtering.

4.3.3 Detection Filter With Observer

In the previous subsection, the problem of the large numbers of unmodeled modes in the detection filter with N = p was solved by introducing a new output transformation. The large improvement that resulted from this was due to the rigid modes that rejected the low frequency noise, and therefore, provided clear detection and identification information. In some cases, however, the model of the flexible structure might contain only one rigid mode or no rigid modes at all. In such a case, the noise rejection properties of the low frequency modes (see Eq. (4.27)) might not be good enough to reject the low frequency noise due to the unmodeled modes (the high frequency noise can always be eliminated with output filtering). The **Detection Filter with Observer** introduced in this subsection is a possible solution when this problem arises. However, it should be made clear that due to a lack of time the properties of such a configuration have not been analyzed in detail, and mainly the motivation for this approach is presented in this thesis.

The problem of model mismatch in detection filters is that the requirement of having small error residuals seems to be incompatible with the requirement of having large failure signatures. The reduction in the error residuals due to model mismatch is achieved by improving the ability of the filter to track the output vector **y**, but in so doing, the ability of the filter to track the output vector **y** in the presence of an actuator failure will also improve, resulting in a smaller failure signature. For example, the error residuals can be reduced by moving the detection space poles to the left in the s plane, but this also results in a smaller failure signature. The Detection Filter with Observer in Fig. 4-46 eliminates the error residuals due to those modes whose shapes and frequencies are known but are not modeled in the reduced order detection filter with N = p, without reducing the

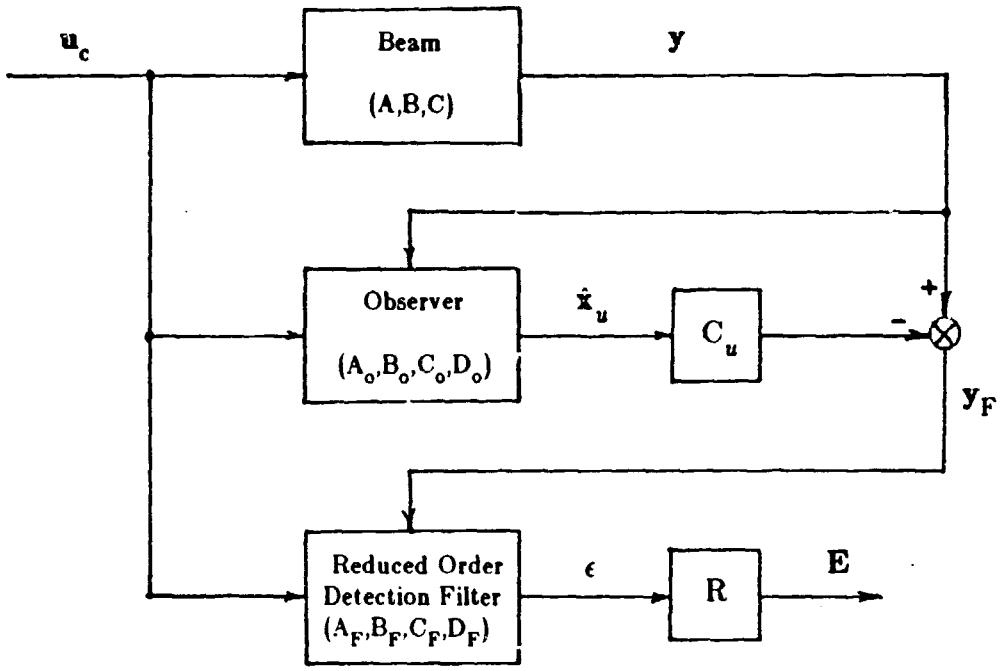

Figure 4-46: The Detection Filter with Observer

failure signature.

The model of the observer contains all the structural modes of the beam that are known, while the model of the detection filter contains as many modes as the number of independent displacement measurements. The equations of the observer are

$$\dot{\hat{x}}_o = A_o \hat{x}_o + B_o u_c + D_o (y - \hat{y})$$

$$\hat{y} = C_o \hat{x}_o$$

and the equations of the detection filter are

$$\dot{\hat{x}}_F = A_F \hat{x}_F + B_F u_c + D_F (y_F - \hat{y}_F)$$

$$\hat{y}_F = C_F \hat{x}_F$$

$$\mathbf{y}_F = \mathbf{y} - C_u \hat{\mathbf{x}}_u$$

where

$$\hat{\mathbf{x}}_o = \begin{bmatrix} \hat{\mathbf{x}}_F \\ \hat{\mathbf{x}}_u \end{bmatrix}$$

$$C_o = [\, C_F \;\; C_u \,]$$

The unmodeled modes of the filter - observer are defined as the modes that are not modeled either in the observer nor in the detection filter. The unmodeled modes of the detection filter are defined as the modes that are modeled in the observer but not modeled in the filter. The purpose of the observer is to obtain good estimates of the amplitudes of the unmodeled modes of the filter in the presence of model mismatch and more important, in the presence of actuator failures. These estimates are multiplied by their corresponding vectors $\mathbf{c}_i$ from matrix C_u, and the results are subtracted from $\mathbf{y}$ to obtain $\mathbf{y}_F$. The detection filter, then, uses $\mathbf{y}_F$ as the measurement vector.

Therefore, when there is no model mismatch between the model of the beam and the model used in the observer and when there is no actuator failure, the estimates of the filter unmodeled modes are correct and the vector $\mathbf{y}_F$ is the one resulting from those structural modes that are modeled in the filter. Hence. since the detection filter does not see any unmodeled modes, the residuals ϵ are zero.

When an actuator failure occurs, the result will depend on the ability of the observer to estimate the amplitudes of the unmodeled modes of the filter in the

presence of the actuator failure. If this ability is good, then the filter measurement vector $\mathbf{y}_F$ will contain very little components resulting from the filter unmodeled modes, and therefore, the error residuals due to the filter unmodeled modes will be very small and identification of the failed component will be possible. On the other hand, if the observer is not good at estimating the amplitudes of the filter unmodeled modes in the presence of actuator failures, when an actuator failure occurs, $\mathbf{y}_F$ will contain large components due to the errors in the estimates of the filter unmodeled mode amplitudes resulting in large error residuals in ϵ that will make the identification impossible.

Therefore, while the detection capabilities of the reduced order filter will be greatly improved by the use of any good observer, the identification capabilities will be improved only if this observer is good at estimating the amplitudes of the filter unmodeled modes in the presence of actuator failures. Note that this requirement is exactly the opposite of the requirement of the detection filter in which we want an actuator failure to produce large errors in the estimates. Furthermore, it seems that in this case, there is no contradiction between requiring the observer to be insensitive to actuator failures and requiring the observer to be insensitive to model mismatch.

A thorough analysis on whether it is possible to design obervers with such properties and how to design them has not been done in this thesis. It is reasonable to expect that observers that rely heavily on the measurements to produce the state estimates will have little sensitivity to actuator failures. An observer with this property has large bandwidth and high frequency poles. This is the case if a detection filter is used as the observer, since the failure signature caused by an actuator failure can be arbitrarily reduced by moving the detection space poles to the left in the s - plane.

The observer used in this thesis was designed using the continuous Kalman filter approach and a seven mode model of the beam. The resulting filter had some high frequency poles very close to the high frequency undamped structural modes, and therefore, it was necessary to use output filtering in the Detection Filter. However, it is believed that the output filtering can be avoided by a more careful design of the observer.

Figure 4-47 shows the result of simulating the filter - observer combination with no model mismatch. That is, the evaluation model of the beam has seven modes, the observer has seven modes and the reduced order detection filter has four modes. The reduced order detection filter used is Detection Filter #3 with the pseudo inverse as the output transformation. The initial conditions of the beam, observer and detection fitler are all zero and actuator 4 fails at T = 1 sec.. Figure 4-47 should be compared with Fig. 4-30 (actually in Fig. 4-30 there is one more unmodeled mode but its contribution to the error residuals is negligible). The failure signature is now clearly visible. The use of the observer produced a remarkable improvement in the detection of the failure, as was expected, and also produced a very large improvement in the identification of the failure.

The eighth structural mode was added to the evaluation model of the beam and the simulation repeated. The effect of the filter - observer unmodeled mode was so small that the output residuals were almost identical to the ones in Fig. 4-47.

Therefore, it can be concluded that the use of the observer was successful in improving the performance of Detection Filter #3 in the presence of unmodeled modes. The performance of the filter - observer configuration was not tested in the presence of parameter errors.

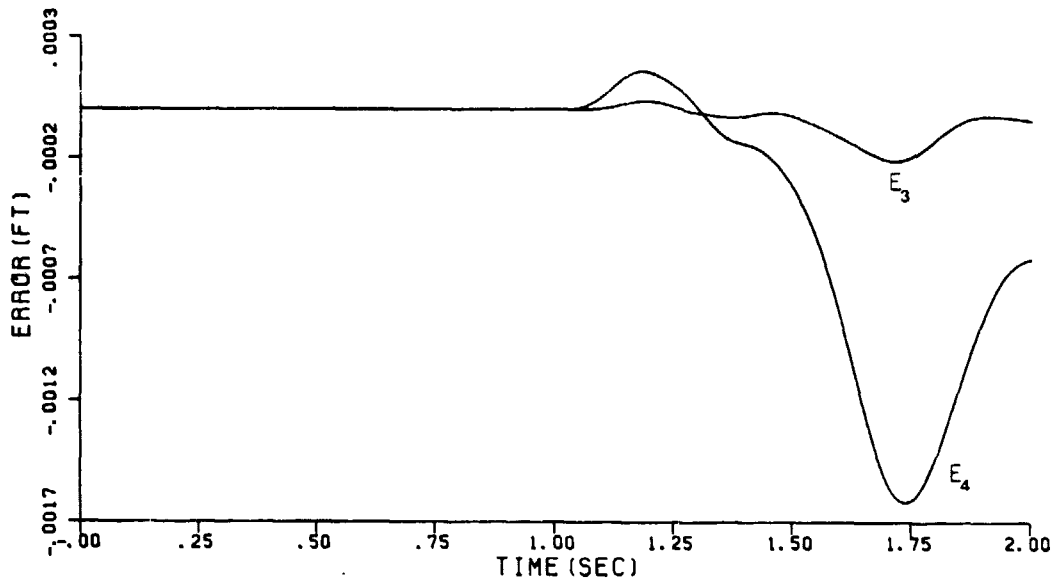

Figure 4-47: Detection Filter #3 with Observer.
Failure of Actuator 4 at T = 1 sec.. Output Filtering.

Chapter 5
Conclusions and Recommendations

When the number of modes modeled into the detection filter was larger than the number of sensors, the detection filter could not be configured to detect more than three actuator failure events, and the corresponding state space was divided into detection and completion spaces. Moreover, the specification of the location of the filter poles did not result in a unique detector gain D. However, the algorithms used in this thesis, suggested by Beard, produced a unique gain matrix D by making the completion spaces invariant. As a result of all this, the filter design was complicated and relied heavily on software.

The dynamics of these filters were very difficult to analyze and produced very unexpected results. The transfer properties of the detection filter that describe its performance in the presence of model mismatch, showed a surprising sensitivity to the location of the completion space poles explaining the results obtained in the simulations. When all of the filter poles were at -10rad/sec., the presence of an unmodeled mode created large low frequency error residuals that completely obscured the failure signature, and the presence of unrealistically low levels of parameter errors also resulted in unsuccessful detections and identification of the failure. By moving the completion space poles to -100rad/sec., the performance of the detection filter in the presence of model mismatch was remarkably improved. However, the detection filter still could not tolerate realistic levels of parameter errors.

The detection filters with N = p (number of modeled structural modes equal

to number of sensors) have several advantages when compared to detection filters with N > p. Perhaps the most important of them is that detection filters with N = p can be configured to detect any number of actuator failure events by placing the filter poles in an appropriate way (e.g., placing all the poles at the same location.) The design of these filters is trivial and does not need any specialized software. Also, their dynamics are very simple and easy to analyze, since they do not involve completion spaces. This in turn allows the designer to make a thorough frequency response analysis of the effects of the different types of model mismatch, and make decisions on how to use the degrees of freedom that he has at his disposal like the location of the detection filter poles, bandwidth of the output filter, choice of output transformation, etc. Finally, another important advantage of these filters is that they perform much better in the presence of parameter errors.

The problem of the detection filters with N = p is their large number of unmodeled modes. The high frequency components of the error residuals due to unmodeled modes lying outside the bandwidth of the filter can always be filtered out without reducing the failure signature. Then, the problem is caused by the components of the residuals lying within the bandwidth of the filter. This problem was dealt with in two different ways. First, the performance of the detection filter in the presence of model mismatch was improved by choosing a different output transformation. This resulted in a detection filter that was able to perform satisfactorily in the presence of the unmodeled modes and in the presence of realistic levels of parameter errors. The second approach was to use an observer to subtract the components of the unmodeled modes from the measurements **y**.

From the analysis and simulations done in this thesis, it appears that a combination of all the techniques explained in subsection 4.3.1 has the best potential to solve the most severe problems of model mismatch in the detection of

actuator failures in flexible structures with displacement sensors. Such a combination refers to a detection filter with N = p, improved output transformation, output filtering and observer.

The recommended areas of research related to the problem analyzed in this thesis are:

1)to investigate whether different methods of assigning the n - ν_F completion poles, that do not require the invariance of the completion spaces, could not result in more robust detection filters,

2)to investigate and develop different ways of reading the detection and identification information from the output error in the presence of model mismatch,

3)to study all the aspects related to the detection filter with observer. For example, to study the design and properties of the observer that best fit this application, and to study the robustness properties of the filter - observer combination,

4)to study the robustness properties of detection filters designed to detect actuator failures in flexible structures with both displacement and rate measurements,

5)to study the performance of the detection filter in a more realistic environment that includes a control system and disturbances.

References

[1] Beard, Richard V.
Failure Accommodation in Linear Systems Through Self-Reorganization.
PhD thesis, Massachusetts Institute of Technology, 1971.

[2] Carignan, Craig R.
Filter Failure Detection For Systems with Large Space Structure Dynamics.
Master's thesis, Massachusetts Institute of Technology, 1982.

[3] Gantmacher, F. R.
The Theory of Matrices.
Chelsea Publishing Co., 1977.

[4] Cole, S. R., Horner, G. and Montgomery, R.
Finite Element Analysis of Experimental Beam.
Technical Report, NASA Langley Research Center, 1980.

[5] Jones, Harold L.
Failure Detection in Linear Systems.
PhD thesis, Massachusetts Institute of Technology, 1973.

[6] Kwakernaak, Huibert and Sivan, Raphael.
Linear Optimal Control Systems.
Wiley-Interscience, 1972.

[7] Major, Carolyn S.
A Demonstration of the Use of Generalized Parity Relations for Detection and Identification of Instrument Failures on a Free-Free Beam.
Master's thesis, Massachusetts Institute of Technology, 1981.